POLYANILINE-ZEOLITIC IMIDAZOLATE FRAMEWORK COMPOSITE NANOFIBERS FOR HYDROGEN GAS SENSING APPLICATION

MSC(Chemistry)

G. MASHAO

2019

POLYANILINE-ZEOLITIC IMIDAZOLATE FRAMEWORK COMPOSITE NANOFIBERS FOR HYDROGEN GAS SENSING APPLICATION

By

GLORIA MASHAO

DISSERTATION

Submitted in fulfilment of the requirements for the degree of

MASTER OF SCIENCE

In

CHEMISTRY

In the

FACULTY OF SCIENCE AND AGRICULTURE

(School of Physical and Mineral Sciences)

At the

UNIVERSITY OF LIMPOPO

SUPERVISOR: DR K. D. MODIBANE

CO-SUPERVISORS: PROF M. J. HATO

DR K. MAKGOPA (TUT)

2019

DEDICATION

TO MY LATE MOTHER

Refilwe Mavis Mashao

DECLARATION BY CANDIDATE

I declare that POLYANILINE-ZEOLITIC IMIDAZOLATE-FRAMEWORK COMPOSITE NANOFIBERS FOR HYDROGEN GAS SENSING APPLICATION is my own work and that all the sources that I have used or quoted have been indicated and acknowledged by means of complete references and that this work has not been submitted before for any other degree at any other institution.

_____	_____
Full Names	Signature
	_____
	Date

ACKNOWLEDGEMENTS

First and foremost, I would like to thank the maker of all things, **GOD MY STRONGHOLD** for making me strong and courageous to overcome all the challenges I faced throughout my studies. Without Him by my side, this achievement would have not been possible.

I have a great pleasure to pass my sincere gratitude to my supervisor Dr K.D. Modibane for his guidance, inspiration and support throughout my postgraduate studies. My special thanks goes to him for his patience, consistent encouragement and also for equipping me with knowledge and problem solving skills.

I would like to pass my acknowledgments to my co-supervisors Prof M.J. Hato and Dr K. Makgopa at Tshwane University of Technology (Acardia) for their immense support throughout the tenure of my studies. I thank them for believing in me and being there when I needed motivation. I thank them greatly for their unwavering support that they have shown in me. My heartfelt gratitude goes to Prof. E.I. Iwouha, Dr M. Masikini and Mr. S.B Mdluli for making me feel at home in the Chemical Science Building, SensorLab at the University of the Western Cape. I am grateful to them for playing an important role in this work, thanks for helping me to understand electrochemical hydrogen gas sensing and fall in love with it. I also want to thank Dr K. Molapo for the great support in helping with electrochemistry aspects.

I would like to express my gratitude to the University of Limpopo, Department of Chemistry more especially Nanotechnology Group at University of Limpopo (NanoRG@UL) lead by Prof Hato for their support. Thanks to Monama G.R, Maponya T.C, Ramohlola K.E, Pesha T, Somo T.R, Ramaripa P.S, Teffu D, Malatji N, and Makhafola M.D.

I also thank the Geology Division at UL for assisting me with XRD analyses.

Special thanks to Sasol Inzalo Foundation and National Research Foundation of South Africa for financial support and making sure that this work is communicated at various conferences and research meetings.

My greatest thanks goes to my father Ngwako Solomon Mashao for constant love, care, support and proper upbringing. I thank him for being by my side at all times. Moyahabo Octocia, Polivia and Puseletso Annelia Mashao for putting up with me during tough times. I thank them for the support and constant encouragement throughout my entire life. I am grateful to my niece Refilwe Praise and Keorapatse Rejoice Mashao for always putting a smile on my face. To my closest friend Eden Motseo, thanks for giving me love, care and courage to complete my studies.

I would like to present my heartfelt thankfulness to my late mother Refilwe Mavis Mashao for the significant role she played in my life, thanks for the love, blessings and for watching over me at all times. I thank her for constantly inspiring me to achieve my dreams, thanks a lot**.**

ABSTRACT

The quest for renewable, sustainable and environmentally compatible energy sources have been on-going for decades. Green technology such as hydrogen fuel cell has attained much attention as an alternative energy carrier to carbon-based fuels owing to its renewability and cleanliness. However, hydrogen gas feed to the fuel cell can easily be ignited if its concentration is above 4 wt.% at room temperature. Thus, hydrogen safety mechanisms such as hydrogen sensors are vital to guarantee people's safety in the hydrogen infrastructure. Sensors based on metals and metal oxides have been widely applied for hydrogen gas detection.

Nonetheless, these materials are only sensitive to hydrogen gas at elevated temperatures (> 100 °C) and they also possess low surface area (< 20 m^2/g). Hence in this work, we present polyaniline (PANI) doped with cobalt-based zeolitic benzimidazolate framework (CoZIF) and zinc-ZIF to fabricate (PANI-CoZIF and PANI-ZnZIF) composite nanofibers as effective electrocatalysts for hydrogen gas sensing application. The composites were synthesised through chemical oxidative polymerisation of aniline monomer in the presence of 3.6 wt.% CoZIF and ZnZIF, respectively.

The structural properties of the synthesised materials were studied using Ultraviolet visible (UV-vis), X-ray diffraction (XRD), Fourier transform infrared (FTIR), Raman spectroscopy and simultaneous thermal analysis (STA). FTIR, Raman and XRD studies showed successful synthesis of CoZIF, ZnZIF and their composites. Furthermore, the studies indicated the co-existence of both CoZIF and ZnZIF in the PANI matrix upon composites formation, indicated by reduction in crystalline size, decrease in band gap and increase in thermal stability. as compared to the neat PANI. Morphological characteristics of the prepared samples were investigated usingscanning electron microscopy (SEM) and transmission electron microscopy (TEM) coupled with both energy dispersive spectroscopy and X-ray (EDS/EDX). PANI-CoZIF revealed the grafting of CoZIF on to the surface of PANI matrix while

PANI-ZnZIF composite showed that PANI is wrapping the cube nanofiber-like structures of ZnZIF also supported by selected area electron diffraction (SAED).

Cyclic voltammetry (CV), Tafel analysis and turn over frequencies (TOFs) were performed to study the electrochemical performance of the synthesised materials through hydrogen evolution reaction (HER) for gas sensing. Both composites presented drastic enhancement in the catalytic H_2 evolution at 0.033 mol.L^{-1} H_2SO_4 with the Tafel slope of 160 mV/dec and exchange current density of 3.98 A.m^{-2} for PANI-CoZIF composite, while the Tafel slope and exchange current density for PANI-ZnZIF composite were 246 mV/dec and 5.01 A.m^{-2}, respectively. Moreover, the TOFs of the PANI-CoZIF composite (0,117 mol H_2.s^{-1}) was higher as compared to neat PANI (0.040 mol H_2.s^{-1}). The TOF values for PANI and PANI-ZnZIF composite were 0.04 and 0.45 mol H_2.s^{-1}, respectively. In addition, the chronoamperometric (CA) results exhibited the significant improvement in the electrochemical hydrogen sensing ability of PANI-CoZIF and PANI-ZnZIF composites with higher current response and sensitivity values of 12 and 10.8 µA.mmol.L^{-1} H_2, respectively. The composites exhibited faster steady state response time of 5 s for PANI-CoZIF composite and 4 s for PANI-ZnZIF composite accompanied by lower detection limit (5.27 µmol.L^{-1}) as compared to the neat PANI matrix. The high electrochemical current response is due to extraordinary specific surface area, more accessible active sites available for the electrolyte provided by CoZIF and ZnZIF and high conductivity supplied by PANI. These results proved that the PANI-CoZIF and PANI- ZnZIF composites are suitable electrocatalytic materials for hydrogen gas sensing application through HER in acidic medium. These results further suggest that the safety of people in mining sectors and other industries can be addressed through simple electrocatalytic gas sensing systems.

RESEARCH OUTPUTS

PUBLICATIONS

i. **Gloria Mashao**, Kabelo E. Ramohlola, Gobeng R. Monama, Mpitloane. J. Hato, and K. Makgopa, Kwena. D. Modibane,. "*Recent developments in polyaniline composites for electrochemical hydrogen gas sensing applications*. Submitted as a review paper in *Electrochemical Energy Reviews (Appendix 1).*

ii. **Gloria Mashao**, Kwena D. Modibane, Siyabonga B. Mdluli, Emmanuel I. Iwuoha, Mpitloane J. Hato, Katlego Makgopa, Kerileng M. Molapo. "*Development of electrochemical gas sensor technology induced by polyaniline doped with cobalt-zeolitic benzimidazolate framework composite for hydrogen safety monitoring*". Revised manuscript submitted in *Electrocatalysis* with provisional acceptance *(Appendix 2).*

iii. **Gloria Mashao**, Mpitloane J. Hato, Kwena D. Modibane, Siyabonga B. Mdluli, Emmanuel I. Iwuoha, Katlego Makgopa. "*Fabrication of polyaniline decorated with zinc-based zeolitic benzimidazolate framework nanocompositeas an effective electrocatalyst for hydrogen gas sensing*". *Revised mauscript submitted in Materials Chemistry and Physics with provisional acceptance (Appendix 3).*

iv. Emmanuel I. Iwuoha, Gobeng R. Monama, Kabelo E. Ramohlola, Mogwasha D. Makhafola, **Gloria Mashao**, Siyabonga B. Mdluli, Mpitloane J. Hato, Kerileng M. Molapo, Katlego Makgopa, Kwena D. Modibane. *Copper(II) phthalocyanine/metal organic framework composite with improved electrocatalytic efficiency for hydrogen production. Published as a Proceeding in the 3rd International Hydrogen Technologies Congress (IHTEC-2018), March 15-18, 2018, Alanya/Antalya, Turkey (Appendix 4).*

v. Gobeng R. Monama, Kwena D. Modibane, Kabelo E. Ramohlola, Kerileng M. Molapo, Mpitloane J. Hato, Mogwasha D. Makhafola, **Gloria Mashao**,

Siyabonga B. Mdluli, Emmanuel I. Iwuoha, "*Copper(II)metal organic framework electrocatalyst for hydrogen evolution reaction applocation*". *International Journal of Hydrogen Energy*. doi.org/10.1016/j.ihydene.2019.02.52 *(Appendix 5).*

vi. Gobeng R. Monama, Siyabonga B. Mdluli, **Gloria Mashao**, Mogwasha D. Makhafola, Kabelo E. Ramohlola, Kerileng M. Molapo, Mpitloane J. Hato, Katlego Makgopa, Emmanuel I. Iwuoha, Kwena D. Modibane, "*Palladium deposition on copper(II) phthalocyanine/metal organic framework composite and electrocatalytic activity of the modified electrode towards the hydrogen evolution reaction*," *Renewable Energy* **119** (2018) 62–72 *(Appendix 6).*

PRESENTATIONS

i. **Gloria Mashao**, Kwena D. Modibane, Kabelo E. Ramohlola, Mpitloane J. Hato, Kerileng M. Molapo, Emmanuel I. Iwuoha. *"Polyaniline doped with zeolitic imidazolate framework composite for hydrogen gas sensing application".* Oral Presentation. Faculty of Science and Agriculture Research Day, Bolivia Lodge, Polokwane, South Africa on the 19th October 2017.

ii. **Gloria Mashao**, Kwena D. Modibane, Kabelo E. Ramohlola, Mpitloane J. Hato, Kerileng M. Molapo, Emmanuel I. Iwuoha. "*Gas sensing through hydrogen evolution reaction induced by polyaniline doped with cobalt-zeolitic imidazolate framework composite".* Oral Presentation. SANI–NanoAfrica 2018 Conference, Salt Rock, Durban, South Africa, 22nd-25th April 2018.

TABLE OF CONTENTS

LIST OF FIGURES

LIST OF TABLES

LIST OF ABBREVIATIONS

ABA	: 3-aminobenzoic acid
ANI	: Aniline
APS	: Ammonium per sulfate
APTMS	: (3-aminopropyl)trimethoxysilane
BIM, BIZ	: Benzimidazole
BOPET	: Biaxially oriented polyethylene terephthalate
CA	: Chronoamperometry
CNTs	: Carbon nanotubes
CoZIF	: Cobalt based Zeolitic benzimidazolate framework
CPs	: Conducting polymers
CSA	: Camphor sulfonic acid
CV	: Cyclic voltammetry
DMSO	: Dimethyl sulfoxide
DSC	: Differential scanning calorimetry
EDS, EDX	: Energy dispersive X-ray spectroscopy
EM	: Emeraldine state
FESEM	: Field Emission Scanning Electron Microscope
FTIR	: Fourier transform infrared
GC	: Gas Chromatography
GO	: Graphene oxide
HER	: Hydrogen evolution reaction
HKUST-1	: Hong Kong University of Science and Technology-1
HRTEM	: High Resolution Transmittance Electron Microscope
ICPs	: Intrinsic conducting polymers

IR	: Infra-red
LE	: Leucoemeraldine
LOD	: Limit of detection
LOQ	: Limit of quantification
LPG	: Liquefied petroleum gas
MOFs	: Metal organic frameworks
NFPA	: National Fire Protection Association
PA	: Polyacetylene
PABA	: Poly(3-aminobenzoic acid)
PANI, PANi	: Polyaniline
PE	: Pernigraniline
PEDOT	: Poly(3.4-ethylenedioxythiophene)
PGMs	: Platinum group metals
PL	: Photoluminescence
PPV, PVP	: Poly(para-phenylene vinylene)
PPY	: Polypyrrole
PTH	: Polythiopene
SAED	: Selected area electron diffraction
SCE	: Saturated calomel electrode
SEM	: Scanning electron microscope
STA	: Simultaneous thermal analysis
SWV	: Square Wave voltammetry
TBAP	: Tetrabutylammonium percholate
TC	: Thermal conductivity
TEM	: Transmission electron microscope
TGA	: Thermogravimetric analysis
TOF	: Turnover frequency
US DoE	: United State Department of Energy
UV	: Ultraviolet
UV-vis	: Ultraviolet visible
XRD	: Powder X-ray diffraction

ZIF	: Zeolitic imidazolate framework
ZnZIF	: Zinc based zeolitic benzimidazolate framework

LIST OF SYMBOLS

A	: Area of the electrode
C	: Concentration
D	: Crystallite size, Diffusion coefficient
Ep	: Peak potential
Ep_a	: Anodic peak potential
Ep_c	: Cathodic peak potential
F	: Faraday constant
I	: Current
Ip	: Peak current
Ip_a	: Peak anodic current
Ip_c	: Peak cathodic current
I_{cat}	: catalytic current
I_L	: limiting currents
j	: current density
k_{cat}	: catalytic rate constant
n	: Number of electrons transferred
Γ	: Surface coverage
v	: Scan rate
V	: Applied voltage
M	: Mass percentage
M	: Mass of per square centimetre

CHAPTER ONE

INTRODUCTION

1.1. BACKGROUND

Energy plays a crucial role in homes, agriculture, industries and transportation for sustaining life. Recent studies have shown that the global population is growing rapidly. As a result, the energy supply must increase in order to meet energy demands [1]. The primary energy source depends on combustion of fossil fuels and they contribute 80% of the energy utilised globally [1]. However, the combustion of fossil fuels emit greenhouse gases such as carbon dioxide (CO_2), nitrogen oxides (Nox), hydrocarbons, carbon monoxide (CO), particulate matter and sulphur dioxide (SO_2) [2-4]. On the other hand, renewable energy sources such as wind, hydrothermal, biomass and nuclear are considered as the alternative route since they produce less pollutants as compared to fossil fuels [5,6]. Nonetheless, these resources are costly and generate limited amount of energy [7]. Hydrogen technology can be considered as a candidate to solve those limitations [8]. It is an appealing energy carrier for a variety of fuel cell applications such as stationary, mobile and portable power technologies [9]. Furthermore, H_2 accounts for 75% of the whole universe's mass and can be produced from water which is in highly abundant [10]. It is renewable in a sense that it gives water as a by-product which can be split further into hydrogen and oxygen gas. In addition, H_2 can be stored as liquid, gas or solid. It can also be transported over large distances using pipelines, tankers, or rail trucks. Moreover, H_2 can be converted into electricity at a relatively high efficiency. Furthermore , hydrogen gives more energy as compared to traditional gasoline based energy resources [11].

1.2. PROBLEM STATEMENT

Hydrogen gas has received much attention as an alternative energy carrier, yet there are still some technically challenging barriers to its widespread usage as a form of energy. One of the crucial limitations for hydrogen technology is its extreme flammability. Hydrogen is highly flammable if its concentration is higher than 4 wt.% at room temperature [12-14]. Therefore, a development of hydrogen gas sensors is essential to alert to the formation of potentially explosive mixture during its production, storage and transportation. According to the United states Department of Energy (US DoE), materials are considered as good hydrogen sensors if they have operating temperature between −30 °C to 80 °C, response time of less than 1 s and 10 years lifetime [15]. Metal oxides (MO_x), metals and their alloys have been used for H_2 sensing due to their high selectivity and sensitivity for the adsorption of H_2 molecule [16-18]. However, these materials are sensitive to hydrogen gas at high temperatures (>100 °C) and also possesses low surface areas (<20 m^2/g) [16]. In addition, high capital cost, long response and recovery time, and difficulty in post-modification process hamper their widespread application [18].

On the other hand, Intrinsic Conducting Polymers (ICPs) such as polyaniline (PANI) and polypyrrole (PPY) have been widely used in the development of electrochemical smart sensors owing to their special conduction mechanism, low fabrication cost, ease of deposition onto a wide variety of substrates, and short response time when used at room temperature [19, 20]. Furthermore, the ability to incorporate specific binding sites into conducting polymers offers the improvement of selectivity and sensitivity [19]. Among ICPs, PANI has been found to be the most promising polymer due to its high environmental stability, mechanical flexibility, simple and reversible doping/dedoping chemistry [21-24]. However, PANI has limited sensitivity towards gas species as compared to metal and metal oxides and its poor processability caused by its insoluble nature in most organic solvents inhibit its use as potential electrochemical hydrogen gas sensor [25]. The poor processability is due to its high aromaticity and its existence in a relative low molecular weight form [26].

1.3. RATIONALE

To circumvent the problems encountered when utilising PANI as a hydrogen sensor, different approaches have been reported [27-30]. The poor processability of PANI can be addressed by development of the PANI based composites and blends [28]. This will introduce new functional groups in the polymer backbone hence making the benzene ring of PANI to be reactive [16]. Incorporation of porous compounds such as metal organic frameworks (MOFs) to the polymer backbone can also help in increasing the electrochemical stability of the polymer [28]. Amongst various types of MOFs, zeolitic imidazolate frameworks (ZIFs) exhibit permanent porosity, high thermal and chemical stability, which make them attractive candidates for many applications [29]. Its small pores (3.4 Å) can be functionalised by tuning the pore sizes to make use of size-exclusive effects for the separation and purification of small molecules such as hydrogen [30]. ZIF/graphene oxide (ZIF/GO) composite had been reported to have large aspect ratio, large surface area to volume ratio and large porosity [31]. These properties play a major role in fabricating a suitable gas sensing materials with larger absorptive capacity for gas analyte [32-33]. Hybridisation of PANI and ZIF to form a composite could results in improved solubility in most organic solvents and also enhanced electrochemical hydrogen sensing properties as compared to pure PANI or ZIF based gas sensors. Based on this information, this study seeks to develop highly efficient electrochemical hydrogen gas sensor induced by PANI-ZIF composites.

1.4. AIM AND OBJECTIVES

1.4.1. Research aim

The aim of this work is to synthesise and determine the efficiency of the PANI-ZIF composite nanofibers for hydrogen gas sensing application.

1.4.2. Objectives

The objectives of this work are to:

i. synthesise PANI and ZIFs (Zn and Co based ZIFs) through chemical polymerisation of aniline monomer and hydrothermal methods, respectively.
ii. prepare PANI doped with cobalt based zeolitic benzimidazolate framework (PANI-CoZIF) and PANI loaded with zinc based zeolitic benzimidazolate framework (PANI-ZnZIF) composites using *in-situ* chemical polymerisation of aniline monomer in the presence of CoZIF and ZnZIF, respectively.
iii. study structural properties of the synthesised nanofibers using X-ray diffraction (XRD), Fourier transform infrared (FTIR), Raman spectroscopy and ultraviolet-visible spectroscopy (UV-vis).
iv. evaluate the thermal stability of the prepared samples by simultaneous thermal analysis (STA), which possess both thermogravimetric analysis (TGA) and differential scanning calorimetry (DSC).
v. perform morphological and elemental characterisations using scanning electron microscopy/energy dispersive spectroscopy (SEM/EDS), transmission electron microscopy/energy dispersive X-ray spectroscopy (TEM/EDX) and high resolution transmission electron microscopy/selected area electron diffraction (HR-TEM/SAED)
vi. study electrochemical behaviour of the synthesised materials using cyclic voltammetry (CV) and square wave voltammetry (SWV).
vii. evaluate HER studies of synthesised materials at room temperature using Tafel parameters and turn over frequency (TOF).
viii. determine the electrochemical hydrogen gas sensing capability of the prepared nanofibers using CV and chronoamperometry (CA).

1.5. DISSERTATION OUTLINE

This dissertation is outlined into six chapters. All the chapters attempt to tune PANI properties by functionalising it with ZIF thus enhancing its electrochemical hydrogen gas sensing capability. Chapter one gives a brief background on PANI and its composites, problem statement, aim and objectives and rational of the study. The outline of the remaining chapters in the dissertation is as follows:

- ✓ **Chapter two**: it gives emphases on recent developments in polyaniline composites for electrochemical hydrogen gas sensing applications wherein it focuses on the literature review of hydrogen technology, hydrogen sensing methods, electrochemical hydrogen gas sensing, polyaniline, polyaniline composites, zeolitic imidazolate frameworks.
- ✓ **Chapter three**: concentrates on the review of analytical techniques employed for structural, thermal, morphological and electrochemical characterisations of the synthesised nanomaterials.
- ✓ **Chapter four**: it is on the development of electrochemical gas sensor technology induced by polyaniline doped with cobalt-zeolitic benzimidazolate framework composite for hydrogen safety monitoring.
- ✓ **Chapter five**: focuses on the fabrication of polyaniline decorated with zinc based zeolitic benzimidazolate framework nanocomposite as an effective electrocatalyst for hydrogen gas sensing.
- ✓ **Chapter six**: general discussion, conclusions and recommendations.

1.6. REFERENCES

[1] J. Goldemberg, “Ethanol for a sustainable energy future”, *Science*, vol. 135, pp. 808-810, 2007

[2] F. A. Rahman, M.M.A. Aziza, R. Saidur, W. Bakar, M.R. Hainin, R. Putrajaya, and N.A. Hassan, “Pollution to solution: Capture and sequestration of carbon dioxide (CO_2) and its utilization as a renewable energy source for a sustainable future”. *Renew Sustain Energy Rev*., vol. 71, pp. 112-126, 2017.

[3] B. C. O’Neill, E. Kriegler, K. L. Ebi, E. Kemp-Benedict, K. Riahi, D. S. Rothman, B. S. van Ruijven., D. P. van Vuuren, J. Birkmann, K. Kok , M. Levy , and W. Soleckim, “The roads ahead: Narratives for shared socioeconomic pathways describing world futures in the 21st century’’, *Glob Environ Chang.*, vol. 42, pp. 169–180, 2017.

[4] E. l. Abd, A. A. Monem, A. M. Azmy, and S.A. Mahmoud. ‘’Effect of process parameters on the dynamic behavior of polymer electrolyte membrane fuel cells for electric vehicle applications’’. *Ain Shams Eng J*., vol. 5, pp. 75–84, 2014.

[5] J. Chow, R. J. Kopp, and P. R. Portney, ‘’Energy resources and global development’’, *Science*, vol. 302, pp. 1528-1531, 2003.

[6] N.L. Panwar, S.C. Kaushik, and S. Kothari, ‘’Role of renewable energy sources in environmental protection-A review’’,*Renew Sustain Energy Rev*., vol. 15, pp. 1513-1524, 2011.

[7] A. Demirbas, ‘’Potential applications of renewable energy sources, biomass combustion problems in boiler power systems and combustions related environmental issues’’, *Prog Energy Combust Sci*., vol. 31, pp. 171-192, 2005.

[8] J. P. Painuly, ‘’Barrier to renewable energy penetration; a framework of analysis’’. *Renew Energy*, vol. 24, pp. 73-89, 2001.

[9] J. A. Turner, ‘’Sustainable hydrogen production, *Science*, vol. 305, pp. 972-974, 2004.

[10] T. Veras, T. S. Mozer , D.C.R.M. Santos, and A. S. Cesar, ‘’Hydrogen: Trends, production and characterization of the main process worldwide’’. *Int J Hydrogen Energy,* vol. 42, pp. 2018-2033, 2017.

[11] S. Satyapal, J. Petrovic, C. Read, G. Thomas, and G. Ordaz, ‘’The US Department of Energy's National Hydrogen Storage Project: Progress towards meeting hydrogen-powered vehicle requirements’’. *Catal Today*, vol. 120, pp. 246-256, 2007.

[12] M. A. Butler, ‘’Micromirror optical-fiber hydrogen sensor’’. *Sens Actuators B*., vol. 22, pp.155-163, 1994.

[13] R. Arsata, X. F. Yub, Y. X. Li, B. W. Wlodarskia, and K. Kalantar-zadeh, ‘’Hydrogen gas sensor based on highly ordered polyaniline nanofibers’’ *Sens Actuators B*., vol. 137, pp. 529–532, 2009.

[14] O. Lupan, V. Postica, F. Labat, I. Ciofini, T. Pauporte, and R. Adelung, “Ultra-sensitive and selective hydrogen nanosensor with fast response at room temperature based on a single Pd/ZnO nanowire”. *Sens Actuators B*., vol. 254, pp. 1259-1270, 2018.

[15] B. W. Abegaz, T. Datta, and S. M. Mahajan, “Sensor technologies for the energy-water nexus – A review”. *Appl Energy*., vol. 210, pp. 451–466, 2018.

[16] E. X. Chen, H. Yang, and J. Zhang, “Zeolitic Imidazolate Framework as Formaldehyde Gas Sensor”, *Inorg Chem.*, vol. 53, pp. 5411−5413, 2014.

[17] V. S. Bhati, S. Ranwa, M. Fenetti, M. Valant, and M. Kumar, “Efficient hydrogen sensor based on Ni-doped ZnO nanostructures by RF sputtering. *Sens Actuators B*”, vol. 255, pp. 588-597, 2018

[18] L.F. Aval, and S.M. Elahi, “Hydrogen gas detection using MOS capacitor sensor based on palladium nanoparticles-gate”, *Electron Mater Lett.*, vol.13, pp .77–85, 2017.

[19] B. Lakard, S. Carquigny, O. Segut, T. Patois, and S. Lakard, “Gas sensors based on electrodeposited polymers”, *Metals*, vol. 5, pp. 1371-1386, 2015.

[20] M.J. Marsella, P.J. Carroll, and T.M. Swager,” Conducting pseudopolyrotaxanes: a chemoresistive response via molecular recognition” *J Am Chem Soc*., vol. 116, pp. 9347-9348, 1994.

[21] J. Pecher, and S. Mecking “Nanoparticles of conjugated polymers”. *Chem Rev.*, vol. 110, pp. 6260-6279, 2010.

[22] S. Bhadra, D. Khastgir, N.K. Singha, and J.H. Lee, “Progress in preparation, processing and applications of polyaniline”. *Prog Polym Sci*., vol. 34 pp. 783-810, 2009.

[23] X. Li, Z. Wang, and G. Wang, “Synthesis of a super-hydrophilic conducting polyaniline/titanium oxide hybrid with a narrow pore size distribution*”. Appl Surf Sci*., vol. 258, pp. 4788–4793, 2012.

[24] A. Z. Sadek, W. Wlodarski, K. Kalantar-Zadeh, C. Baker, and R. B. Kaner, “Doped and dedoped polyaniline nanofiber based conductometric hydrogen gas sensors”. *Sens Actuators* A, vol. 139, pp. 53–57, 2007.

[25] A. G. MacDiarmid, and A. J. Epstein, “The concept of secondary doping as applied to polyaniline” *Synth Met.*, vol. 65, pp. 103-116, 1994.

[26] M. Jaymand, “Recent progress in chemical modification of polyaniline”. *Prog Polym Sci*., vol. 38 , pp. 1287-1306, 2013.

[27] X. P. Chen, J.K. Jiang, Q. H. Liang, N. Yang, H. Y. Ye, M. Cai, L. Shen, D. G. Yang, and T. L. Ren, “First-principles study of the effect of functional groups on polymer backbone”. *Sci Rep.*, vol. 5, pp. 1-7, 2015.

[28] H. L. Jiang, and Q. Xu, “Porous metal−organic frameworks as platforms for functional applications”, *Chemical Communications*, vol. 47, pp. 3351−3370, 2011.

[29] G. Lu, and J. T. Hupp, “Metal−organic frameworks as sensors: a ZIF−8 based Fabry−Pérot device as a selective sensor for chemical vapors and gases”. J Am *Chem Soc.*, vol. 132, pp. 7832−7833, 2010.

[30] N. Chang, Z. Y. Gu, X. and P. Yan, “Zeolitic imidazolate framework−8 coated capillary for molecular sieving of branched alkanes form linear alkanes along with high−resolution chromatographic separation of linear alkanes”.J Am *Chem Soc* , vol. 132, pp. 13645−13647, 2010.

[31] T. David, J. K. Mathad, T. Padmavathi, and A. Vanaja, “Synthesis of polyaniline and carboxylic acid functionalized SWCNT composites for

electromagnetic interference shielding coatings". *Polymer*, vol. 55, pp. 5665-5672, 2014.

[32] W. Zhang, Y. Tan, Y. Gao, J. Wu, J. Hu, A. Stein, and B. Tang, "Nanocomposites of zeolitic imidazolate frameworks on graphene oxide for pseudocapacitor applications", *J Appl Electrochem.*, vol. 46, pp. 441-450, 2016.

[33] B. Chen, Y. Zhu, and Y. Xia, "Controlled in situ synthesis of graphene oxide/zeolitic imidazolate framework composites with enhanced CO_2 uptake capacity", *RCS Adv*, vol. 5, pp. 30464-30471, 2015.

CHAPTER TWO

RECENT DEVELOPMENTS IN POLYANILINE COMPOSITES FOR ELECTROCHEMICAL HYDROGEN GAS SENSING APPLICATIONS-REVIEW

This chapter was submitted for possible publication in *Electrochemical Energy Reviews*

CHAPTER SUMMARY

The emergence of hydrogen gas (H_2) sensors is essential for hydrogen to gain wide acceptance as a fuel. This review gives an insight on different hydrogen sensing methods, their advantages and limitations. Metals and metal-oxide based catalysts are considered as good materials for hydrogen gas sensing; nonetheless they are not cost effective and they operate at elevated temperatures. Furthermore, they are not selective towards hydrogen gas and their calibration curves are prone to moisture deviations. Therefore, it is of great importance to develop highly effective and reliable hydrogen gas sensors which have the capability to operate at room temperature. In this work, more focus is on hydrogen gas sensors induced by PANI composites and their distinctive parameters such as response time, selectivity and sensitivity are being reviewed. PANI is a conducting polymer which grasped much attention in gas sensing applications owed to its easy synthesis and ability to detect various gases. Moreover, it has become one of the most studied and reviewed conducting polymers in the past decades due to its outstanding conductivity, chemical and thermal stability. This review chapter also gives an overview on the latest developments in electrochemical hydrogen sensors based on PANI composites; their drawbacks and future prospects are being discussed. New nanotechnological approaches which uses PANI composites for electrochemical hydrogen gas sensing are still in their infancy stage and numerous electrochemical hydrogen sensors induced by these composites are expected to increase in the near future in order for hydrogen gas to be utilised in practical fuel cell applications.

2.1. INTRODUCTION

Hydrogen technology has attained considerable attention as a clean and effective alternative energy carrier for a variety of fuel cell applications such as stationary, mobile and portable power applications [1]. It is expected to play a significant role in the near future by supplying the world with green, renewable and sustainable energy by replacing traditional fossil fuels. Hydrogen gas is highly abundant in fossil fuels, water (H_2O), plants and animals but only exists as a free element only in trace amounts [2]. Combustion of hydrogen gas generates no pollutants; only water is formed as a bi-product [3]. In addition, hydrogen gives more energy (about 2.75 times) greater as compared to traditional gasoline based energy resource [4]. For fuel cell application, hydrogen gas is converted from chemical into electric energy in a simple and clean way using electrochemical process [5]. Moreover, an electrocatalyst is required in a fuel cell to increase the reaction rate, thus lowering the activation energy of the process. The curve of overpotential as a function of current density (Tafel curve) is usually employed to determine the exchange current density (i_0), which is related to electrocatalytic performance of a material [5]. The higher the exchange current density, the higher the electrochemical performance of the electrocatalyst [6]. Noble metals such as palladium and platinum have shown better electrocatalytic performance hence they are found at the apex of the volcano plot (Figure 2.1) [5]. However, they are not ideal for practical use since they are not cost effective.

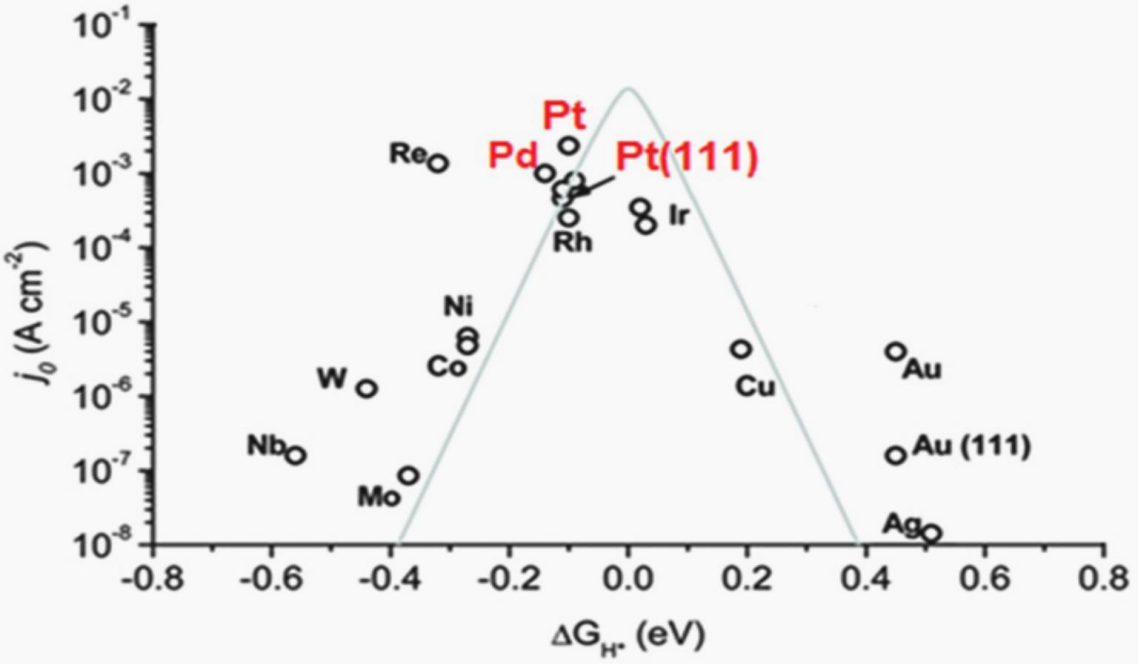

Figure 2. 1: Volcano curve for hydrogen adsorption on different metals [5]

Due to the above mentioned limitations of noble metals, there is a continued search in the science community to find better electrocatalysts for fuel cell applications. Furthermore, to construct a fuel cell for electric motor and batteries applications using hydrogen as energy carrier, there is still a need to solve the challenges which are encountered in hydrogen technology which includes hydrogen extreme flammability [7]. Hydrogen can easily be ignited if its concentration in air is above 4wt% [7]. For that reason, hydrogen gas sensors are needed to assist in preventing the explosion hazards which might take place during its production, storage and transportation [8], hence this review focuses on the overview of hydrogen sensing technologies.

2.2. HYDROGEN SENSING TECHNOLOGY

Hydrogen is the least combustible gas at 4 wt.%, however its flammability window is larger (4–75% v/v H_2) as compared to ethane, natural gas, propane and gasoline [8]. Therefore, it is vital for a hydrogen sensing material to possess a wider measuring

range (1–99% v/v H_2) to monitor hydrogen gas [8]. Furthermore, hydrogen is the lightest element and the tiniest molecule, as a result, it tends to leak easily [9]. Moreover, hydrogen cannot be detected by human senses and its leakage can be more risky and challenging [10]. Based on this information, the emergence of hydrogen sensing materials is essential for hydrogen to be used universally as a fuel [10]. Sensors are devices which are capable of responding to an external stimulus and give a specific signal [11]. According to the National Fire Protection Association (NFPA), for a hydrogen sensing material to grasp extensive acceptance to be used within the hydrogen infrastructure of production, storage, transportation, and utilisation, it must have good performance, be reliable and cost effective [12]. The United States Department of Energy (US DoE) set a target that a hydrogen sensor must possess a compact size, easy fabrication and control system, fast response, operational temperature between -30 °C and 80 °C, excellent sensitivity and selectivity, lifetime of 10 years, must not be responsible for false alarms and be non- contaminating [12,13]. Different hydrogen sensing methods have been widely studied which includes gas chromatography, metal oxides**,** thermal conduction**,** pellistor**,** palladium based and electrochemical sensors [13].

2.2.1. Gas chromatography (GC)

A gas chromatography is a separation instrument which uses carrier gas as a mobile phase. GC separates the component of a mixture based on their boiling points [12]. GC principle involves the interaction between gases of interest with walls of the column resulting in the elution of the gases at different times (retention time). Gas chromatography is one of the most selective and sensitive applied measuring principle for hydrogen detection [12]. The drawbacks of GC include its long response time caused by time-consuming expensive handling procedures and sample preparation [14]. Furthermore, it has the ability to measure other gases such as carbon dioxide, nitrogen and oxygen in the presence of hydrogen which adds time to the total analysis [14].

2.2.2 Metal oxides (MO_X) sensors

Metal oxide sensors are also known as semiconductor-based sensors since they use a semiconducting film as the sensing element [15]. Their sensing principle involves heating them up to elevated temperatures (300–500 °C) in the presence of oxygen wherein the grain boundary is formed in the MOx thus resulting in detection of gases. The MO_X sensors such as zinc oxide and tin oxide are compact, inexpensive and they have good sensitivity towards hydrogen gas [15]. However, MOx are only sensitive to hydrogen gas at elevated temperatures for them to obtain a stable conductivity thus resulting in complex configurations in comparison to other sensing materials operating at room temperature [16]. The reported high operational temperature of MOx is due to the reaction temperature of O^- [16]. Other challenges facing MOx sensors include structural instability, low surface area, moisture deviations, long response and recovery time [15-17]

2.2.3. Thermal conduction sensors (TC)

Thermal conductivity (TC) sensors are widely used for hydrogen gas sensing and they depend upon a change in temperature of an electrically heated sensing element when exposed to the analyte [14]. The TC sensors are heated to a temperature in which the resistance of the sensing element deviates from the linear limit of Ohm's law [18]. They possess advantages such as wide measuring range, long term stability, robustness and they do not require O_2 to operate. Moreover, they are resistant to poisoning and they have simple and low cost construction [14]. Nonetheless, they exhibit higher low detection limit, cross-sensitive to He and the reaction with heating wire can occur and [19].

2.2.4. Pellistor sensors

Pellistor sensors uses noble metals such as platinum as catalysts which surrounds a ceramics that is electrically heated at 550 °C, thus offering a catalytic surface for hydrogen ignition [14]. This lead to a change in the resistance and improvement in the temperature of the sensing device [14]. Pellistor sensors have good stability, wider operational temperature and longer lifetime [20]. However, they are not selective and cannot distinguish between different flammable gases [20]. Moreover, they are prone to poisoning by sulphur (S) , phosphorus (P), and silicon (Si), they require more power and oxygen (O) to operate [21] .

2.2.5. Palladium based sensor

Palladium has attained much attention for hydrogen gas sensing due to its fast response towards hydrogen gas [22]. Their operating principle involves the dissociation of hydrogen in its molecular state to its elemental state (this is the rate-determining step), followed by the diffusion of elemental hydrogen into the palladium lattice causing it to expand and a phase transition from conductive phase to less conductive phase occurs [12,22]. The shortcomings of palladium based hydrogen sensors are their high operational temperature (above 100 °C) [12]. The high operational temperature causes structural change of the sensor therefore resulting in the response differences and instability [12]. Furthermore, elevated temperatures are threats when detecting flammable gases.

2.2.6. Electrochemical sensors

Electrochemical sensor consists of a sensing, reference and a counter electrode, separated by a thin layer of electrolyte [13]. Electrochemical sensors show significant advantages of being highly sensitive, selective and portable at a modest cost [23] . They have shown excellent analytical performance with low energy and power

consumption [13]. Potentiometric and amperometric based sensors are the most widely investigated types of electroctrochemical based sensors.

2.2.6.1. Potentiometric sensors

For potentiometric sensors, a local equilibrium is established at the sensor interface, where either the electrode or membrane potential is measured, and information about the composition of a sample is obtained from the potential difference between two electrodes (potential is independent of the dimensions of the sensor) [13]. They are miniaturised and they generate power that can be easily be measured precisely [24].

2.2.6.2. Amperometric sensors

In amperometric sensors, an electroactive species undergo oxidation or reduction resulting from the applied potential between a working and reference electrode to measure the current which is directly proportional to gas concentration [13,25]. Hydrogen can easily be sensed by electrochemical sensors, particularly amperometric devices available commercially [13]. The mechanism of a hydrogen sensor involves the diffusion of hydrogen through the gas diffusion barrier to the electrode and become absorbed on the sensing electrode. This is followed by the occurrence of electrochemical reaction accompanied by the transfer of electron and generation of hydrogen proton. The proton conducting membrane facilitates the movement of proton to the counter electrode, thus the product desorbs from the counter electrode and diffuses away. Lastly, the electronic charge moves from or to the electrode followed by appearance of current [13]. Amperometric gas sensors are known to be physically small, have good sensitivity, and usually have a broad linear range [26]. Drawbacks include moderate selectivity and poor sensitivity as compared to metals [27]. They are very stable with lifetimes of up to 5 years or more. According to the US DoE a material is considered a good hydrogen sensor if its lifetime is 10

years [13]. Therefore there is a growing interest in the development of new sensors to satisfy the US DoE requirements.

2.2.6.3. Key parameters for electrochemical gas sensing

There are several parameters, which influences the performance of an electrochemical sensing material. Those key parameters include sensor sensitivity, response time, selectivity and stability.

2.2.6.3.1. Sensitivity

Sensor sensitivity is the measure of how fast a sensor can detect the analyte of interest. It is the measure of how the signal change per analyte concentration unit [11]. The detection limit of a material is the minimum value of an analyte that can be measured by the sensor and it can be related to sensitivity [8]. The lower the limit of detection of a sensor the higher the sensitivity. In electrochemical gas sensing, the sensitivity can be determined from the slope of the calibration curve of current response against different gas concentrations generated from amperometric or potentiometric results [11].

2.2.6.3.2. Selectivity

Selectivity is also the key factor in gas sensing and is defined as the ability of the sensor to differentiate between the target analytes and other materials [11]. It measures the capability of a sensor to respond selectively to a specific analyte in a group of analytes. Numerous sensors need functionalisation with recognition elements for the selectivity to increase [8].

2.2.6.3.3. Stability

Stability is another key parameter used to evaluate the performance of a sensor. Stability means the ability of a sensor to give the same response signal for an identical stimulus over time. According to Bochenkov and SergeeV stability is the ability of a sensor to provide reproducible results for a certain period of time and the parameters such as selectivity, sensitivity, response, and recovery time are retained [11]. To probe the stability of a sensor over time, current-time responses at a fixed potential must be performed using electrochemical techniques such as chronoamperometry and chronopotentiometry [8]. A material is regarded as a good sensor if it remains stable over the lifespan of the sensor [22].

2.2.6.3.4. Response and recovery time

Response time is the time the sensor needs to increase up to the 90% of its final stable output after introducing the analyte [8]. It is the time needed for the sensor to respond to a step concentration change from zero to a certain concentration value [11]. The recovery time is the time the sensor takes to drop to the 10% of its baseline after the removal of the analyte [11].

2.2.6.4. Sensing electrode materials for electrochemical gas sensing

The relationship between the key operating characteristics and kinetic factors such as mass transfer of the analyte to the electrode and the electrocatalytic activity of the sensing electrode are of great importance in electrochemical sensing [8]. Moreover, the performance of the electrochemical gas sensor depends on the structural properties of the material from which the sensor is made-up of. Furthermore, sensor dimensions and geometry have a profound effect on the response time, sensitivity, signal stability and selectivity of the hydrogen sensor [8]. Additionally, to control sensor kinetics and thermodynamics, materials are selected based on their

fundamental electrochemical and electronic properties, stability and specific chemical interactions [25]. Realisation and commercialisation of hydrogen technology requires the emergence of highly abundant, reliable and active electrocatalyst for hydrogen gas sensing. Therefore, more research to find reliable electrocatalyst for hydrogen sensing has increased recently. Materials such as carbon nanotubes, metal oxide nanostructures, noble metals and intrinsic conducting polymers have been investigated for hydrogen sensing [25,28,29].

2.2.6.4.1. Noble metals

Noble metals such as gold, palladium and platinum have being exploited in electrochemical hydrogen sensing as the working electrodes and they are capable of making a defined interface with the electrolyte in the cell to allow efficient diffusion of the gas phase to a large-area and reactive electrode-electrolyte interface [8]. To date, noble metals are the most studied materials for electrochemical hydrogen gas sensing owed to their exceptional stability under polarised potential [25]. Korotcenkov *et al.* reported that palladium electrodes have fast response (10 s) for all hydrogen concentrations from 1-100% to achieve a signal level of 90% [8].

2.2.6.4.2. Carbon based materials

Carbons based material such as graphite, carbon nanotues (CNTs) and glassy carbon are used as popular sensing electrodes [8]. Carbon is conductive and the sensing electrode made of it can achieve an optimum combination properties such as porosity and conductivity [8]. If carbon can be combined with noble metals such as platinum, carbon provides good electrical contact between the grains of the metal thus improving the performance [8].

2.2.6.4.3. Intrinsic conducting polymers (ICP)

Among these materials, intrinsic conducting polymers (ICP) are the promising candidates for gas sensing due to their ability to conduct electricity and their extended π-electrons system in their structure [25,28]. The first ICP to be discovered was polyacetylene (PA) in the 1970s by Shirakawa Louis et al [30]. ICPs possess low energy optical transition, low ionisation potential and high electron affinity [3]. The conductivity of these polymers can be influenced by factors such conjugation length, polaron length, overall polymer length and the charge transfer to adjacent molecule [31]. They have been studied extensively due to their great electrical and optical properties, redox reversibility redox, flexibility in processing and ease of synthesis [32,33]. Conducting polymer based gas sensors are having an advantage as compared to the inorganic based sensors due to their variety, natural conductivity, fast response, low cost, light weight, easy synthesis and sensitivity at the room temperature. The first conducting polymer to be applied for gas sensing was polypyrrole [32]. Nonetheless, it was found that this polymer lacks adsorption-desorption reversibility. Furthermore, its longer response time and poor sensitivity has hampered its wide application as a gas sensing material. Therefore, there is a continued need to find reliable and better performing polymer based gas sensing materials. Recently, PANI as one of the conducting polymers has grasped much attention in various applications such as HER, water treatment as well as gas sensing. Huang and co-authors [34] studied the response towards 100 ppm of HCl and NH_3 vapor induced by PANI nanofiber. The authors found that the PANI nanofiber showed better sensing performance.

2.3. POLYANILINE

2.3.1. Background of polyaniline

The term PANI corresponds to a class of polymers having up to 1000 repeating units (also called monomers) and was first reported in 1862 where it was formed through oxidation of aniline monomer under mild conditions [19]. PANI exists in different chemical structures due to different oxidation states of the polymer backbone. It exists in fully reduced state, half oxidised state and fully oxidised known as leucoemeraldine, emeraldine and pernigraniline respectively [35] . PANI in its half oxidised state is highly stable at room temperature. The most common synthesis of PANI involves oxidative polymerisation, in which the polymerisation may be accomplished either electrochemically or chemically [34]. Furthermore it is known to be soluble in some polar organic solvents such as N-methylpyrrolidone and dimethyl sulfoxide [3].

The electrochemical performance and the redox states of PANI are usually investigated by employing cyclic voltammetry (CV). Song and Choi documented some key electrochemical behavior of PANI (Figure 2.2) and further explained that the electrochemical response depends on factors such as applied potential and the type of material used [36]. They further explained that working temperature, surface area of the electrode and the electrolyte composition also play a huge role on the electrochemical behaviour of PANI [36]. The CV results give an insight about the structural formula for PANI as it undergoes redox processes and such distinctive plot is presented in Figure 2.2.

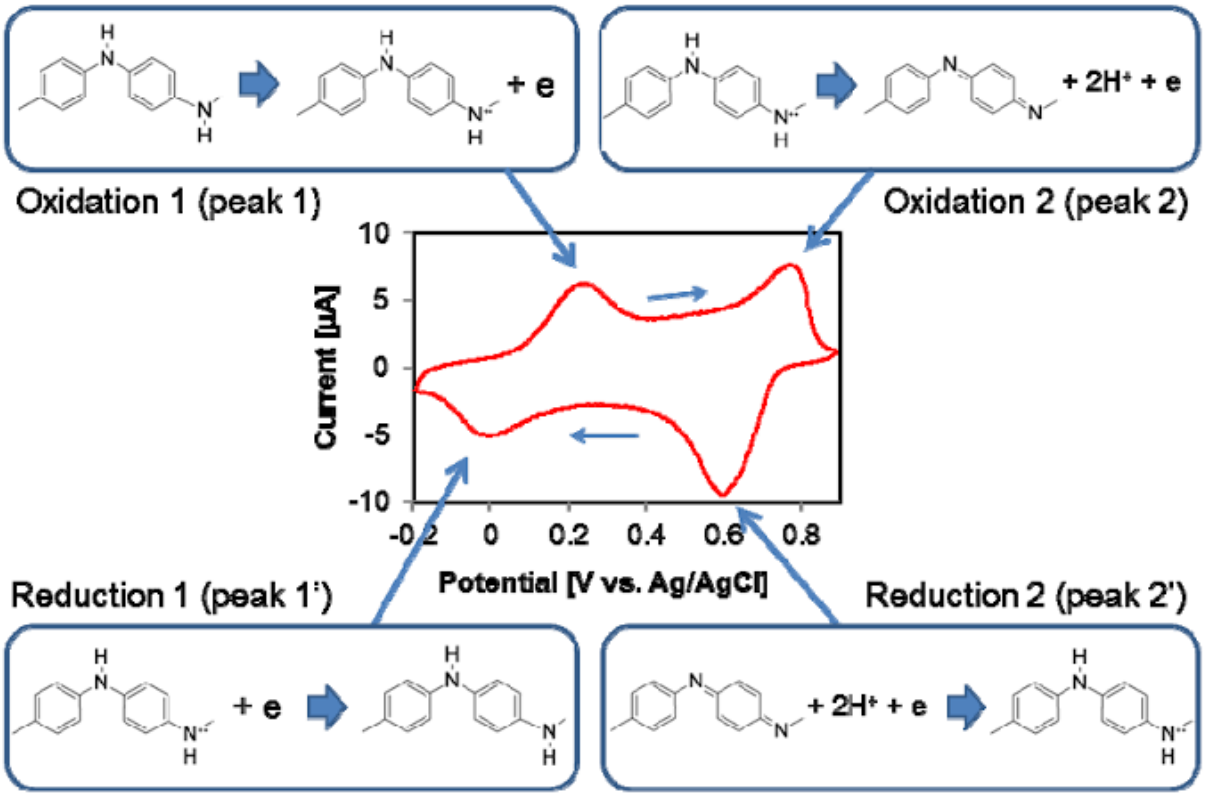

Figure 2.2: A typical cyclic voltammetry (CV) curve of PANI in HCl (pH 1) showing two sets of redox couples. The direction of potential scan is shown with the arrows [36]

It displays two distinctive redox couples wherein the redox couple at around 0 and 0.25 V using Ag/AgCl reference electrode pertains to where fully reduced leucoemeraldine base is converted to the partly oxidised emeraldine, and the redox couple appearing around 0.6 and 0.8 V is due to emeraldine being converted to fully oxidised pernigraniline state [36].

PANI has been found to be the most promising and attractive conducting polymer due to its low cost, easy synthesis, high environmental stability, mechanical flexibility, simple and reversible doping/dedoping chemistry [3,38]. Moreover, it has become one of the most studied and reviewed conducting polymers in the past decades due to its high conductivity [38]. It has found its potential applications in

multidisciplinary areas such as water treatment, supercapacitors as well as sensing due to its easy synthesis, high conductivity and capability to detect various gases [33,39]. Surface acoustic wave sensor based on PANI nanowire with the diameter between 30-50 nm was used for detection of hydrogen and possessed the detection limit of about 0.06% and response time of about 100 s [36]. However, its poor processibility and limited sensitivity towards gas species as compared to metal oxides limits its potential to be used in gas sensing application [34]. Different methods have been employed to address the encountered limitations of PANI which includes formation of PANI composites [3]. Furthermore, through oxidation-reduction and doping, the conductivity of ICPs can also be improved [3]. The main focus of this review is on the development of electrochemical hydrogen sensors induced by PANI based composites.

2.3.2. PANI composites based sensors

PANI based composites comprise of PANI and one or more components such as semiconductors, metal nanoparticle, organic compounds and inorganic compounds [38,39]. This improves polymer backbone structure and its functionalities [37]. Composites are synthesised using a number of methods like physical mixing, sol–gel technique, *in-situ* chemical polymerisation, emulsion technology and sonochemical process [3,35,39]. Lina and the co-authors [40] studied the characterisation and gas sensitivity study of PANI/SnO_2 hybrid material prepared by hydrothermal route. The PANI/SnO_2 hybrid material constitutes of PANI as the polymeric matrix and SnO_2 as the semiconducting component, it exhibited good sensitivity towards ethanol and acetone at 60 or 90 °C [40]. Moreover, it showed good reversibility, short response and recover time within 1 minute. The material emerged overwhelmed the drawbacks of longer response time of PANI and lowered the operational temperature of SnO_2, hence it can be opted for practical use [40]. Pandey compiled a comprehensive report based on a highly sensitive and selective chemiresistor gas/vapor sensors induced by PANI nanocomposite [40]. Gas sensing parameters

such as sensitivity, response and recovery time for different gases such as NO_2, NH_3, H_2 and H_2S were briefly discussed [40].

Sen *et al.* reported about PANI/Fe_2O_3 nanocomposite for room temperature liquefied petroleum gas (LPG) sensing [41]. PANI/Fe_2O_3 (3 wt.%) nanocomposite exhibited excellent gas response at a low gas concentration of 50 ppm with a response time of 60 s [41]. Moreover, Yan *et al*. prepared NO_2 gas sensing with PANI nanofibers synthesised by a facile aqueous/organic interfacial polymerisation [39]. Mekki *et al.* investigated the chemiresistive gas sensing properties of PANI–silver (Ag) films on (3-aminopropyl)trimethoxysilane (APTMS) modified biaxially oriented polyethylene terephthalate BOPET and pristine BOPET achieved by the exposing 10 ppm of each test gases such as NH_3, H_2S, Cl_2, NO, NO_2, CO, CH_4, and C_2H_5OH [42]. The sensor showed better performance on H_2S than other gases as shown on Figure 2.3 and Table 2. 1 shows PANI based nanocomposites used for detection of various gases.

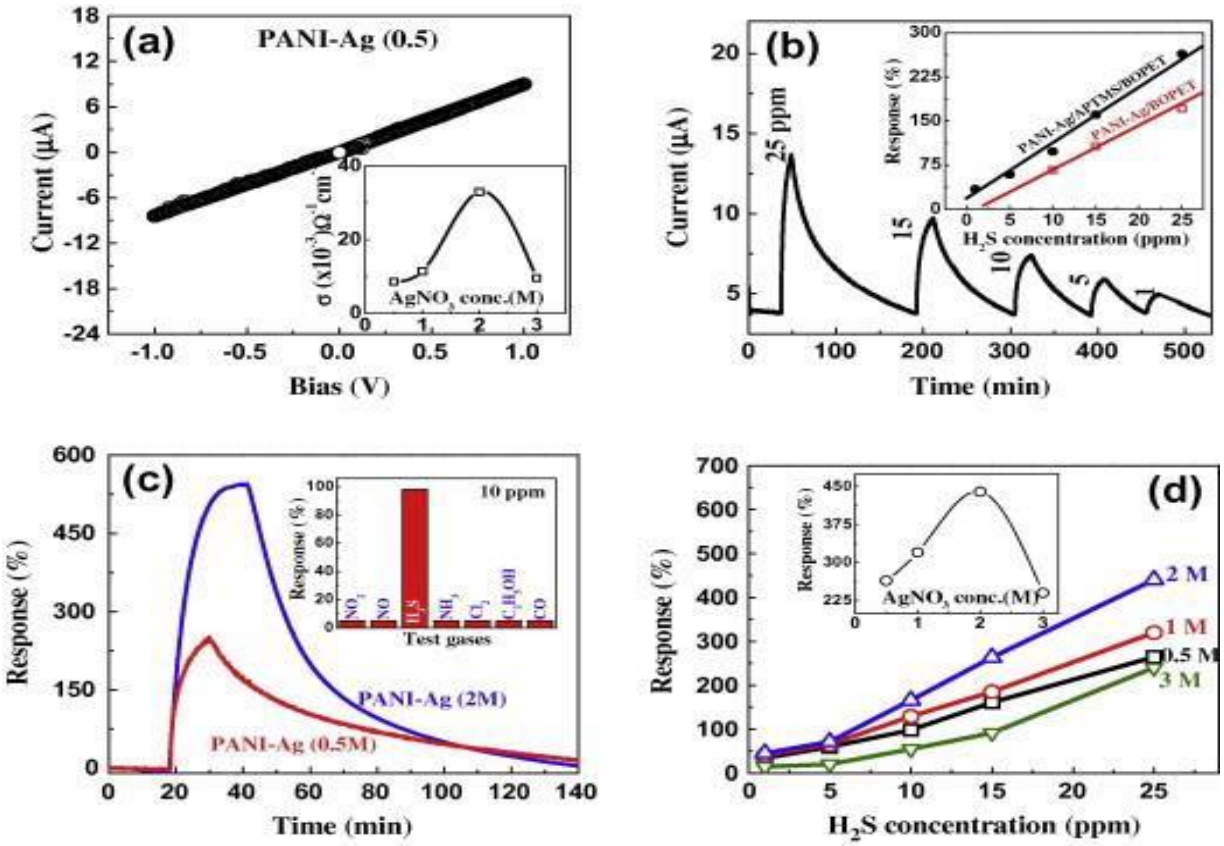

Figure 2.3: (a) Current–voltage characteristics of PANI–Ag films. Inset: base resistance of the films versus $AgNO_3$ concentration (b) Response curve for PANI–Ag (0.5 M) films at various H_2S concentration. Comparative response (%) as a function of H_2S concentrations (c) Comparative response curve for PANI–Ag (0.5 M) and PANI–Ag (2 M). Inset: the selectivity histogram of PANI–Ag (0.5 M) at 10 ppm concentration of different gases. (d) Response as a function of concentrations of H_2S and $AgNO_3$. Inset: the response (%) of PANI–Ag films prepared varying concentration of $AgNO_3$ at 25 ppm of H_2S exposure [42].

Table 2.1: Summary of PANI based composites for gas sensing application

Sensor	Gas detected	Range (ppm)	Response time	Sensitivity	Refs.
PANI/TiO_2	NH_3	23–141	2s	-	[43]
PANI/SnO_2	N_2	10ppm	-	3.01×10^2	[44]
	NH_3	100	46 s	91%	[45]
PANI/SnO_2-CSA					
RGO/PANI	NH_3	50	- -	59.2	[18]
PANi/Fe_2O_3	LPG	50	60s	-	
PANI/$ZnMoO_4$	LPG	800-1800	-	45.8%	[46]

Zheng and co-workers [47] studied the electrochemical glucose sensing induced by Cu/PANI/graphene. The composite exhibited the sensitivity, detection limit and response time of 150 mA cm^{-2} M^{-1}, 0.27 µM and 3 s, respectively [47]. Lata *et al.* [23] also reported an amperometric H_2O_2 biosensor based on cytochrome c immobilized onto nickel oxide nanoparticles/carboxylated multiwalled carbon nanotubes/PANI (NiO/MWCNT/PANI) modified gold electrode. The biosensor was non-enzymatic and exhibited good reproducibility, fast response, longer stability and broad linear range [23]. Tovide *et al.* [48] investigated the electrochemical sensing behaviour of graphenated-PANI nanocomposite systems based on amperometric and voltammetric signal transductions. The authors obtained the dynamic linear range and detection limit of 0.012–1000 µM and 0.0044 µM, respectively. These results show that PANI can be used for electrochemical sensing application.

2.3.3. PANI based composites for hydrogen (H_2) gas sensing

PANI is one of the intrinsic polymers which is studied extensively in hydrogen technology [34]. Ramohlola *et al.* [3] elaborated on its electrochemical performance (Figure 2.4) on hydrogen production and as an electrocatalysts for hydrogen evolution reaction using Tafel plot. The results showed that formation of polyaniline composite further improves the electrochemical performance of PANI as an electrocatalyst in acidic medium which was indicated by an increase in exchange current density. The exchange current density and Tafel slope were found to be 7.943 $A.m^{-2}$ and 199.3 $mV.dec^{-1}$, respectively [3]. The authors further studied the composite formed from PANI derivative poly(3-aminobenzoic acid) (PABA) incorporated metal organic framework (MOF) denoted as PABA-MOF with exchange current density and Tafel slope of 35.48 $A.m^{-2}$ and 130.5 $mV.dec^{-1}$, respectively [6].

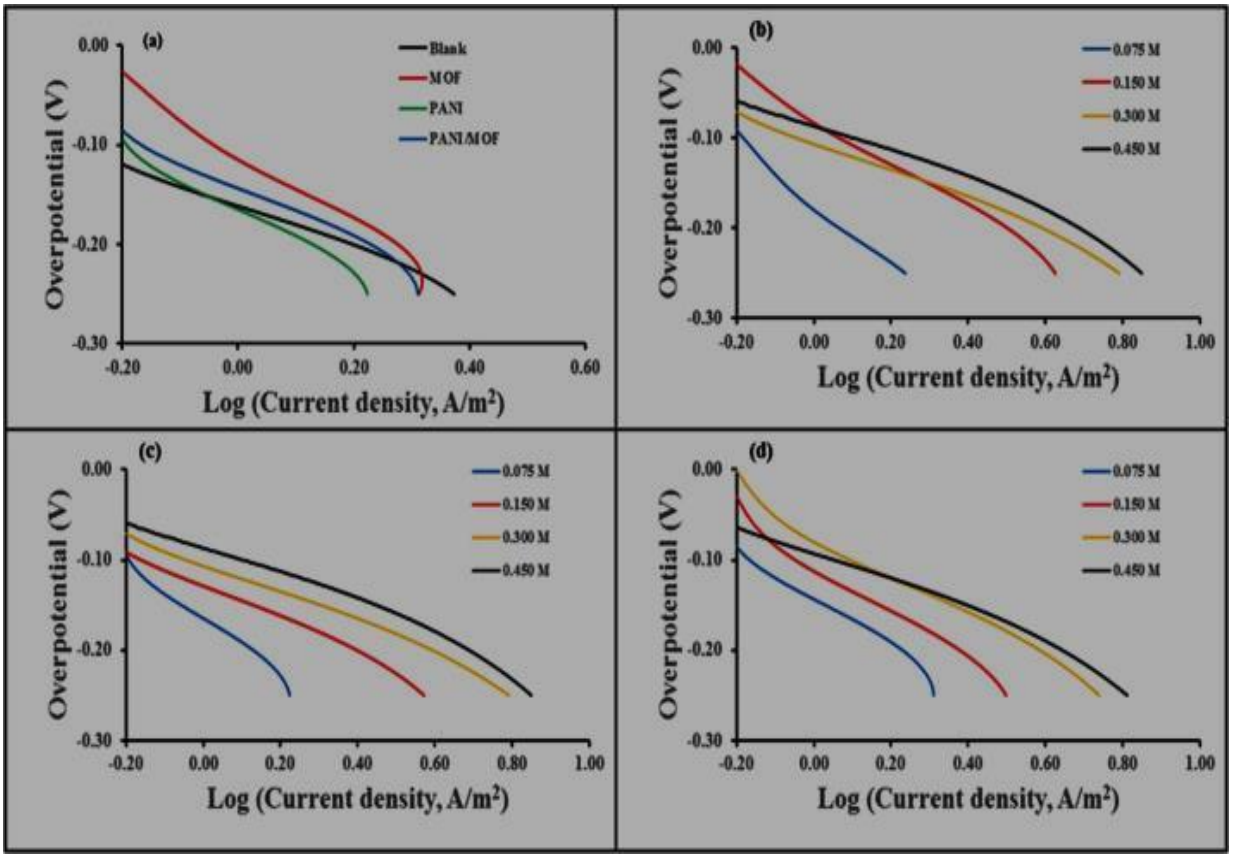

Figure 2.4: Tafel plots of (a) blank, PANI, MOF and PANI/MOF composite (~2.0x10^{-4} mol/L) in the presence 0.075 M H_2SO_4 at 0.10 Vs^{-1} (b) MOF (c) PANI and (d) PANI/MOF composite in different concentrations of H_2SO_4 and 0.10 Vs^{-1} scan rate on Au electrode in 0.1 M TBAP/DMSO electrode system [3].

2.3.3.1. PANI doped with metal oxides for H_2 sensing

PANI doped with metal oxides composites have been widely investigated for hydrogen gas sensing application. Hydrogen sensor based on PANI/WO_3 was investigated for hydrogen detection in the range 0.06 - 1%, and showed better performance with the response and recovery time of 40 and 100 s, respectively [40]. In another report, PANI (emeraldine)/ anatase TiO_2 was also investigated for sensing 0.8% of hydrogen gas. The sensor exhibited the recovery and response time of

around 130 and 83 s respectively, with the sensitivity of around 1.63% towards hydrogen gas [40]

2.3.3.2. PANI doped with carbon based materials for H_2 sensing

PANI doped with carbon based materials such as graphene/PANI have been used for hydrogen gas sensing application [38]. The graphene/PANI sensor was used to sense hydrogen concentration between 0.06 - 1% and possessed the sensitivity of about 16.57% [38]. In another study a chemiresistive hydrogen sensor based on Graphene/PANI with the diameter of less than 25 - 50 nm showed faster response of about 1 minute towards hydrogen [36]. Furthermore, chemiresistive sensor induced by PANI doped with camphor sulphonic acid (CSA) denoted as PANI/CSA with diameter of 100 nm was also used for hydrogen sensing and exhibited the detection limit of less than 1% [36].

2.3.3.3. PANI doped with multi-components for H_2 sensing

In another study [40], a hydrogen sensor was fabricated using a multicomponent Al-SnO_2/PANI composite fibre and the sensor showed faster response and recovery time of around 2 s with the sensitivity of 275% towards 1000 ppm of hydrogen. Recently, Do *et al*. [25] studied the planar solid-state amperometric hydrogen gas sensor based on Nafion/platinum/nano-structured polyaniline/gold/aluminium oxide (Nafion®/Pt/nsPANi/Au/Al_2O_3) electrode. The sensor exhibited the specific sensitivity and the response time of 338.50 mA ppm^{-1} g^{-1} and 100-250 s, respectively, for measuring 10-10,000 ppm hydrogen as shown in Figure 2.5. Based on these results, this sensor did not meet the US DoE requirements. Therefore, Nafion®/Pt/nsPANi/Au/Al_2O_3 cannot be regarded as an ideal material for electrochemical hydrogen sensing. The long response time of Nafion®/Pt/nsPANi/Au/Al_2O_3 hydrogen sensing electrode might be attributed to the

incorporation of platinum since noble metal Pt is known to work best at elevated temperatures [21].

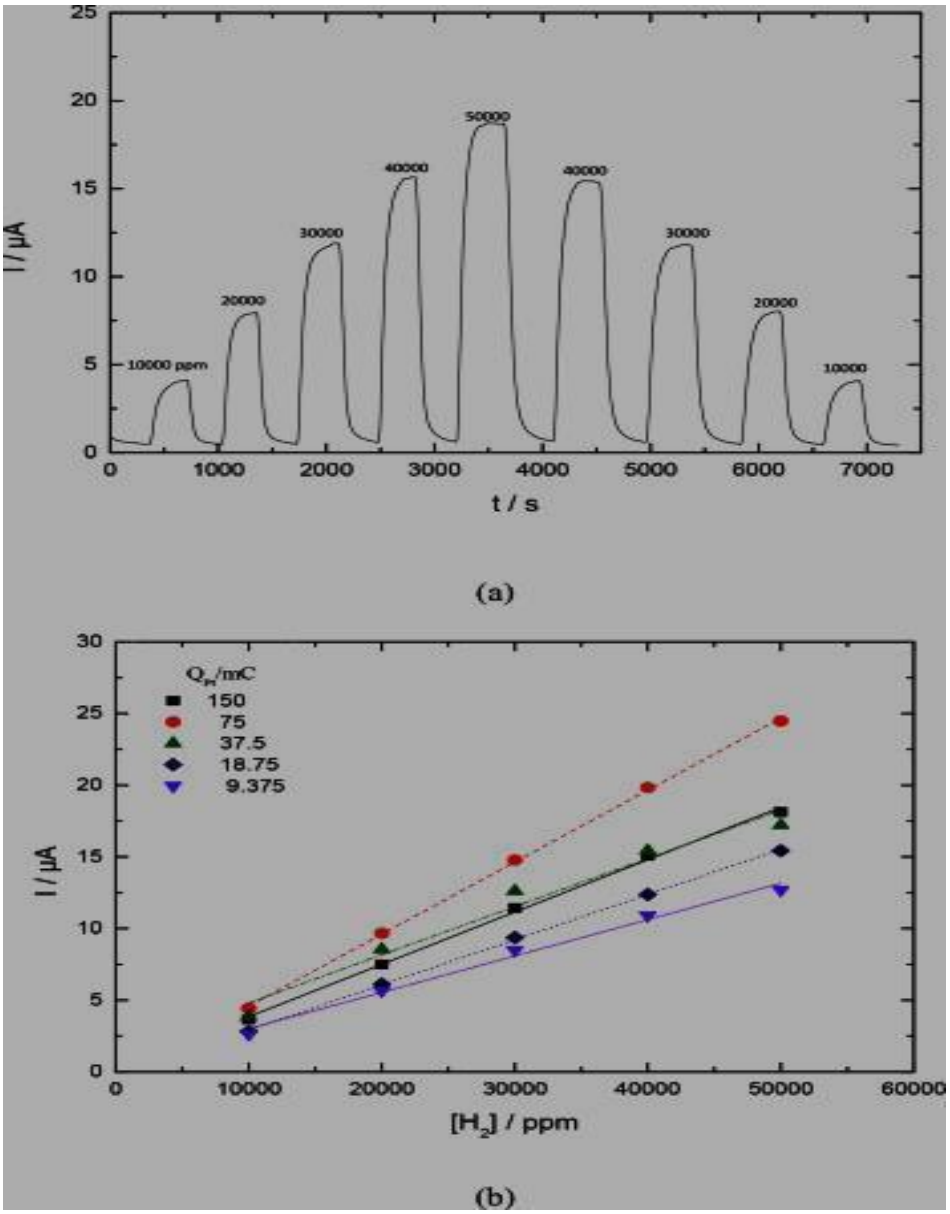

Figure 2.5: Relationships of (a) the sensing current and run time on Nafion®/Pt (Q_{Pt} = 150 mC)/ns PANI (QPANI = 30 mC)/ Au/Al_2O_3, and (b) the sensing current and concentration of H_2 on Nafion®/Pt/nsPANI (QPANI = 30 mC)/Au/Al_2O_3 for Pt prepared with the various charges (Q) passed. Counter electrode: Au/Al_2O_3, reference electrode: Au/Al_2O_3, applied potential = 0.2 V, solid electrolyte: Nafion®

film prepared by casting 5 µl 5 wt.% Nafion® solution, gas flow rate = 200 ml.min^{-1}, relative humidity = 100% [25]

Table 2.2: Summary of hydrogen sensors based on PANI composites.

Sensor	Concentration	Response time (s)	Recovery time (s)	Sensitivity	Refs.
PANI/WO_3	0.06 -1%,	40	100	-	[40]
PANI (emeraldine)/ anatase titanium dioxide (TiO_2)	0.8%	83	130	1.63%	[40]
Aluminum/ Tin oxide (Al-SnO_2) /PANI	1000 ppm	2	2	275%	[40]
Graphene/PANI	0.06-1%	-	-	16.57%	[38]

2.4. CURRENT CHALLENGES AND FUTURE PROSPECTS

Even though PANI composites have made an excessive progress as hydrogen sensors, there are still some challenges facing them regarding their wide acceptance in sensing technology. According to the US DOE a material must have a short response time (1 s) and operational temperature between -30 to 80 °C for it to gain wide acceptance as a hydrogen sensor [13]. Nonetheless, to the best of our knowledge there is no existing hydrogen sensing technology which has met the US DoE requirements and ideal for all applications. From literature, there are many reports on PANI composites for hydrogen gas sensing applications. However, PANI composites based sensors suffer from longer response time and poor sensitivity as

compared to metal oxides [36]. Much work is currently underway to address these issues with some areas already showing signs of success, and the number of publications for these composites is expected to increase in the near future. One of the available methods to overcome the above-mentioned challenges is by development of PANI composites for electrochemical hydrogen gas sensing. Electrochemical gas sensors are known to be good at sensing low concentrations (ppm level) of hydrogen gas within a short response time and do not require heating. However, reports on PANI composites for hydrogen gas detection at room temperature are still scarce and their sensing mechanisms are not well understood.. In another report, Do *et al*. [25] designed an amperometric hydrogen gas sensor (10- 10,000 ppm H_2) based on a multi-components Nafion®(5.7 µm)/Pt/nsPANI/Au/Al_2O_3 sensing electrode with a Pt loading of 1.87 mg and obtained response time and specific sensitivity of 100-250 s and 338.50 mA ppm^{-1} g^{-1}, respectively. On the other hand, organic–inorganic hybrid materiasl continues to be an exciting area of research in the past due to their flexibility in different applications [18]. Furthermore, organic-inorganic hybrids exhibit both properties of the organic part and the inorganic part. For example, PANI-graphene oxide composite and also carbon nanotubes nanocomposite have been reported to exhibits excellent electrical, mechanical and optical properties such as surface hardness, modulus, strength, transparency and high refractive index and used for gas sensing [18]. Yet, composites between PANI with inorganic porous materials such as metal organic frameworks have not been studied well for electrochemical hydrogen gas sensing application. Wu and the co- authors [49] designed a hydrogen gas sensor based on zinc oxide@zeolitic imidazolate framework-8 (ZnO@ZIF-8) core–Shell nanorod film. It was observed that the introduction of ZIF-8 to form a composite introduced more oxygen vacancies in the complex film, thus improving the sensitivity of ZnO@ZIF-8 towards hydrogen as compared with the raw ZnO nanorod film. Moreover, the sensor was more porous and selective towards hydrogen than carbon monoxide upon incorporating ZIF-8 [49]. Very recently, Yuan and Liu developed an electrochemical sensor based on Nafion/PANI/(ZIF-8) nanocomposite for the determination of dopamine. The sensor exhibited the limit of detection of about 1.2×10^{-8} mol. L^{-1} [50]. It also showed good

selectivity, outstanding stability and high reproducibility wherein ZIF-8 provided larger surface area and electrocatalytic activity while PANI provided the electrical conductivity [50]. In the same manner, herein, we present for the first time that PANI based ZIF is a promising electrochemical hydrogen gas sensor at a low operating temperature.

2.5. CONCLUSIONS

Hydrogen sensors play a vital role for safety monitoring and for hydrogen to gain wide acceptance as a fuel. In addition, they are important during hydrogen production, transportation and utilisation. Briefly, this comprehensive review focused on the basic principles, advantages and limitations of different types of hydrogen gas sensors. The electrochemical based hydrogen gas sensors induced by PANI composites were the core of interest and their distinctive parameters such as response time, selectivity, stability and sensitivity were reviewed. This conducting polymer matrix has advantages over metals and semiconductors owing to its ease of synthesis, low fabrication cost and room temperature operation. Nevertheless, it possesses low sensitivity to hydrogen gas as compared to metals and metal oxides. Moreover, its poor processibility due to it being insoluble in many organic solvents limits its application in electrochemical gas sensing. PANI based composite electrochemical sensors have been found to possess enhanced sensitivity and short response time as compared to neat polymer. However, previous reports have not yet satisfied the US DOE requirements, thus more work has to be done on electrochemical hydrogen sensing induced by these composites. Therefore, there is still plethora of work on electrochemical sensing performance of based on polyaniline composites focusing on other gases. Unfortunately, only a few reports exist on hydrogen gas sensing via electrochemical route. This poses a serious challenge in the science community and numerous electrochemical hydrogen sensors induced by PANI composites are therefore expected to increase in the near future. To the best of our knowledge, there are no attempts made for studying how this conducting PANI

interact with ZIFs for electrochemical hydrogen gas sensing. Based on this information, this has motivated our study to focus on PANI doped with different types of zeolitic imidazolate framework materials as promising candidates for electrochemical hydrogen gas sensing.

2.6. REFERENCES

[1] G. R. Monama, S. B. Mdluli, G. Mashao, M. D. Makhafola Mdluli, K.E. Ramohlola, K.M. Molapo, M.J. Hato, K. Makgopa, E.I. Iwuoha, and K.D. Modibane, “Palladium deposition on copper(II) phthalocyanine/metal organic framework composite and electrocatalytic activity of the modified electrode towards the hydrogen evolution reaction,” *Renew. Energy*, vol. 119, pp. 62–72, 2018.

[2] C. Koroneos, A. Dompros, G. Roumbas, and N. Moussiopoulos, “Life cycle assessment of hydrogen fuel production processes,” *Int. J. Hydrogen Energy,* vol. 29, pp. 1443–1450, 2004.

[3] K. E. Ramohlola, G. R. Monana, M. J. Hato, K. D. Modibane, K. M. Molapo, M. Masikini, S. B. Mduli, and E. I. Iwuoha, Polyaniline-metal organic framework nanocomposite as an efficient electrocatalyst for hydrogen evolution reaction” *Compos. B: Eng.*, vol. 137, pp. 129–139, 2018

[4] N. L. Panwar, S. C. Kaushik, and S. Kothari, “Role of renewable energy sources in environmental protection : A review,” *Renew. Sustain. Energy Rev.*, vol. 15, pp. 1513–1524, 2011.

[5] M. C. Santos, L. S. Parreira, F. D. M. Souza, J. C. Junior, and T. Gentil, “Fuel Cells : Hydrogen and Ethanol Technologies,” *Reference Module Mater. Sci. Mater. Eng.*, doi:10.1016/B978-0-12-803581-8.09263-8.

[6] K. E. Ramohlola, M. Masikini, S. B. Mdluli, G. R. Monama, M. J. Hato, K. M. Molapo, E. I. Iwuoha, K. D. Modibane “Electrocatalytic Hydrogen Production Properties of Poly(3- aminobenzoic acid) doped with metal organic frameworks,” *Int. J. Electrochem. Sci.*, vol. 12, pp. 4392–4405, 2017.

[7] J. Villatoro, D. Luna-moreno, and D. Monzon-Hernandez, “Optical fiber hydrogen sensor for concentrations below the lower explosive limit,” *Sens. Actuators B*, vol. 110, pp. 23–27, 2005.

[8] G. Korotcenkov, S. Do Han, J. R. Stetter, P. H. Sensors, and C. Sensors, “Review of electrochemical hydrogen sensors,” *Chem. Rev.*, vol. 109, pp. 1402–1433, 2009.

[9] D. B. Myers, G. D. Ariff, B. D. James, J. S. Lettow, C. E. S. Thomas, and R. C. Kuhn, “Cost and performance comparison of stationary hydrogen fueling appliances,” *Proc. 2002 US. DOE Hydrogen Program Rev.*, NREL/CP-610-32405.

[10] S. Phanichphant, “Semiconductor metal oxides as hydrogen gas sensors,” *Procedia Eng.*, vol. 87, pp. 795–802, 2014.

[11] V. E. Bochenkov and G. B. Sergeev, Metal oxide nanostructures and their applications, (Eds.) A. Umar, and Y-B. Hahn, “Sensitivity, selectivity and stability of gas-sensitive metal-oxide nanostructures,” American Scientific Publishers, vol. 3, pp. 31–52, 2010.

[12] P. Soundarrajan, and F. Schweighardt, "Hydrogen Sensing and Detection", *Hydrogen Fuel: Production, Transport, and Storage*, Taylor and Francis Group, LLC, doi:10.1201/9781420045772.ch15.

[13] W. J. Buttner, M. B. Post, R. Burgess, and C. Rivkin, “An overview of hydrogen safety sensors and requirements,” *Int. J. Hydrogen Energy*, vol. 36, pp. 2462–2470, 2011.

[14] P. Soundarrajan and F. Schweighardt, *Hydrogen Sensing and Detection*, *Hydrog Fuel Prod Transp Storag*, vol.13, pp. 495-500, 2016

[15] I. Simon, N. Barsan, M. Bauer, U. Weimar, “Micromachined metal oxide gas sensors : opportunities to improve sensor performance,” *Sens. Actuators B*, vol. 73, pp. 1-26, 2001.

[16] B. Wei, M. Hsu, P. Su, H. Lin, R. Wu, and H. Lai, “A novel SnO_2 gas sensor doped with carbon nanotubes operating at room temperature,” *Sens Actuators* vol. 101, pp. 81–89, 2004.

[17] H. Kim and J. Lee, "Chemical Highly sensitive and selective gas sensors using p-type oxide semiconductors : Overview,” *Sens Actuators B. Chem.*, vol. 192, pp. 607–627, 2014.

[18] J. M. Chem, “Ammonia gas sensing,” *Sens Actuators B,* vol. 223 pp. 22488–22495, 2012.

[19] A. Z. Sadek, W. Wlodarski, K. Kalantar-Zadeh, C. Baker, and R. B. Kaner, “Doped and dedoped polyaniline nanofiber based conductometric hydrogen

gas sensors," *Sens. Actuators A,* vol. 139, pp. 53–57, 2007.

[20] . Liu X. "A survey on gas sensing Technology". *Sensors (Basel)*, vol. 12, pp. 9635–9665, 2012.

[21] S. Boulter, "Sensor selection - getting it right for flammable gases."Crowcon Detection Instruments.

[22] J. Noh, J. M. Lee, and W. Lee, "Low-dimensional palladium nanostructures for fast and reliable hydrogen gas detection," *Sensors,* vol. 11, pp. 825–851, 2011.

[23] S. Lata, B. Batra, N. Karwasra, and C. S. Pundir, "An amperometric H_2O_2 biosensor based on cytochrome c immobilized onto nickel oxide nanoparticles / carboxylated multiwalled carbon nanotubes/polyaniline modified gold electrode," *Process Biochem.*, vol. 47, pp. 992–998, 2012.

[24] T. Kokulnathan, T. S. K. Sharma, S. M. Chen, T. W. Chen, and B. Dinesh, "Ex-situ decoration of graphene oxide with palladium nanoparticles for the highly sensitive and selective electrochemical determination of chloramphenicol in food and biological samples," *J. Taiwan Inst. Chem. Eng.*, vol. 89, pp. 26-38, 2018.

[25] J. Do, Y. Chen, and M. Tsai, "Planar solid-state amperometric hydrogen gas sensor based on Nafion ®/Pt/nano-structured polyaniline/Au/Al_2 O_3 electrode," *Int. J. Hydrogen Energy*, vol. 43, pp. 14848–14858, 2018.

[26] V. Mani, R. Devasenathipathy, S. M. Chen, S. T. Huang, and V. S. Vasantha, "Immobilization of glucose oxidase on graphene and cobalt phthalocyanine composite and its application for the determination of glucose," *Enzyme Microb. Technol.*, vol. 66, pp. 60–66, 2014.

[27] Q. Yi, A. Chen, W. Huang, J. Zhang, X. Liu, G. Xu, and Z. Zhou "Titanium-supported nanoporous bimetallic Pt-Ir electrocatalysts for formic acid oxidation," *Electrochem. Commun.*, vol. 9, pp. 1513–1518, 2007.

[28] A. Ramanavicius, A. Ramanaviciene, and A. Malinauskas, "Electrochemical sensors based on conducting polymer—polypyrrole," *Electrochim Acta.,* vol. 51, pp. 6025–6037, 2006.

[29] S. Kempahanumakkagari, K. Vellingiri, A. Deep, E. E. Kwon, N. Bolan, and K.

Kim, “Metal–organic framework composites as electrocatalysts for electrochemical sensing applications,” *Coord. Chem. Rev.*, vol. 357, pp. 105–129, 2018.

[30] E. Sezer, “The new frontiers of organic and composite nanotechnology”, (Eds.) V. Erokhin, M. Ram, and O. Yavuz, *Conducting nanocomposite systems*, Elsevier Science, doi.org/10.1016/B978-0-08-045052-0.x5001-5.

[31] M. K. Ram, O. Yavuz, V. Lahsangah, and M. Aldissi, “CO gas sensing from ultrathin nano-composite conducting polymer film,” *Sens. Actuators B. Chem.* vol. 106, pp. 750–757, 2005.

[32] J. Qi, X. Xinxin, X. Liu, and K. Tong, “Chemical fabrication of textile based conductometric polyaniline gas sensor,” *Sens. Actuators B. Chem*., vol. 202, pp. 732–740, 2014.

[33] I. Fratoddi, I. Venditti, C. Cametti, and M. Vittoria, “Chemical Chemiresistive polyaniline-based gas sensors : A mini review,” *Sensors Actuators B. Chem.*, vol. 220, pp. 534–548, 2015.

[34] R. Arsat, X. F. Yu, Y. X. Li, W. Wlodarski, and K. Kalantar-zadeh, “Chemical Hydrogen gas sensor based on highly ordered polyaniline nanofibers,” *Sensors Actuators B. Chem*., vol. 137, pp. 529–532, 2009.

[35] S. Srivastava, S. S. Sharma, S. Kumar, S. Agrawal, M. Singh, and Y. K. Vijay, “Characterization of gas sensing behavior of multi walled carbon nanotube polyaniline composite films,” *Int. J. Hydrogen Energy*, vol. 34, pp. 8444–8450, 2009.

[36] E. Song and J. Choi, “Conducting polyaniline nanowire and its applications in chemiresistive sensing,” *Nanometerials*, vol. 3, pp. 498–523, 2013.

[37] K. E. Ramohlola, G. R. Monana, M. J. Hato, K. D. Modibane, K. M. Molapo, M. Masikini, S. B. Mduli, E. I. Iwuoha, “Polyaniline-metal organic framework nanocomposite as an efficient electrocatalyst for hydrogen evolution reaction,” *Compos. Part B Eng.*, vol. 137, pp. 129–139, 2018.

[38] L. Al-Mashat, K. Shin, K. Kalantar-zadeh, J. D. Plessis, S. H. Han, R. W. Kojima, R. B. Kaner, D. Lin, X. Gou, S. J. Ippolito, and W. Wlodarski, “Graphene/polyaniline nanocomposite for hydrogen sensing,” *J. Phys. Chem.*

C, vol.114, pp. 16168–16173, 2010.

[39] X. B. Yan, Z. J. Han, Y. Yang, and B. K. Tay, "NO_2 gas sensing with polyaniline nanofibers synthesized by a facile aqueous/organic interfacial polymerization," *Nanometerial*, vol. 123, pp. 107–113, 2007.

[40] S. Pandey, "Highly sensitive and selective chemiresistor gas/vapor sensors based on polyaniline nanocomposite : A comprehensive review," *J. Sci. Adv. Mater. Devices*, vol. 1, pp. 431–453, 2016.

[41] T. Sen, N. G. Shimpi, S. Mishra, and R. Sharma, "Polyaniline/γ-Fe_2O_3 nanocomposite for room temperature LPG sensing," *Sensors Actuators B. Chem.*, vol. 190, pp. 120–126, 2014.

[42] A. Mekki, N. Joshi, A. Singh, Z. Salmi, P. Jha, P. Decorse, S. Lau-Truong, R. Mahmoud, M. M. Chehimi, D. K. Aswal, and S. K. Gupta, "H_2S sensing using in situ photo-polymerized polyaniline–silver nanocomposite films on flexible substrates," *Org. Electron.*, vol. 15, pp. 71–81, 2014.

[43] H. Tai, Y. Jiang, G. Xie, J. Yu, X. Chen, and Z. Ying, "Influence of polymerization temperature on NH_3 response of PANI/TiO_2 thin film gas sensor," *Sens. Actuators B Chem.,* vol. 129, pp. 319–326, 2008.

[44] L. Geng, Y. Zhao, X. Huang, S. Wang, S. Zhang, and S. Wu, "Characterization and gas sensitivity study of polyaniline/SnO_2 hybrid material prepared by hydrothermal route," *Sens. Actuators B Chem.*, vol. 120, pp. 568–572, 2007.

[45] G. D. Khuspe, S. T. Navale, M. A. Chougule, and V. B. Patil, "Ammonia gas sensing properties of CSA doped PANi-SnO_2 nanohybrid thin films," *Synth. Met.*, vol. 185, pp. 1–8, 2013.

[46] B. A. Bhanvase, N. S. Darda, N. C. Veerkar, A. S. Shende, S. R. Satpute, and S. H. Sonawane, "Ultrasound assisted synthesis of PANI/$ZnMoO_4$ nanocomposite for simultaneous improvement in anticorrosion , physico-chemical properties and its application in gas sensing," *Ultrason. - Sonochemistry*, vol. 24, pp. 87–97, 2015.

[47] W. Zheng, L. Hu, L. Yoon, S. Lee, and K. Wong, "Copper nanoparticles/polyaniline/graphene composite as a highly sensitive electrochemical glucose sensor," *J. Electrochem. Chem.*, vol. 781, pp. 155-

160, 2016.

[48] O. Tovide, “Electro-oxidation of anthracene on polyanilino-graphene composite electrode,” *Sensors Actuators B Chem.*, vol. 205, pp. 184–192, 2014.

[49] X. Wu, S. Xiong, Z. Mao, S. Hu, and X. Long, “A designed ZnO@ZIF-8 core–shell nanorod film as a gas sensor with excellent selectivity for H_2 over CO,” *Chem. Eur. J.*, vol. 23, pp. 7969–7975, 2017.

[50] J. Qian, F. Sun, and L. Qin, “Hydrothermal synthesis of zeolitic imidazolate framework-67 (ZIF-67) nanocrystals,” *Mater. Lett.*, vol. 82, pp. 220–223, 2012.

CHAPTER THREE

CHARACTERISATION TECHNIQUES

3.1. INTRODUCTION

The aim of this chapter is to give a comprehensive review on characterisation techniques, their general description, basic principles, advantages and limitations. Characterisation techniques are set of methods used to characterise the structural, physical, chemical, electrochemical and morphological nature of a material [1]. They can also be used for quantitative analysis of certain species in a material. They are used to identify and isolate components of a sample. Many characterisation techniques have been practiced for centuries and new ones are constantly emerging [1-3]. The emergence of electron microscopy and secondary ion mass spectroscopy in the 20^{th} centuries have made it easy to analyse structures and composition of materials thus making it possible to understand why different materials exhibit different behaviour and properties [1]. Characterisation techniques can be divided into different categories including physical, spectroscopy, microscopy, and electroanalytical techniques. Common examples of microscopy instruments include optical microscope, scanning electron microscope, transmission electron microscope and atomic force microscope [2]. Spectroscopic techniques such as Ultraviolet- visible (UV-vis) spectroscopy, photoluminescence (PL) and FTIR are used to reveal the chemical composition, and photoelectric properties [1-3]. In this work, the following analytical techniques were employed for characterisation and electrochemical hydrogen sensing studies of the parent materials (PANI and ZIFs) and PANI-ZIF composites.

3.2. PHYSICAL METHODS

Physical methods are characterisation techniques employed for determining the structural properties such as crystallinity, surface area, mechanical and thermal stability of the materials. Those methods include X-ray diffraction (XRD) and simultaneous thermal analysis (STA) in this study.

3.2.1. X-ray diffraction (XRD)

XRD is a rapid, non-destructive analytical tool used for phase identification of crystalline materials and can also supply information on unit cell dimensions [4]. Moreover, it is used to measure the average spacing between layers or rows of atoms, determines the orientation, size, shape and internal stress of a single crystal or grain, and determines the crystal structure of an unknown material such as minerals and inorganic compounds [5]. It is based on constructive interference of monochromatic X-rays and a crystalline sample of which interaction of the incident rays with the sample induces constructive interference and Bragg's law has to be satisfied. This law is mathematical expressed in Equation 3.1 as follows [6].

$$n\lambda = 2d\sin\theta \qquad (3.1)$$

Wherein n is an integer usually equal to 1, λ is the wavelength of the radiation beam, d is the interplanar spacing between two diffracting lines and θ is the diffraction angle [7]. Conversion of the diffraction peaks to d-spacing allows identification of material because each material has a set of unique d-spacing. This is achieved by comparison of d-spacing with standard reference patterns. In this work, it was used to identify the phases of the synthesised materials (PANI, ZIF and PANI-ZIFs) and d- spacing. In addition, it was used to monitor the composite formation by using the

obtained *d*-spacing values and the crystallite sizes. The crystallite sizes were determined by using Debye Scherrer's equation (Equation 3.2) [8].

$$D=\frac{k\lambda}{\beta\, cos\theta} \tag{3.2}$$

where, k = 0.9, λ is the CuK_{α} radiation wavelength (1.5406 Å), β is the full-width at half maximum in radians, θ is the Bragg's angle [8]. Zheng *et al.* [9] reported typical XRD diffraction peaks of PANI (Figure 3.1b) which exhibited a broad peak at around 2θ = 20° corresponding to (110) reflection as an indicative of ordered structure. On the other hand, Li *et al.* [10] showed that the XRD pattern of ZIF-7 is composed of pure ZIF-7 and free of ZnO as an impurity phase and there is no preferential orientation for this material as given in Figure 3.2(a).

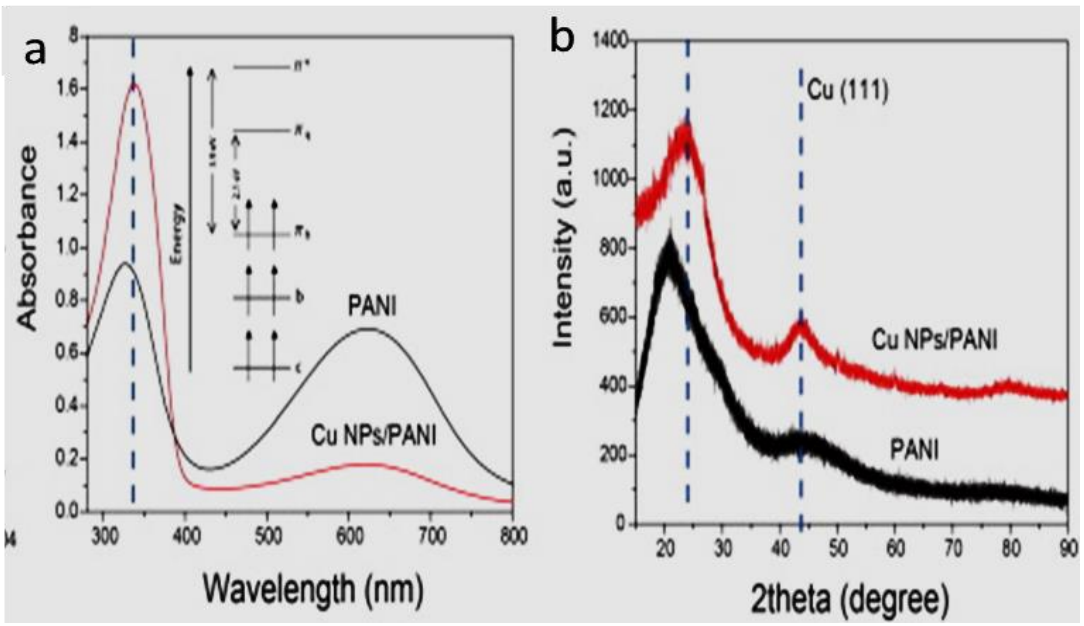

Figure 3.1: (a) UV–vis spectra of PANI and CuNPs/PANI (discussed in the spectroscopy section), insert is the schematic energy level diagram of PANI; (b) XRD pattern of PANI and CuNPs/PANI [9].

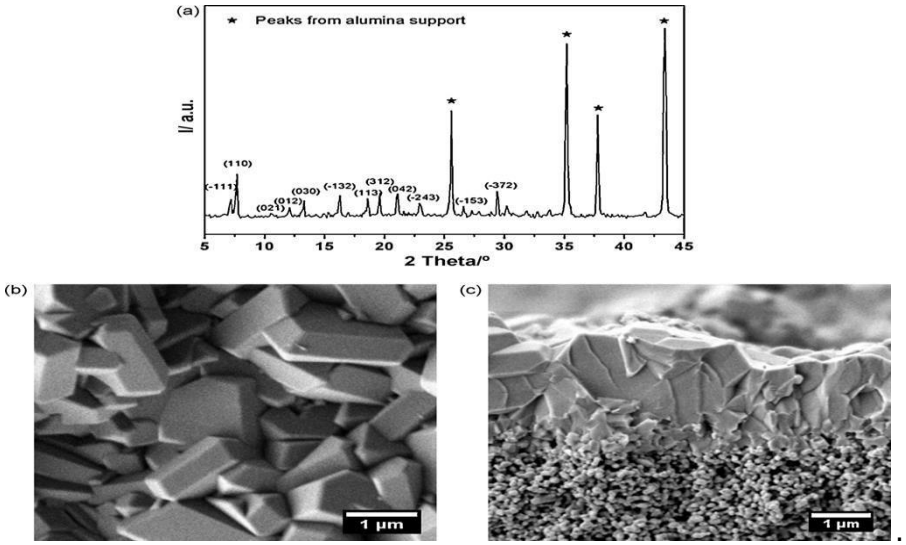

Figure 3.2: (a) XRD pattern, (b) SEM Top view, and (c) SEM cross-sectional view of the ZIF-7 membrane (discussed in the spectroscopy section) [10].

3.2.2. Simultaneous thermal analysis (STA)

STA comprises of simultaneous themogravimetric analysis (TGA) and differential scanning calorimmetry (DSC) techniques. TGA is a type of thermal analysis in which physical and chemical changes of materials as a function of increasing temperature are measured. One heating source is used and the heating rate must remain constant. It gives information about thermal processes such as vaporisation, sublimation, and adsorption and desorption. Information about chemical phenomenon such as dessolvation and chemisorption is revealed [11]. During TGA analysis, either mass loss or gain is observed upon decomposition. In the case of DSC, the technique measures the difference in the amount of heat needed to increase the temperature of a sample as function of temperature. Throughout the experiment, the sample and reference samples are maintained at the same temperature and the sample holder temperature increases linearly as a function of time [11]. It is a fast, simple thermal analysis method used for quantitative analysis. Generally, if a material is thermally stable, no change in mass will be observed [12].

STA does not require a series of standards for calculation of an unknown and instrumental errors are limited but it is only for single elemental analysis [13]. In the present work, STA was used to check the thermal stability of the synthesised material (PANI, ZIF and PANI-ZIF composites) achieved by checking the degradation steps (weight loss) which appears when samples are heated from 25 to 525 °C. The thermal analysis was investigated using STA (Perkin-Elmer 6000) and samples ranging from 1 - 4 mg were heated and scanned at the speed of 20 °C/min under inert environment. STA was used to monitor changes phase transitions (heat flow rate) as temperature increases. Bhanvase *et al.* [14] gave a report on a typical TGA of PANI (Figure 3.3) and showed that the TGA curve of PANI synthesised by ultrasound assisted emulsion polymerisation shows three stage thermal degradation steps. The first thermal degradation step of PANI staged around 39% up to 250 °C was ascribed to the removal of water molecules. The second weight loss around 33% in a temperature range of 250 – 400 °C might be owed to the phase transition occurred in PANI.

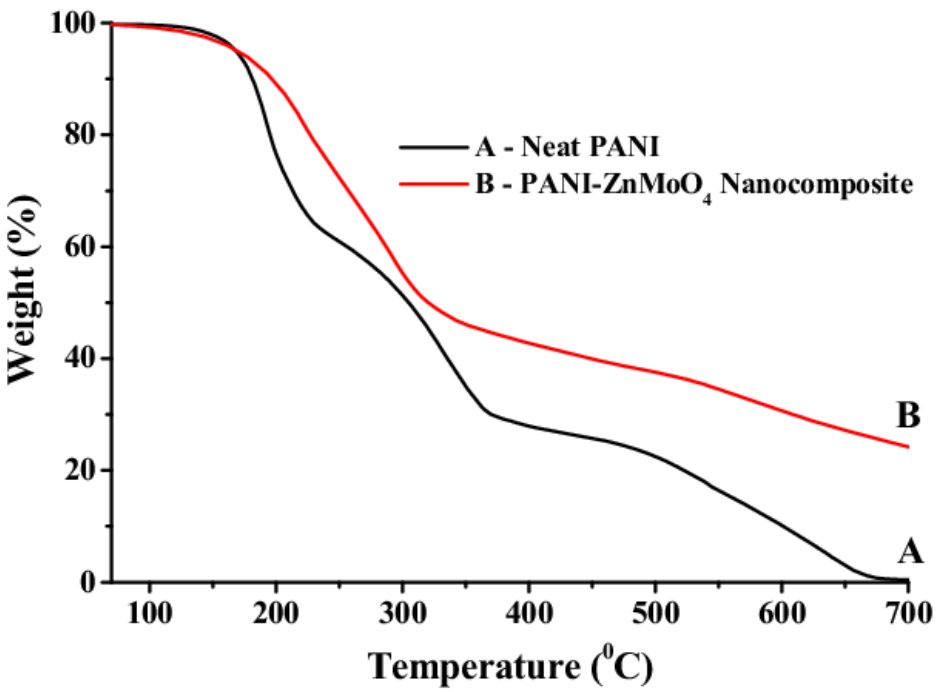

Figure 3.3: TGA plot of (A) of neat PANI and (B) PANI/ZM nanocomposite [14].

In another report, Zakzeski *et al.* [15] explained that the TGA plot of ZIF (Figure 3.4) displayed four weight loss steps between 320 and 880 K. The first weight loss of 14.6% at around 400 K corresponds to the removal of a portion of the DMF and H_2O contained in the framework Co-ZIF-9. The second degradation steps of about 22.3% between 560 and 680 K along with two small weight-loss steps of 3% and 3.5% (680–880 K) were due to the decomposition of the ZIF framework. It was concluded that ZIF is stable under reaction conditions, but temperatures exceeding 560 K have a deleterious effect on the framework resulting in its decomposition.

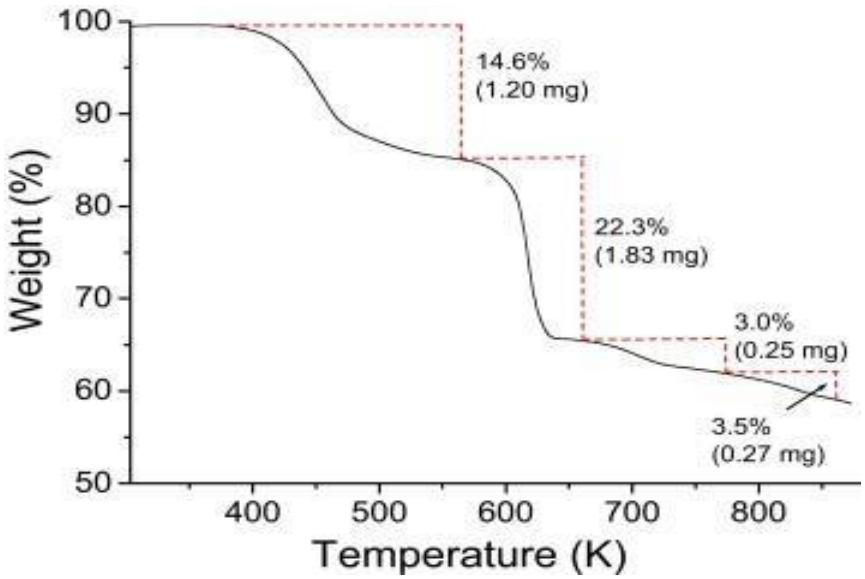

Figure 3.4: Thermal gravimetrical analysis of Co-ZIF-9 [15].

3.3. SPECTROSCOPY

Spectroscopy is the field of science which uses spectroscope in order to study the interaction between electromagnetic radiation and matter, thus giving rise to UV electronic excitations or IR molecular vibrations (IR).

3.3.1. Fourier transform infrared spectroscopy (FTIR)

FTIR is a technique based on the vibrations of the atoms of a molecule. It is used to obtain absorption or emission infrared spectrum of a solid, liquid or a gas [16]. It is used for structure identification using functional groups present which give rise to characteristics bands in terms of intensity and position [17]. The energy at which any peak in an absorption spectrum appears corresponds to the frequency of a vibration of a part of a sample molecule. This technique was used in this study to determine functional groups present [18-19] in ZIF, and polyaniline and to check whether they are consistent with previous reports qualitative analysis. It was also used to check changes on PANI spectra upon loading 3.6 wt% of ZIF.

Ramohlola *et al.* [20] gave a report on FTIR spectroscopy of PANI as depicted in Figure 3.5(a). The FTIR showed peaks at around 806, 1138, 1493, 1575 and between 2500 and 3500 cm^{-1} relating to C-H out of plane deformation bending of the benzene ring, $–NH^{+}$= vibration mode, C=N stretching vibration, C=C stretching vibration and = N-H stretching vibration, respectively. Figure 3.6 shows FTIR basic components and explains how the analysis can be performed.

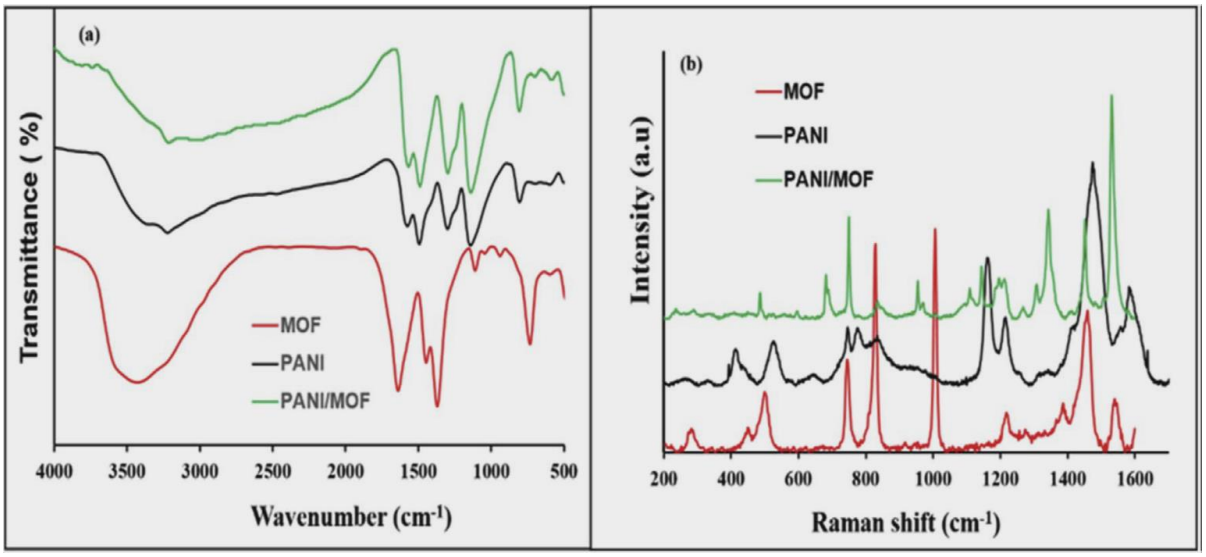

Figure 3.5: (a) FTIR and (b) Raman spectra of MOF, PANI and PANI/MOF composite [20].

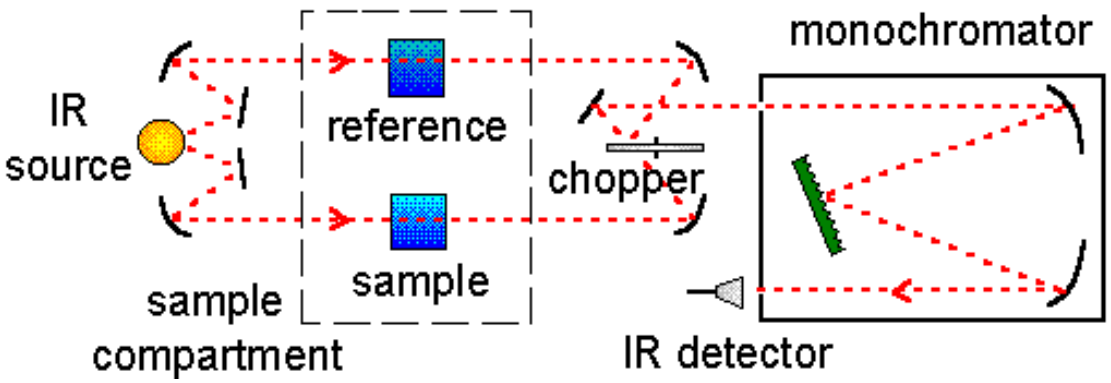

Figure 3.6: Basic components of FTIR [16].

The FTIR of ZIF (ZIF-9) was reported by Lien *et al*. [21] as presented in Figure 3.7 and shows that the ZIF-9 revealed a significant difference as compared to that of benzimidazole linker. FT-IR spectra of benzimidazole, showed a strong and broad band at the range from 3400 to 2200 cm^{-1} with the maximum at approximately 2800 cm^{-1} indicating the presence of the N–H bond. The important feature observed

for the FT-IR spectra of the ZIF-9 as compared to those of benzimidazole was the disappearance of this absorption band, proving that the benzimidazole linkers were entirely deprotonated upon ZIF-9 formation.

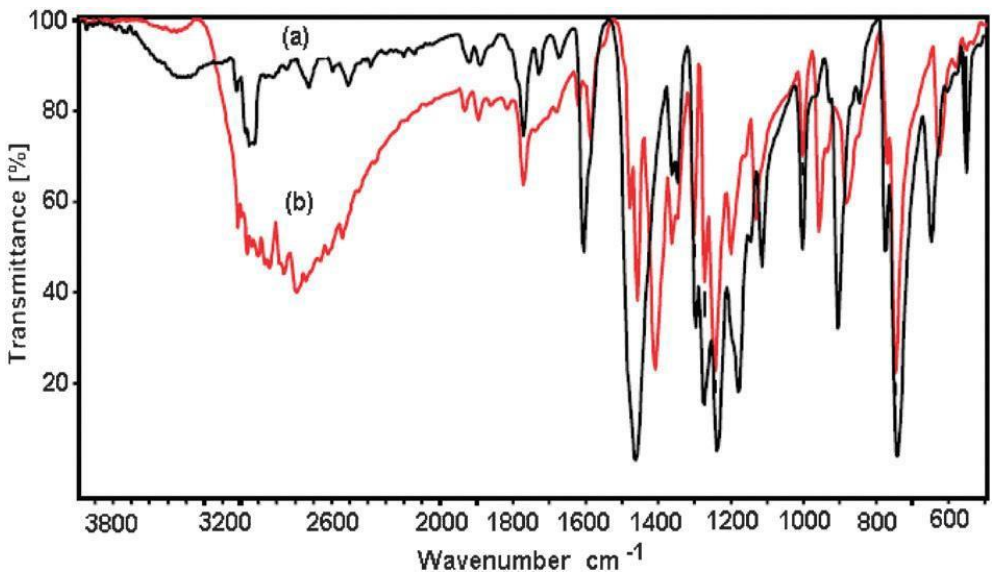

Figure 3.7: FTIR spectra of (a) ZIF-9 and (b) benzimidazole [21].

3.3.2. Ultraviolet-visible (UV-Vis) spectroscopy

UV-vis spectroscopy is the absorption spectroscopy that uses light in the visible and near infrared region to study the electronic transitions that molecules undergo when they are exposed to light [22-23]. When molecules are exposed to light the π electrons or non-bonding electrons absorb the energy in the form of ultraviolet or visible light and get promoted from ground state to higher energy state as summarised in Figure 3.8 [22,24].

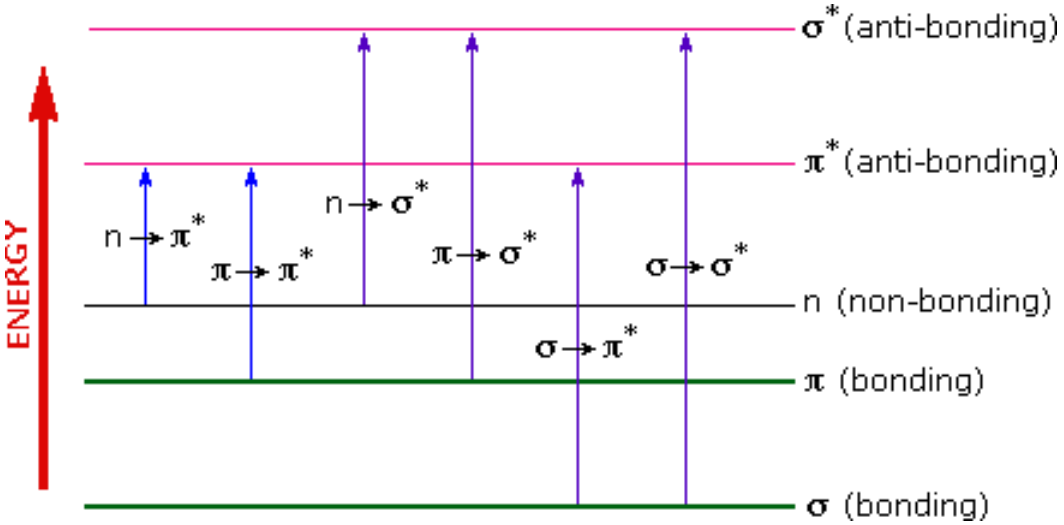

Figure 3.8: Possible electronic transitions of π and n electrons [19]

The relationship between the energy of the ultra-violet radiation absorbed and the energy difference between the ground state and the excited energy state is given by the Equation 3.3 [25];

$$E = hv \tag{3.3}$$

in which, *E* is the energy, *h* is the Planck constant and *v* is the frequency. Different molecules absorb light at different wavelengths, *λ*, so energy and wavelength are related using Equation 3.4 [25].

$$E = \frac{hc}{\lambda} \tag{3.4}$$

where *c* is the speed of light of the molecule. The intensity of light absorbed by the molecule is called absorbance denoted by *A*, can be related to the transmittance of light by the equation [25].

$$A = -logT \tag{3.5}$$

In this work UV was used to check the relationship between absorbance and concentration governed by Beer Lambert ‘s law given by Equation 3.6 [25].

$$\mathrm{A} = abc \tag{3.6}$$

where A is the absorbance, a is the absorptivity constant, b is the path length of a cell and c is the concentration of the analyte [25]. Since the concentration of the analyte is commonly measured in molarity, M (moles per litre), the Beer's law was rearranged to determine the molar absorptivity (ε) of polyaniline and the composite. The expression can be written as shown in Equation 3.7 [25].

$$\varepsilon = abc \tag{3.7}$$

The molar absorptivity of the material can be used to determine the conductivity of the materials. Furthermore, in this communication, the UV-vis spectroscopy was used to monitor composite formation by examining the optical properties, red shift blue shift and also band gab of the composite as compared to PANI. Zheng *et al.* [9] also gave a report on a typical UV-vis spectrum of PANI (Figure 3.1a) where the spectrum of the polymer matrix showed two peaks at about 334 and 653 nm attributed to the π − π* and πb (benzenoid) – πq (quinoid) electron transfers, respectively. They further showed that when they embedded CuNPs in PANI to form CuNPs/PANI composite, both peaks were red-shifted, indicating that CuNPs have lifted the πb energy level. Such energy level change is ascribed to the electron transfer from CuNPs to PANI that would lead to the changes in peak intensity. Zakzeski *et al.* [15] evaluated the catalytic oxidation of aromatic oxygenates by the heterogeneous catalyst Co-ZIF-9 and they included a typical UV-vis spectrum of ZIF in that communication as displayed in Figure 3.9.

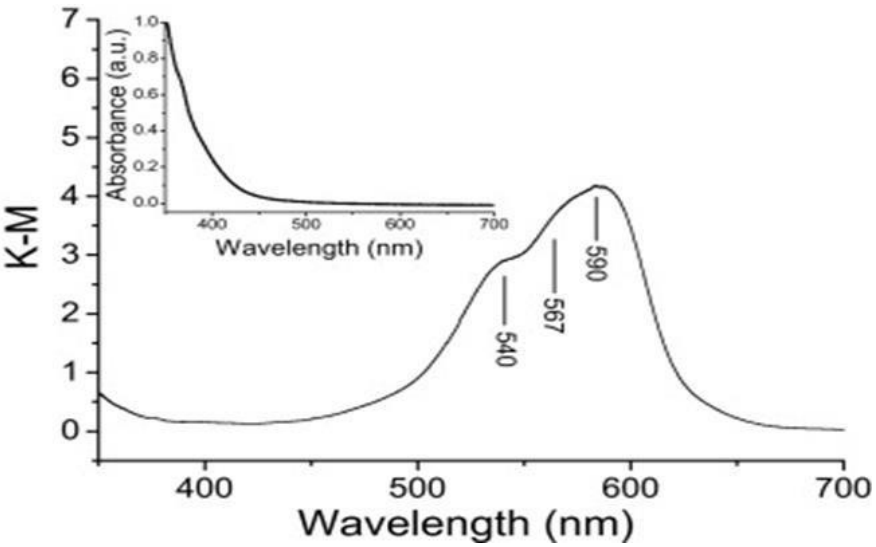

Figure 3.9: UV–vis diffuse reflectance spectrum of Co-ZIF-9 sample and UV–vis of reaction solution after 12 h at 423K following hot filtration (inset) [15].

3.3.3. Raman spectroscopy

Raman spectroscopy is a spectroscopic technique used to observe vibrational, rotational, and other low-frequency modes in a system which mostly appears in the fingerprint regions of FTIR. IR inactive molecules such as metal oxides vibrations can also be determined using this type of spectroscopy. It is mostly employed in chemistry to provide a fingerprint by which molecules can be identified [22]. This technique offers several advantages for microscopic analysis. Since, it is a scattering technique, specimens do not need to be fixed and that its spectra can be collected from a very small volume. However, it faces difficulties when separating the weak inelastic scattered light from the intense Rayleigh scattered laser light. It is most applicable in chemistry since vibrational information is specific to the chemical bonds and symmetry of molecules [22]. In this study it was used to determine vibrations corresponding to polyaniline and zeolitic imidazolate frameworks in the composite. Ramohlola *et al.* [20] also gave a report on Raman spectroscopy of polyaniline as depicted in Figure 3.5b. The Raman spectrum of PANI showed vibrations at

approximately 1197, 1220, 1500 and 1610 cm^{-1} corresponding to C-H in-plane bending vibration of benzenoid ring, C-N bonding modes of benzenoids ring, C=N stretching vibrations of unprotonated quinoid ring and C-C stretching of emeraldine salt, respectively.

Tanaka *et al.* [26] reported on adsorption and diffusion phenomena in crystal size engineered ZIF-8 MOF and showed that the Raman spectra of ZIF-8 is dominated by intense bands corresponding to methyl group and imidazole ring vibrations as shown in Figure 3.10. Furthermore, the band observed at 282 cm^{-1} was assigned to Zn−N stretching, while the bands observed at 685, 1146, and 1460 cm^{-1} were attributed to imidazolium ring puckering, C5−N stretching, and methyl bending, respectively. The Raman modes of all samples are all in the same position and intensity, indicating structural equality.

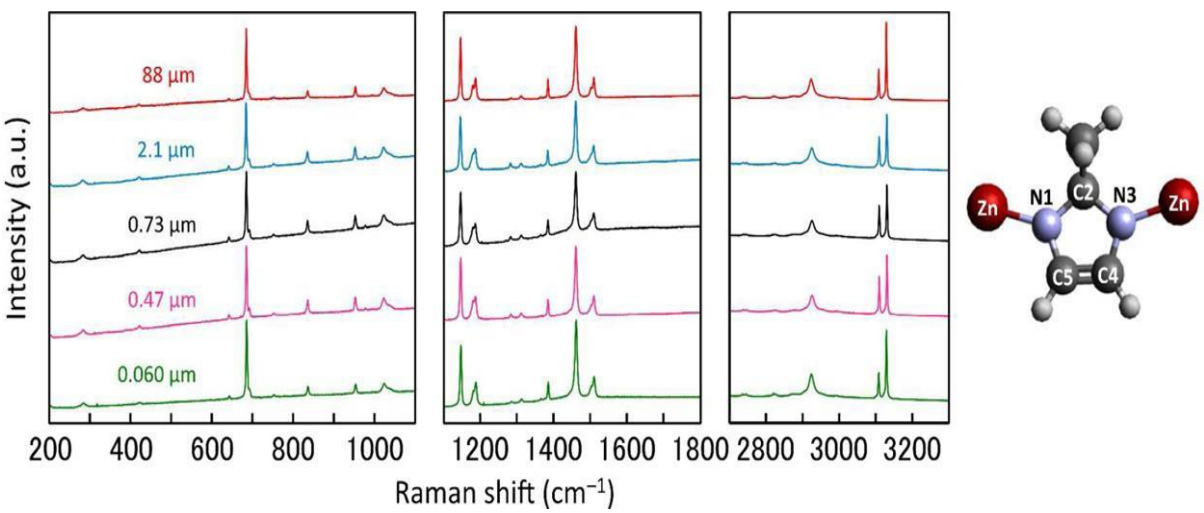

Figure 3.10: Raman spectra of the crystal-size-engineered ZIF-8 samples. Schematic illustration shows the atom nomenclature used for the imidazolium ring, where N is shown in purple, C in black, H in gray, and Zn in red [26].

3.4. MICROSCOPY

Microscopy involves techniques with different methods, which can be used to characterise objects which cannot be detected by simple spectroscopic techniques (UV-vis or IR) or naked eyes. Microscopy can be classified into optical microscopy (uses visible light to produce enlarged images), scanning probe microscopy (uses a probe to scan object) and electron microscopy (uses an electron beams to create an image of an object).

3.4.1. Scanning electron microscopy (SEM)

SEM is a great method which uses focused beam of electrons for high-resolution imaging of surfaces of the materials. It uses tungsten filament or field emission gun to create a beam of electrons [27]. The electron beam is accelerated through a high voltage (e.g. 20 kV) and pass through a system of apertures and electromagnetic lenses to produce a thin beam of electrons [28,29]. Electrons are emitted from the specimen by the action of the scanning beam and detector is used to collect them. In this work, the SEM was used to check morphology of the synthesised materials and confirm composite formation. Khuspe *et al.* [30] reported on ammonia gas sensing properties of camphor sulfonic acid (CSA) doped PANi-SnO_2 nanohybrid thin films and showed that PANI possesses fibrous morphology with high porosity as shown in Figure 3.11.

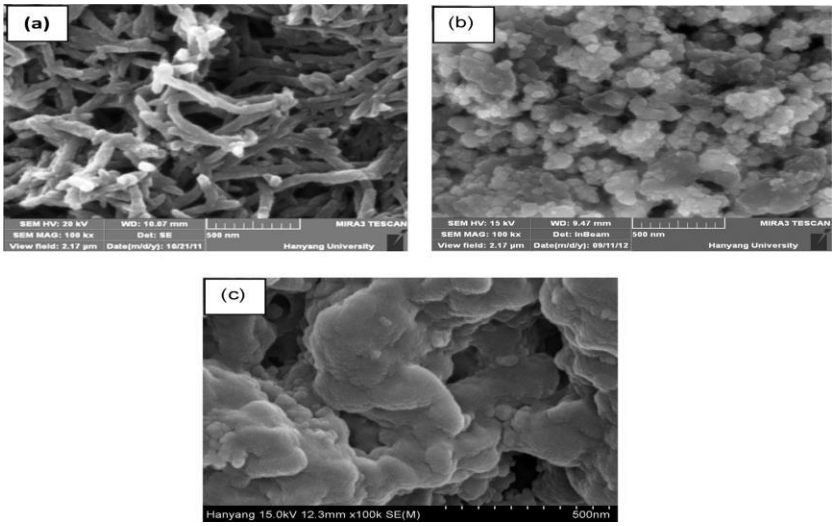

Figure 3.11: FE-SEM micrographs of (a) PANi, (b) PANi-SnO_2 (50%) and (c) 30% CSA doped PANi-SnO_2 nanohybrid [30].

On the other hand, the SEM results for ZIF were also reported by Li *et al.* [10] as depicted in Figure 3.11(b and c) and showed that the ZIF-7 layer consists of randomly oriented grains, which coincided with the XRD results shown in Figure 3.2(a).

3.4.2. Transmission electron microscopy (TEM)

TEM is a very powerful tool for material science. A high energy beam of electrons is shone through a very thin sample, and the interactions between the electrons and the atoms can be used to observe features such as the crystal structure and features in the structure like dislocations and grain boundaries [31]. Chemical analysis can also be performed. TEM can be used to study the growth of layers, their composition and defects in semiconductors. High resolution can be used to analyze the quality, shape, size and density of quantum wells, wires and dots. The TEM operates on the same basic principles as the light microscope but uses electrons instead of light.

Because the wavelength of electrons is much smaller than that of light, the optimal resolution attainable for TEM images is many orders of magnitude better than that from a light microscope [32]. Thus, TEMs can reveal the finest details of internal structure [33]. In this communication, it was used for internal characterisations of the synthesised materials, check the crystalinity and calculate the *d*-spacing and compare it with the one from XRD. Ramohlola *et al.* [20] also reported the TEM results of PANI (Figure 3.12(a)) coupled with SAED (inset) for crystallinity analysis and showed that it has nanofibers/tubular structures and a disordered (amorphous) structure, which indicated that the molecules are arranged to a certain definite position in the lattice.

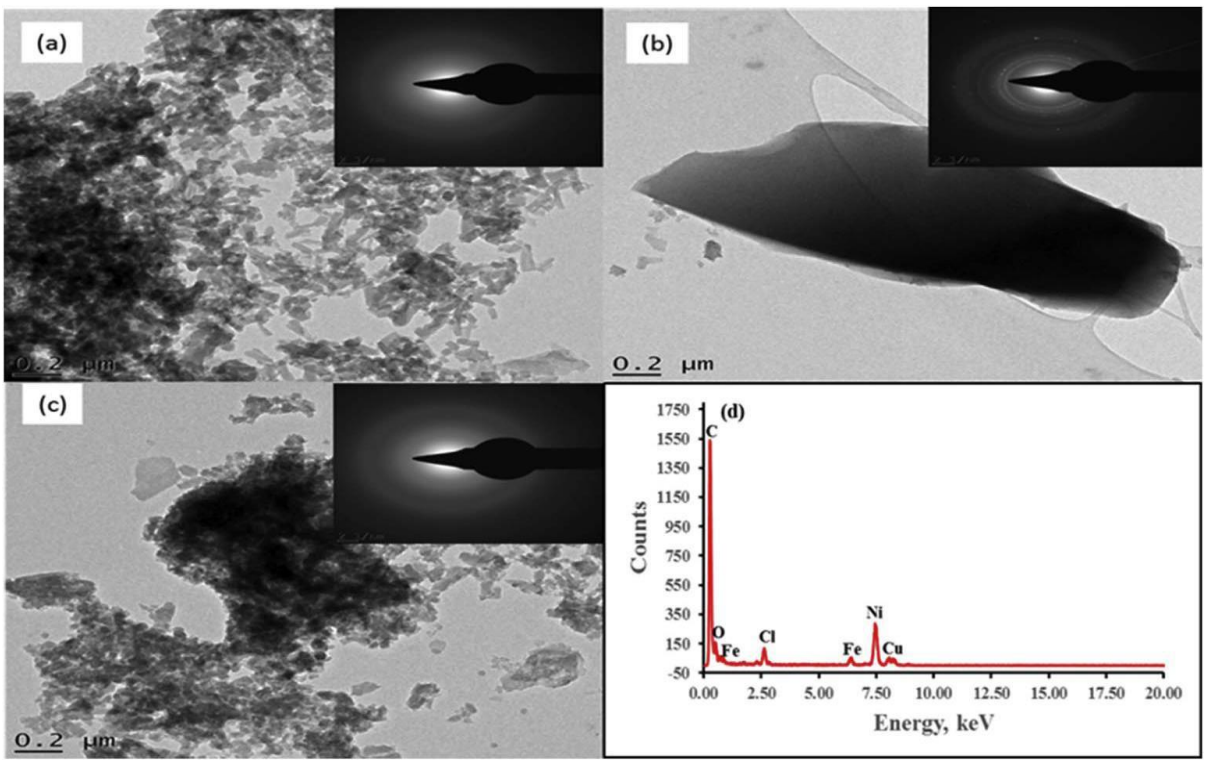

Figure 3.12: TEM images (a) PANI (b) MOF (c) PANI/MOF composite and (d) EDX spectrum of PANI/MOF composite. Inset: SAED images of various samples [20].

Lien *et al.* [21] gave a report on Metal–organic frameworks for catalysis: the Knoevenagel reaction using zeolite imidazolate framework ZIF-9 as an efficient heterogeneous catalyst. The TEM micrograph of ZIF-9 indicated that it possessed a porous structure (Figure 3.13) and TEM results appeared to suggest that the pore structure of the ZIF-9 was complex, containing both microporous and mesoporous pores.

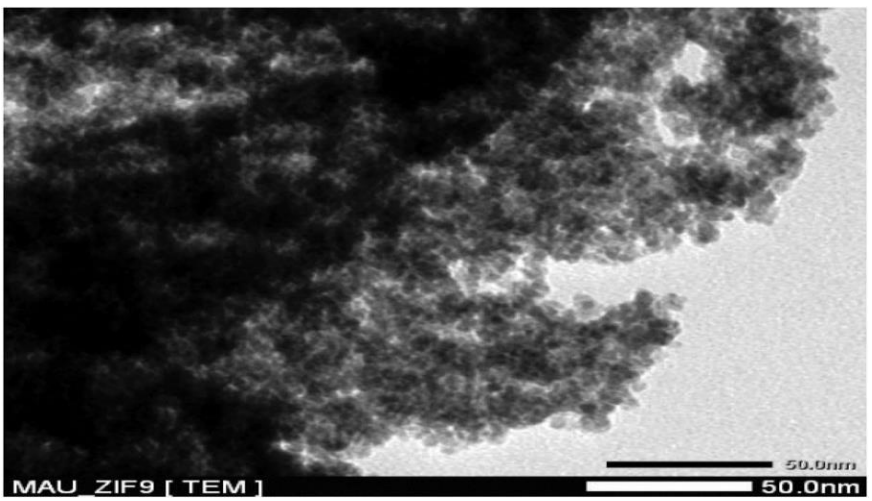

Figure 3.13: TEM micrograph of the ZIF-9 [21].

3.5. ELECTROANALYTICAL METHODS

Electroanalytical methods are a class of techniques in analytical chemistry, which study an analyte by measuring the potential (volts) and/or current (amperes) in an electrochemical cell containing the analyte. These methods can be broken down into several categories depending on which aspects of the cell are controlled and which are measured. The three main categories are potentiometry (the difference in electrode potentials is measured), coulometry (the cell's current is measured over time), and voltammetry (the cell's current is measured while actively altering the cell's potential) [33, 34]. Electroanalytical techniques follow the basics of electrochemistry whereby redox reactions occur during operations and use the

electrochemical cell principles. This means that there is an electron loss and gain between the species in question. In a three compartment electrode system working, counter and reference electrodes are placed in an electrolytic solution [35]. The most commonly used working electrodes are such as gold, glassy carbon and mercury. During operations, there must be a standardisation process, which occurs in reference electrode [36]. The potential in reference electrode is fixed and the potential change is monitored on working electrode. Silver/silver chloride (Ag/AgCl) and saturated calomel electrode (SCE) are the most commonly used reference electrodes. Counter electrodes serves as a sink for electrons so that the current can be passed from the external circuit [36]. The electroanalytical technique which are used in this wok are voltammetry and amperommetry.

3.5.1. Cyclic voltammetry (CV)

CV is an electrochemical technique which uses electrochemical cell to measure current in excess voltage, predicted by the Nernst equation [35].The CV is performed by cycling the potential of a working electrode, and measuring the resulting current. This technique consists of three electrodes namely; working, reference, and counter electrode [35]. In order to provide sufficient conductivity electrolytic solution needs to be added to the sample solution. CV is often used to study a variety of redox processes, to determine the stability of reaction products, the presence of intermediates in redox reactions, reaction and electron transfer kinetics and the reversibility of a reaction [34-37]. The CV was used to evaluate the electrochemical properties of polyaniline and composite. CV was also used for hydrogen evolution studies using Tafel plot. Eftekhari *et al.* [37] documented some key CV electrochemical behavior of PANI (Figure 3.14a) and reported that it consists of three redox pair reactions over a wide range of potential, which includes the redox transition between leucoemeraldine (insulating) and protonated emeraldine (conducting), the transition between pbenzoquinone and hydroquinone, and the redox transition between the emeraldine and the pernigraniline.

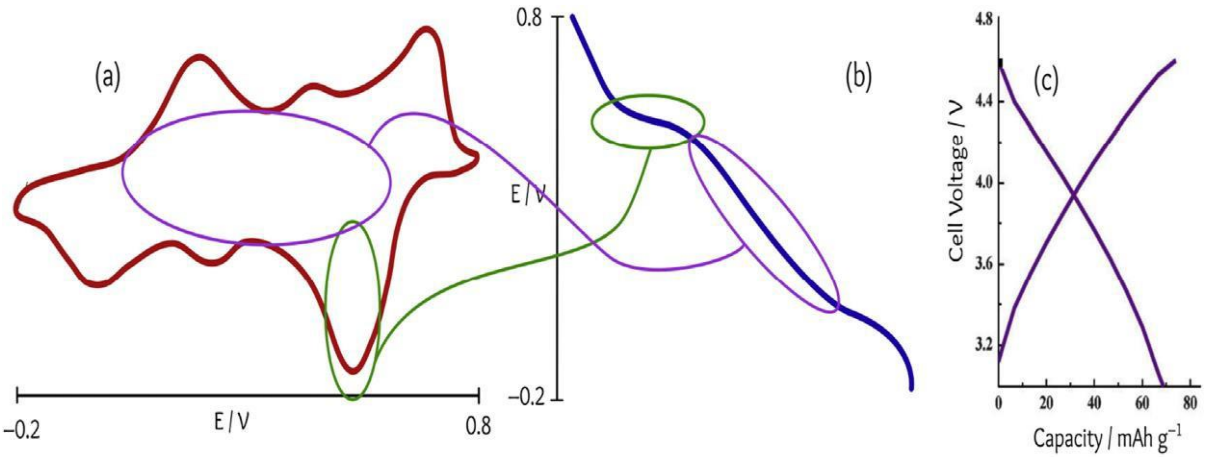

Figure 3.14: (a) Cyclic voltammogram and (b) discharge profile of a typical PANI electrode. (c) Experimental charge/discharge profile of a lithium-ion cell employing a PANI cathode [37].

3.5.2. Square wave voltammetry (SWV)

SWV is a form of linear potential sweep voltammetry which has found numerous applications in various fields. In SWV experiments the current at a working electrode is measured while the potential between the working electrode and a reference electrode is swept linearly in time [38]. Its advantage is that it can be used to perform an experiment much faster than the other electrochemical techniques. SWV is more effective than cyclic voltammetry due its high sensitivity. In the current work, SWV was used to support the CV analysis for evaluating electrochemical properties of the synthesised materials. Ramohlola *et al.* [20] used SWV to support CV as shown in Figure 3.15 (a and b).

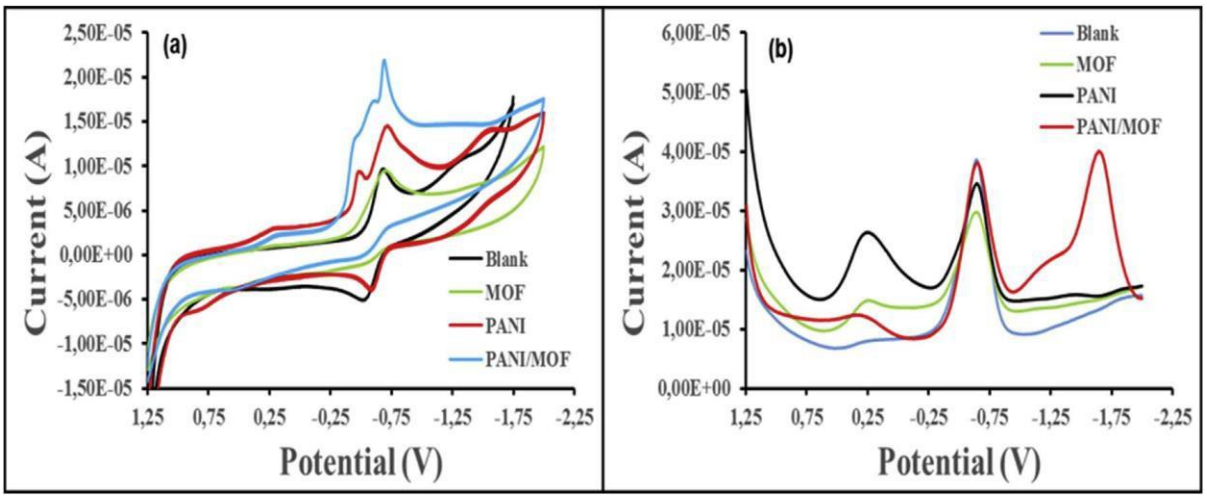

Figure 3.15: (a) CV and (b) SWV curves of MOF, PANI and PANI/MOF (~3.0 × 10^{-3} mol/L) in 0.1 M TBAP/DMSO electrolyte solution on Au electrode [20].

3.5.3. Chronoamperometry (CA)

In a CA experiment, current 'amp' is measured as a function of time 'chrono'. The chronoamperometry electrochemical technique involves stepping the potential applied to the working electrode, where initially it is held at a value at which no Faradaic reactions occur before jumping to a potential at which the surface concentration of the electroactive species is zero, wherein the resulting current-time dependence is recorded [39]. This technique is commonly used either as a single potential step, in which only the current resulting from the forward step is recorded, or double potential step, in which the potential is returned to a final value following a time period. The mass transport process throughout this process is solely governed by diffusion, and as such the current-time curve reflects the change in concentration at the electrodes surface. This involves the continuing growth of the diffusion layer associated with the depletion of reactant, thus a decrease in the concentration gradient is observed as time progresses [39]. The most important equation in chronoamperometry is the Cottrell equation, which describes the observed current

(planar electrode of infinite size) at any time following a large forward potential step in a reversible redox reaction (or to large overpotential) as a function of $t^{-1/2}$ [39].

$$I = nFACD^{1/2}P^{-1/2}t^{-1/2} \quad (3.8)$$

where *n* is the stoichiometric number of electrons involved in the reaction, *F* is the Faraday's constant, *A* is the area of the electrode, *C* is the concentration of electrocatalyst and *D* is the diffusion coefficient [39]. In this work, chronoamperometry was used to determine the sensor sensitivity, limit of detection (LOD), limit of quantification (LOQ), response time, catalytic rate constant and diffusion coefficient. Yin *et al*. [40] presented a typical chronoamperogram as shown in Figure 3.16 below.

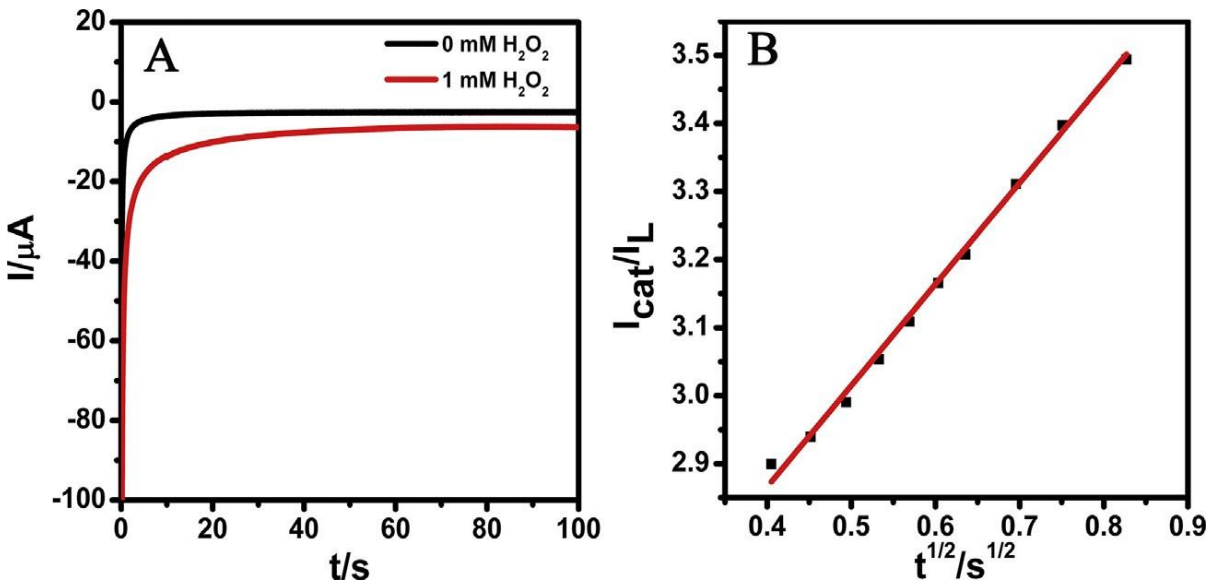

Figure 3.16: (A) Chronoamperograms of Zr-PorMOF/MPC-2/GCE in the absence and presence of 1 mM H_2O_2 concentration in PBS (pH 7.4) recorded at -0.2 V. (B) Calibration curve of I_{cat}/I_L versus $t^{1/2}$ [40].

3.6. CONCLUSIONS

Briefly, this chapter focused on different types of analytical instruments, their principle behind, advantages, limitations and previous reports on their application in characterising PANI, ZIF and their composites. FTIR was detailed to help with the identification of functional groups corresponding to PANI and ZIF and in one report it was used to confirm composite formation, displayed by the appearance and disappearance of vibration bands. It was shown from the previous reports that the STA (TGA-DSC) is employed to study the thermal properties such as degradation steps of PANI and ZIF. The crystallinity, phase identification, interplanar *d*-spacing and crystallite sizes of the synthesised materials are evaluated by using XRD. Morphological characterisation techniques such as SEM/EDS and TEM/EDX were reviewed and show to provide information about the surface and internal structural morphology, elemental composition and mapping. The electrochemical properties of the PANI and ZIF using CV potentiostat and SWV were reviewed in this chapter which will help in understanding the electrochemical behaviour of the synthesised materials. Chronoamperometry is the core of this study and it was reviewed in detail in order to have a better understanding in its practical application for electrochemical hydrogen gas sensing.

3.7. REFERENCES

[1] K. S. Zhang, L. L. Ashok, ‘’Materials characterization techniques’’, *Boca Raton CRC Press*, 2009.

[2] L. Yang, ‘’Materials Characterization: Introduction to Microscopic and Spectroscopic Methods’’, *Wiley*, 2009.

[3] S. Zhang, Materials Characterization Techniques. *CRC Press*, 2008.

[4] F. C. Adams, “X-Ray absorption and diffraction-overview,” *Encyclopedia of Analytical Science,* 3rd Ed, pp. 1-14, 2017.

[5] G. M. Hansford, “Nuclear instruments and methods in physics research A X- ray diffraction without sample preparation: Proof-of-principle experiments,” *Nucl. Inst. Methods Phys. Res. A*, vol. 728, pp. 102–106, 2013.

[6] G. P. Stahly and D. Ph, “Advantages of a Cu vs . Co X-ray diffraction source,” pp. 5629, 2012.

[7] D. Rennes and D. Loue, “Powder X-Ray Diffraction, Applications,” *Encyclopedia of Spectroscopy and Spectrometry,* 3rd Ed., 2017.

[8] A. Mekki, N. Joshi, A. Singh, Z. Salmi, P. Jha, P. Decorse, S. Lau-Truong, R. Mahmoud, M. M. Chehimi, D. K. Aswal, and S. K. Gupta, “H_2S sensing using in situ photo-polymerized polyaniline–silver nanocomposite films on flexible substrates” *Org. Electron*., vol. 15, pp. 71–81, 2014.

[9] W. Zheng, L. Hu, L.Y.S. Lee, and K. Wong “Copper nanoparticles/polyaniline/graphene composite as a highly sensitive electrochemical glucose sensor” *J. Eletrochem*., vol. 30, pp. 3456-3466, 2016.

[10] Y. Li, F. Lianga, H. Buxa, W. Yangb, J. Caroa “Zeolitic imidazolate framework ZIF-7 based molecular sieve membrane for hydrogen separation” *J. Memb. Sci.*, vol. 354, pp. 48–54, 2010.

[11] S. Loganathan, R. B. Valapa, R. K. Mishra, G. Pugazhenthi and S. Thomas, “Thermogravimetric analysis for characterization of nanomaterials, ”*Nanomaterials,* vol. 60, pp. 67-80, 2015.

[12] P. Thirunathan, P. Arnz, J. Husny, A. Gianfrancesco, and J. Perdana, “Thermogravimetric analysis for rapid assessment of moisture diffusivity in

polydisperse powder and thin film matrices," *Food Chem*., vol. 242, pp. 519–526, 2018.

[13] C. Karakaya, S. Ricote, D. Albin, E. Sánchez-cortezón, B. Linares-zea, and R. J. Kee, "Thermochimica acta thermogravimetric analysis of $InCl_3$ sublimation at atmospheric pressure," *Thermochim. Acta.*, vol. 622, pp. 55–63, 2015.

[14] B.A. Bhanvase, N.S. Darda, N.C. Veerkar, A.S. Shende , S.R. Satpute, S.H. Sonawane, "Ultrasound assisted synthesis of PANI/$ZnMoO_4$ nanocomposite for simultaneous improvement in anticorrosion, physico-chemical properties and its application in gas sensing", *Ultrason Sonochem*, vol. 24, pp. 87–97, 2015.

[15] M. A. Mohamed, J. Jaafar, A. F. Ismail, M. H. D. Othman, and M. A. Rahman, "Fourier Transform Infrared (FTIR) Spectroscopy," *Membrane Charact*, vol 355, pp. 3-29, 2017.

[16] J. Zakzeskia, A. Debczaka, P.C.A. Bruijnincxa, and B.M. Weckhuysena, "Catalytic oxidation of aromatic oxygenates by the heterogeneous catalyst Co-ZIF-9", *Appl Catal A Gen*, vol. 394, pp. 79–85, 2011.

[17] L.C. Lee, C. Liong, and A.A. Jemain, "A contemporary review on data preprocessing (DP) practice strategy in ATR-FTIR spectrum," *Chemom. Intell. Lab. Syst*., vol. 163, pp. 64–75, 2017.

[18] M. C. Rehbein, S. Husmann, C. Lechner, C. Kunick, and S. Scholl, "Fast and calibration free determination of first order reaction kinetics in API synthesis using in-situ ATR-FTIR," *Eur. J. Pharm. Biopharm*., vol. 30, pp. 1–6, 2017..

[19] G.E. Tranter, and U. Kingdom, "FTIR Spectroscopy of Aqueous Solutions," Encyclopedia of Spectroscopy and Spectrometry, 3rd Ed, pp. 762–769.

[20] K.E. Ramohlola, G.R. Monana, M.J. Hato, K.D. Modibane, K.M. Molapo, M. Masikini, S.B. Mduli, E.I. Iwuoha, Polyaniline-metal organic framework nanocomposite as an efficient electrocatalyst for hydrogen evolution reaction" *Compos. Part B: Eng.*, vol. 137, pp. 129–139, 2018.

[21] T. L.N. Lien, K. A. L. Ky, X. T. Hien, and T. S. P. Nam "Metal–organic frameworks for catalysis: the Knoevenagel reaction using zeolite imidazolate

framework ZIF-9 as an efficient heterogeneous catalyst" *Catal. Sci. Technol*., vol. 2, pp 521–528, 2012

[22] M. Clugston, R. Flemming, and D. Vogt, "Chemistry: An introduction for southern African students", *Oxford University Press*, 1st Ed , 2002.

[23] J. McMurry, "Organic Chemistry", *Brooks/Cole, Thomson Learning, Inc,* 7th Ed., 2008.

[24] D.A. Skoog, D.M. West, and F.J. Holler, "Fundamentals of Analytical Chemistry", *Saunders College Publishing*, 8th Ed., 1992.

[25] http://www.chemicool.com/img1/graphics/ir.gi.

[26] S. Tanaka, K. Fujita, Y. Miyake, M. Miyamoto, Y. Hasegawa, T. Makino, S. Van der Perre, J. C. S. Remi, T. Van Assche, G. V. Baron, and J.F.M. Denayer, "Adsorption and diffusion phenomena in crystal size engineered ZIF-8 MOF", *J. Phys. Chem*., vol. 119, pp. 28430−28439, 2015.

[27] A. Yoshida, Y. Kaburagi, and Y. Hishiyama, "Scanning Electron Microscopy," *Mater. Sci. Eng.*, vol. 30, pp. 71-93, 2016.

[28] M. D. A. Pereira-da-silva and F. A. Ferri, "Scanning electron microscopy," *Nanocharacterization Tech.*, vol. 66, pp. 1-35, 2017.

[29] T.L. Kirk, "A review of scanning electron microscopy in near field emission mode," *Adv. Imaging Electron Phys.*, vol. 204, pp. 232-239, 2017,

[30] G.D. Khuspe, S.T. Navale, M.A. Chougule, and V.B. Patil". Ammonia gas sensing properties of CSA doped PANi-SnO_2 nanohybrid thin films", *Synth. Met*., vol. 8, pp. 185–186, 2013.

[31] Z.L. Wang, "Transmission electron microscopy of shape-controlled nanocrystals and their assemblies," *J. Phys. Chem. B.,* vol.104, pp. 1153–1175, 2000.

[32] P.G. Callahan, J. C. Stinville, E.R. Yao, M.P. Echlin, M.S. Titus, M. Graef, D.S. Gianola and T.M. Pollock, "Ultramicroscopy transmission scanning electron microscopy : defect observations and image simulations," *Ultramicroscopy*, vol. 186, pp. 49–61, 2018

[33] J. McMurry,. Organic Chemistry, *Brooks/Cole, Thomson Learning, Inc*, 7th Ed, 2008.

[34] http://www.chemicool.com/img1/graphics/ir.gi.

[35] A.J. Bard, L.R. Faulkner, “Electrochemical Methods: Fundametals and applications”. *John wiley & Sons Inc*, 2nd Ed., 2001.

[36] https://openi.nlm.nih.gov/imgs/512/389/2871148/PMC2871148_ijms-11-01956f1.png.

[37] A. Eftekhari, L. Li, Y. Yang “Polyaniline supercapacitors,” *J. Power Sources*, vol. 347, pp. 86-107, 2017.

[38] https://openi.nlm.nih.gov/imgs/512/389/2871148/PMC2871148_ijms-11-01956f1.png.

[39] D. A. C. Brownson and C. E. Banks, *Interpreting Electrochemistry*. 2014

[40] D. Yin, J. Liu, X. Bo, M. Li, L. Guo, “Porphyrinic metal-organic framework/macroporous carbon composites for electrocatalytic applications *Electrochimic. Acta.*”, vol. 247, pp. 41–49, 2017.

CHAPTER FOUR

DEVELOPMENT OF ELECTROCHEMICAL GAS SENSOR TECHNOLOGY INDUCED BY POLYANILINE DOPED WITH COBALT-ZEOLITIC BENZIMIDAZOLATE FRAMEWORK COMPOSITE FOR HYDROGEN SAFETY MONITORING

This chapter was submitted for possible publication in *Electrocatalysis (revised manuscript is under review with provisional acceptance).*

CHAPTER SUMMARY

The quest for smart sensors with excellent sensitivity, fast response and high accuracy for hydrogen gas detection has been ongoing for decades. In this chapter, PANI doped with CoZIF (ZIF-9) to fabricate the (PANI-CoZIF) composite for electrochemical hydrogen gas sensing is presented. The composite was synthesised through chemical oxidative polymerisation of aniline with 3.6 wt.% CoZIF present in the composite. The structural properties of the synthesised materials were studied by employing UV-vis, XRD, FTIR and Raman spectroscopy, and simultaneous thermal analysis (STA). The SEM/EDS and TEM/EDX were used for morphological characterisation and revealed grafting of CoZIF on to the surface of PANI upon composite formation. The XRD diffraction pattern and SAED results showed that PANI and the composite structures are amorphous in nature and the presence of CoZIF did not alter the amorphous nature of PANI. Spectroscopic analyses using FTIR and Raman revealed the coexistence of CoZIF and PANI in the composite displayed by a characteristic peak intensities corresponding to both CoZIF and polymer. From the Tauc plot results, it was found that PANI and the resultant composite possessed the energy band gap of 2.5 and 2.3 eV, distinctively, indicating that they are both semi-conductors. STA studies showed that the PANI-CoZIF composite exhibits an enhancement in thermal stability in comparison to PANI as indicative of improvement of thermal properties. CV, Tafel analysis and TOFs were

performed to study the electrochemical perfomance of the synthesised materials through HER for gas sensing application. The PANI-CoZIF composite showed drastic enhancement in the catalytic H_2 evolution and the TOFs as compared to neat PANI. In addition, the CA results exhibited the significant improvement in electrochemical hydrogen sensing ability of PANI-CoZIF composite. The composite shows great potential as a tool for practical applications for hydrogen fuel technology.

40.1. INTRODUCTION

Hydrogen is an appealing energy carrier for fuel cell application due to its high abundance, renewability, environmental friendliness, fuel efficiency and produces more energy as compared to gasoline [1]. Unfortunately, hydrogen is extremely flammable if its concentration is higher than 4% in air [2]. Therefore, a development of hydrogen gas sensors is vital to preclude explosion risks during its production, storage and transportation [3]. Hydrogen sensors employing metals and metal oxides such as tin oxide and zinc oxide have been widely studied [4,5]. Nonetheless, these materials are only sensitive to hydrogen gas at high temperatures (>100 °C) and they also possess low surface areas [6].

Conducting polymers have shown an increasing significance in the development of smart sensors owing to their inexpensive fabrication price, deposition simplicity onto different types of substrates, high sensitivity and short response time when used at room temperature [7]. In addition, the ability to incorporate specific binding sites into conducting polymers offers the improvement of selectivity and sensitivity [8]. Intrinsic conducting polymers (ICPs), such as PANI, poly (p-phenylene-vinylene) (PPV) and polypyrrole (PPY) have been extensively investigated for gas sensing owing to their special conduction mechanism [9]. Among ICPs, PANI has been found to be the most promising polymer due to its high environmental stability, mechanical flexibility, simple and reversible doping/dedoping chemistry [10]. However, PANI has limited sensitivity towards gas species as compared to metal oxides [11]. Furthermore, its

poor solubility in many organic solvents hampers its application [11]. This can be addressed by development of the PANI based composites and blends [12]. Incorporation of novel porous compounds such as metal organic frameworks (MOFs) to PANI structure form a composite can help in order to increase the electrochemical stability of the polymer [13]. As discussed in the previous chapters, ZIFs exhibit permanent porosity, large structural diversity and outstanding chemical and thermal stability, thus making them attractive candidates for various applications [14]. The ZIF crystal structures are constructed from aluminosilicate zeolite nets, wherein the tetrahedral Si(Al) sites are substituted by transition metal such as Co and Zn tetrahedrally coordinated by imidazole ligands [15]. Herein, we present for the first time that PANI-CoZIF is a promising hydrogen gas sensor through HER mechanism at room temperature. The CoZIF is a kind of ZIF constructed from benzimidazole organic linker and Co^{2+} ions, establishing three dimensional microporous metal organic networks. PANI-CoZIF composite synthesised by in-situ oxidative polymerisation was characterised using FTIR, Raman, XRD, UV-vis, STA, SEM/EDS, HR-TEM/EDX, SWV, CV and CA. High sensitivity towards hydrogen was successfully achieved by employing PANI-CoZIF composite for electrochemical hydrogen gas sensing application. The PANI-CoZIF composite have great potential as a tool for practical applications in the hydrogen fuel technology.

40.2. EXPERIMENTAL SECTION

4.2.1. Materials

Aniline was procured from Sigma Aldrich, South Africa and it was distilled first before use. Absolute ethanol, methanol, benzimidazole ($C_7H_6N_2$), tetrabutylammonium percholate (TBAP) and cobalt nitrate hexahydrate $Co(NO_3)_2.6H_2O$ were all obtained from Merck, South Africa. Ammonium per sulfate (APS) was procured from Riedel- de Haen. Iron chloride ($FeCl_3$) was purchased from Educhem. The dimethyl sulfoxide (DMSO) was bought from Rochelle chemicals. In addition, Hydrochloric acid (HCl),

and sulphuric acid (H_2SO_4) were also bought from Rochelle chemicals. H_2SO_4 standard solutions were prepared in 0.1 mol.L^{-1} TBAP-DMSO electrolyte lest specified else way.

4.2.2. Methods

4.2.2.1. Preparation of PANI, CoZIF and PANI-CoZIF composite

PANI was synthesised through oxidative polymerisation of aniline monomer in accordance to previous method reported elsewhere [16]. The CoZIF was synthesised according to the route reported previously with some modifications where methanol and benzimidazole (BIM) were used instead of distilled water and 2- methyl imidazole, respectively [17]. PANI-CoZIF composite was synthesised via in- situ chemical oxidative polymerisation according to the synthetic method reported by Ramohlola *et al*. [18,19] with some slight modifications, wherein aniline monomer and CoZIF replaced 3-amino-benzoic acid monomer and MOF, respectively.

4.2.2.2. Characterisation techniques

Varian Cary 300 UV-Vis-NIR spectrophotometer was employed for absorption studies at room temperature in the wavelength region 300 to 900 nm. The structural characterisation of PANI, CoZIF and PANI-CoZIF composite was achieved by using X-ray diffraction (XRD Phillips PW 1830 with CuKα radiation at wavelength of 1.5406 Å. The thermal analysis was investigated using STA Perkin-Elmer 6000 and samples which range from 1 - 4 mg were heated at a working temperature from 30-500 °C at the scan speed of 20 °C.min^{-1} under inert environment. FTIR spectrometer (Spectrum II Perkin-Elmer) was used to confirm composite formation in the wavenumbers between 400 and 4500 cm^{-1} obtained at room temperature. At a resolution of 4 cm^{-1} a minimum of 32 scans were collected. SEM images were taken by Auriga field emission-scanning electron microscope (FE-SEM) coupled with EDS

detector to check the composition of the elements. They were carried out using accelerating voltage of 200 kV. TEM investigation was made by using FEI Tecnai G2 20 TEM coupled with EDX to study the interior morphology of the prepared materials. All the electrochemical results were achieved by employing EPSILON electrochemical workstation. The results were obtained using bare gold working electrode (3 mm diameter, 0.071 cm^2 area). In addition to that, platinum (Pt) and Silver-Silver chloride Ag/AgCl were used as counter and reference electrode, respectively. PANI, CoZIF, and PANI-CoZIF composite (~2.0 x 10^{-4} $mol.L^{-1}$) solutions readings were done at a scan speed of 0.02 - 0.10 $V.s^{-1}$ swept from -1.0 to 1.0 V. Electrochemical behavior of the materials were investigated in 10 mL of 0.1 $mol.L^{-1}$ TBAP-DMSO as the electrolyte. Hydrogen evolution reaction was investigated using
0.033 $mol.L^{-1}$ of H_2SO_4 as the source of hydrogen source and ~2.0 x 10^{-4} $mol.L^{-1}$ of PANI, CoZIF and PANI-CoZIF as electrocatalysts and hydrogen sensing material. Electrochemical experiments were done at 22 $\pm$ 2 °C controlled by water bath.

4.3. RESULTS AND DISCUSSION

4.3.1. Structural characterisations

Figure 4.1(a) displays the FTIR spectra of $Co(NO_3)_2.6H_2O$, BIM and as-synthesised CoZIF. The spectrum of BIM possesses the vibrations at around 3200, 3000, 1650 and 1200 cm^{-1} for N-H, C-H, C=C and C-N, respectively. Huang et al. reported that benzimidazole organic linker shows the aromatic C-H stretching vibrations between 3100–3000 cm^{-1} and the stretch band of N-H group which absorbs strongly at 3250–2500 cm^{-1} [20]. On the other hand, the cobalt nitrate shows vibration around 3000 cm^{-1} for moisture/H_2O and intense peaks at around 1350 cm^{-1} for nitrate groups. The significant feature observed for the FTIR spectrum of the CoZIF as compared to the one of BIM, it is the disappearance of the strong and broad N-H bands between 3250–2500 cm^{-1}, substantiating that the benzimidazole linker has been fully deprotonated during CoZIF formation [20]. This was supported by the

appearance of characteristic Co-N stretching band at 3050 cm^{-1} in spectrum of CoZIF, attributed to the interaction of Co^{2+} with nitrogen in the benzimidazole linker [20] .

The FTIR results of the synthesised PANI-CoZIF composite with reference to PANI and CoZIF spectra are presented in Figure 4.1(b). The composite has similar characteristic peak in comparison to the neat PANI. Both PANI-CoZIF composite and the undoped PANI showed peaks at 806 cm^{-1} (C-H out-of-phase bonding corresponding to benzenoid ring), 1177 cm^{-1} (C-H in-phase bonding ascribed to benzenoid ring), 1338 cm^{-1} and 1505 cm^{-1} (C-N stretches of benzenoid and quinoid rings, respectively) and 1605 cm^{-1} (C=C attributed to aromatic ring) [16]. The peak at 3495 cm^{-1} is attibuted to N-H bonding of the polymer [21]. The observed absorption peaks for PANI are in accordance with previous reports, proving its successful synthesis [19]. The composite showed an increase in aromaticity upon doping with CoZIF as evidence that there was interaction between PANI and CoZIF.

The existence of CoZIF in the PANI-CoZIF composite was further confirmed using Raman spectroscopy as depicted in Figure 4.1(c). The Raman spectrum of CoZIF exhibits the strong bands at ~1200 cm^{-1} ascribed to benzene ring (C=C) of the organic ligand [22]. The noticeable peaks at around 610 and 810 cm^{-1} attributed to C-H bending vibrations of the ring [23,24] . The peak around 1000 cm^{-1} in spectrum of PANI is the characteristic of conductive PANI and discerned from charge delocalisation of polymer backbone [25]. The results for CoZIF provide characteristic band at around 500 cm^{-1} assigned to Co-C and Co-N coupled vibrations. On the other hands, the introduction of CoZIF in PANI showed the presence of benzene at around 1000 cm^{-1} and Co-N/C vibration at around 550 cm^{-1}. The peak intensities of the PANI peaks drastically improved upon composite formation, which further indicates that both CoZIF and PANI coexist in the PANI-CoZIF composite.

UV-vis spectroscopy was employed for optical studies of PANI and PANI-CoZIF composite using DMSO as a solvent as shown in Figure 4.1(d). Figure 4.1(d) shows that PANI has two distinctive bands at ~347 and 500 nm. The peak at around 347 nm is ascribed to the π-π^* transitions of the benzoid rings, and the broad peak at approximately 500 nm is due to the π-π^* transitions of the quinine-imine groups

confirming emerladine state of PANI [26]. Nonetheless, upon composite formation, there is slight red shift and increase in absorbance of the benzoid and quinoid absorption peaks, which is due to improved solubility in DMSO thus increasing the electron density in the PANI backbone [19]. Based on this interpretation, it is obvious that incorporation of CoZIF was a success and this has been supported with both Raman and FTIR analyses. Figure 4.1(e) shows the effect of concentration on the absorbance PANI-CoZIF composite. The higher the concentration, the higher the absorbance of the composite, thus the Beer-Lambert law is obeyed [26]. An increase in concentration does not shift the position of the peaks hence the conduction band on the composite did not change [19].

Figure 4.1(f) presents Tauc plot variation of $(\alpha h\nu)^2$ as a function of $h\nu$ for the determination of the band gap of the synthesized materials [27]. The energy band gap was determined by a linear extrapolation of the Tauc curve where it cuts the abscissa. Abdulla *et al*. [28] reported that PANI possesses the energy band of 2.8 eV which shows strong absorption for visible light and after doping it with TiO_2 the optical band gap became 2.21 eV. Herein, the energy band gap values were found to be 2.5 and 2.3 eV for PANI and PANI-CoZIF composite (8% reduction), respectively. These results agree very well with the previous report published elsewhere [28]. The CoZIF is reported to have band gap of 3.01 eV [29] which is close to 3.25 eV obtained in this current work. From these observations, it can be deduced that CoZIF has an insulator characteristic due to organic linker and both PANI and PANI-CoZIF are semiconductors [27]. There was a drop in the energy band gap upon composite formation as expected [28]. This is attributed to an increase in electrons on the composite in comparison to undoped PANI [16].

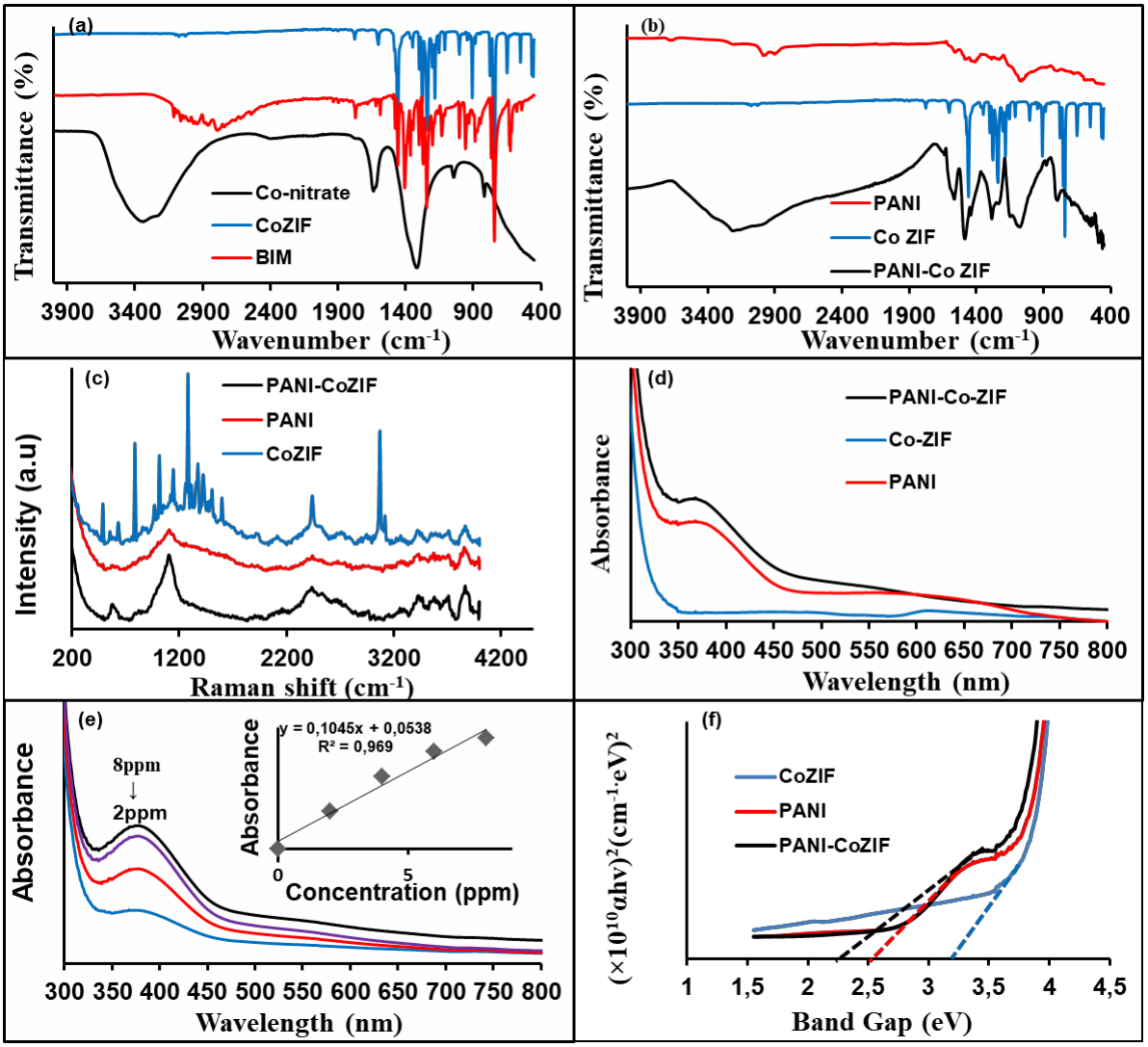

Figure 4.1: (a) FTIR spectra of $Co(NO_3)_2.6H_2O$, BIM and as synthesised CoZIF (b) FTIR, (c) Raman spectra and (d) UV results at 2ppm for PANI, CoZIF, and PANI-CoZIF composite, (e) UV spectra of the composite obtained at varying concentrations; 2ppm to 8ppm in DMSO and (f) Tauc curve of PANI, CoZIF and PANI-CoZIF composite.

The XRD analysis was employed to examine the crystallinity and phase structure of PANI, CoZIF and PANI-CoZIF composite. The diffraction patterns of the samples are depicted in Figure 4.2(a). As shown in Figure 4.2(a), the peaks at 2θ angle of 6.98, 9.13, 13.03, 14.01, 15.44, 16.22, 18.73, 19.75, 21.14, and 23.04° are corresponding

to the main peaks of CoZIF, which is in agreement with the isostructural CoZIF reported by Shensuo et al. [30]. The diffraction peak of the pattern that appeared at 2θ angle of 6.98°, accounting for the reflection (011) was used to determine the interplanar d spacing of 12.4 Å (estimated using Bragg's equation: $n\lambda = 2d\sin\theta$ [31] where n, λ and θ are the integer, wavelength and theta, respectively). The XRD diffraction pattern of PANI displays a broad peak at around 2θ angle of 20 and 23 corresponding to (100) and (200) planes, respectively [16]. This shows that PANI was successfully synthesised and the results are in agreement with the previously reported data [21]. The average crystallite sizes of PANI (at 2θ angle of 21°) and PANI-CoZIF (at 2θ angle of 21°) were estimated from peak width using Debye Scherrer formula (Equation 4.2) [32]:

$$D = \frac{0.9\lambda}{\beta COS\theta} \qquad (4.2)$$

Where β is the full-width at half-maximum (FWHM) measured in radians, λ is the X-ray wavelength of Cu-Kα radiation (1.5406 Å) and θ is the Bragg's angle. The crystallite sizes were found to be 4.04 nm and 3.22 nm for PANI-CoZIF and PANI respectively. In situ polymerisation of PANI in the presence of CoZIF caused shift in the XRD diffraction peaks intensities which reveal the coexistence of both PANI and CoZIF in the composite [19].

Thermal analysis of solid materials is essential to detect the degradation behaviour of the as-synthesised materials when subjected to elevated temperatures. It is also important to check the exact weight loss ratio corresponding to every component in a sample. Thermograms of mass loss versus temperature for PANI, CoZIF and PANI-CoZIF were recorded at a heating rate of 10 °C/ min in a nitrogen atmosphere. The results are depicted in Figure 4.2(b) below. The most important feature in the TGA result for CoZIF was the 3% weight loss in the temperature ranges 22 - 220 °C. This indicates that the CoZIF was still stable at that temperature range. This little weight loss is owing to loss of moisture, solvent and unreacted species [33]. As the temperature increased from 225 °C to 550 °C, little weight-loss step of over 8% was

observed, indicating little thermal decomposition of the CoZIF in that temperature range [20]. After 575 °C, around 92% of the starting weight remained, which shows that CoZIF is applicable across a wide temperature range. TGA results for PANI display two weight loss steps in the temperature range between 25 °C and 575 °C. The first weight loss is ascribed to the evaporation of moisture [34]. The main degradation at 275 °C can be attributed to the collapse of the polymer chains of PANI [35]. Thermogravimetric analysis of PANI-CoZIF composite shows that the structure-directing agent and solvent molecules are trapped within the porous cavities of the frameworks. Furthermore, the composite shows slow and less steeper degradation steps in comparison to undoped PANI. This suggests that there is an enhanced thermal stability and a alteration in morphology upon composite formation [16].

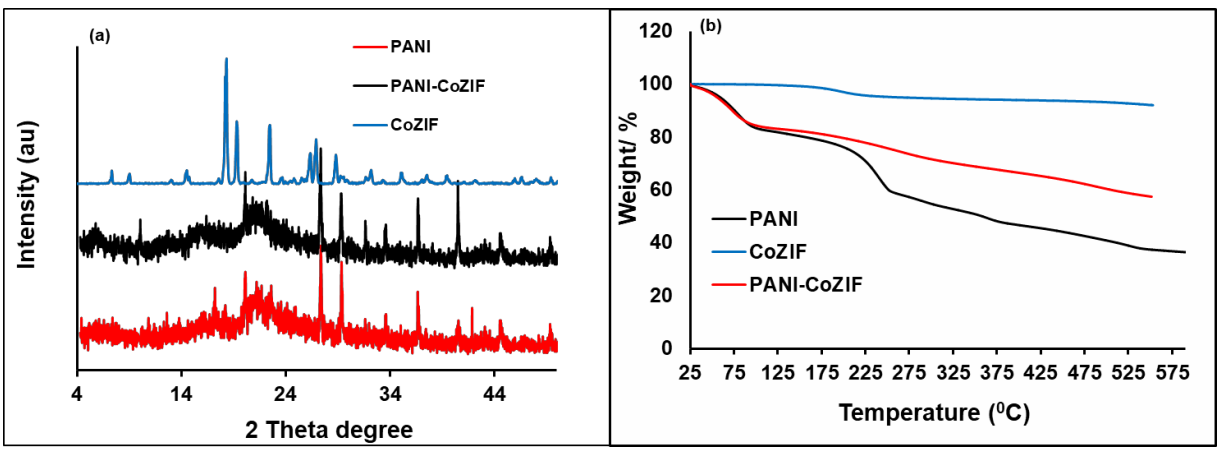

Figure 4.2: (a) XRD patterns and (b) TGA curves of PANI, CoZIF and PANI-CoZIF composite.

4.3.2. Morphological characterisations

The FE-SEM images helped to determine the morphological properties of the materials as shown in Figure 4.3 (a, c, and e). SEM image of CoZIF (Figure 4.3(a)) exhibited the spherical shaped crystals similar to morphology to the CoZIF crystals as reported in literature [20], [36] and its the EDS (Figure 4.3(b)) shows the presences of C-, N- and Co- atoms in the CoZIF network. The SEM image of PANI

presented in Figure 4.3(c) shows some fibrous rod-like structures together with the agglomerated structures [16]. The fiber-like morphology might be ascribed to soft template-assisted development of polyaniline [19]. Its corresponding EDS results (Figure 4.3(d)) revealed the existence of impurities of Fe, O, Cl and S. The impurities are owed to the oxidising agents and HCl utilised through the synthetic procedure [37]. The SEM image further revealed the grafting of spherical CoZIF particles on the surface of PANI matrix. On the other hand, EDS analysis of the PANI-CoZIF composite (Figure 4.3(f)) displayed an increase in C and O percentage compositions.

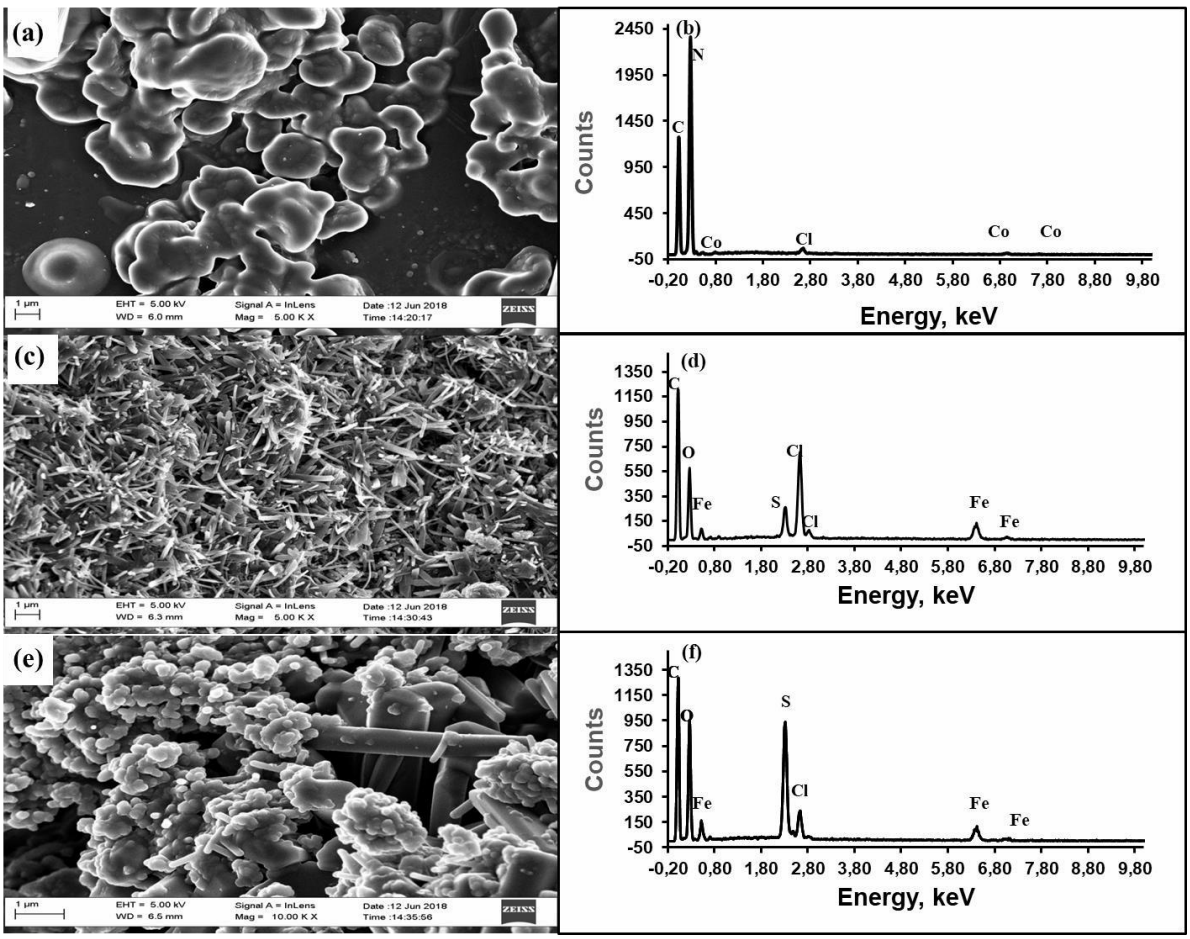

Figure 4.3: SEM results of (a) CoZIF, (c) PANI and (e) PANI-CoZIF; composite and EDS spectrum of (b) CoZIF, (d) PANI and (f) PANI-CoZIF composite.

Figure 4.4(a, c and e) present TEM images for CoZIF, PANI and PANI-CoZIF, respectively. PANI and CoZIF showed tubular morphological structures (Figure 4.4a and c). PANI tubings are twisted together thus forming the aggregates. Upon composite formation there is intertwinement of tubings of CoZIF and PANI, hence, the morphology was modified showing the presence of both PANI and CoZIF. The EDX spectra (Figure 4.4(d) and (f)) show the presence of various elements in the synthesised PANI and PANI-CoZIF materials. The PANI structure consists of Fe, S, O and Cl due to the oxidant and acidic medium used during the synthetic procedure [38]. The composite PANI-CoZIF shows a decrease in the composition of carbon which might be due to the interaction between PANI and CoZIF (Figure 4.4(f)). These findings prove the existence of CoZIF in the composite resulting in the modification of polyaniline morphology. The presence of small peaks of Cu is due to copper grid used during TEM experiments.

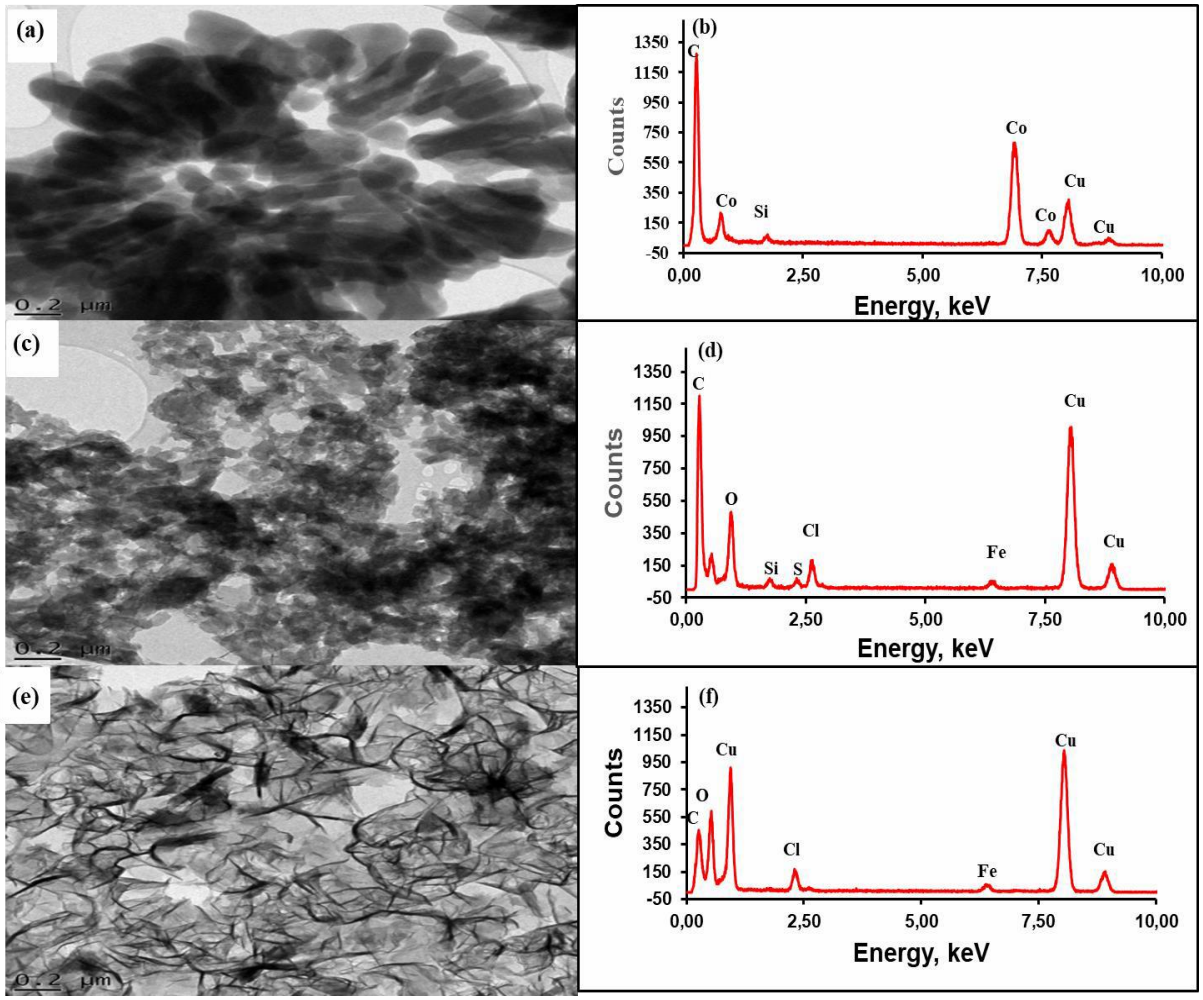

Figure 4.4: TEM images of (a) CoZIF, (c) PANI and (e) PANI-CoZIF composite and EDX spectrum of (b) CoZIF, (d) PANI and (f) PANI-CoZIF composite

HR-TEM was employed to study the internal morphologies of PANI, CoZIF and PANI-CoZIF. The results are presented in Figure 4.5(a-c) together with the images of SAED to check if the materials were crystalline. The SAED findings of CoZIF displayed patterns of clearly visible rings confirming that it is crystalline which is in agreement with the XRD patterns (Figure 4.2(a)). The SAED showed the d- spacing of 1.7 nm which correspond to XRD *d*-spacing of 1.24 for the orientation (011). The neat PANI displayed no clear rings, which indicated that is was in an amorphous

state [16]. Furthermore, the composite retained the amorphous nature of the polymer. Moreover, the structure of PANI was modified upon composite formation.

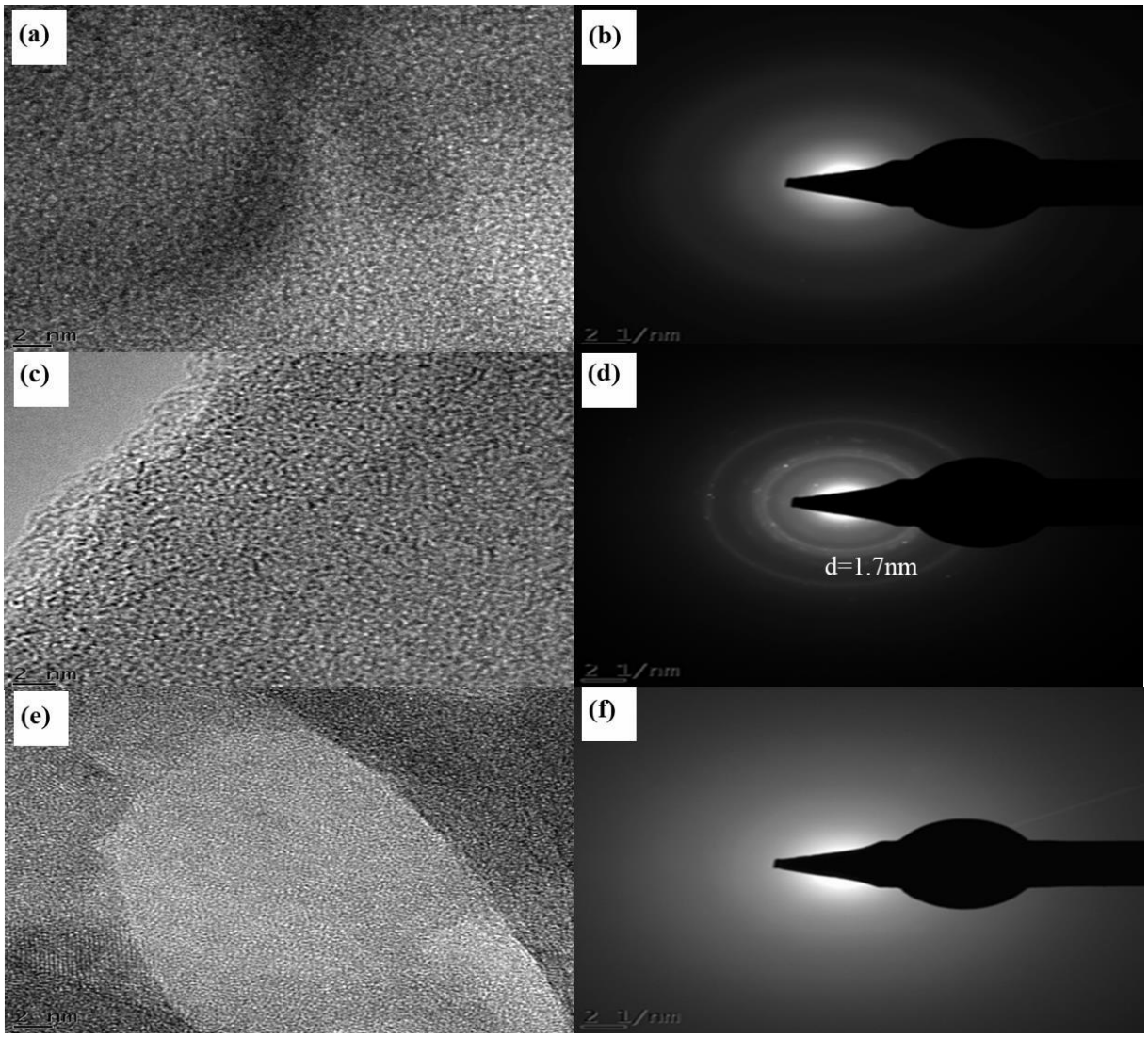

Figure 4.5: HRTEM images of (a) PANI, (c) CoZIF and (e) PANI-CoZIF composite; and SAED patterns of (b) PANI, (d) CoZIF and (f) PANI-CoZIF.

4.3.3. Electrochemistry

4.3.3.1 *Electrochemical characterisation*

The studies of Cyclic voltammetry (CV) and Square wave voltammetry (SWV) were conducted to check the redox potentials and the electrochemical behavior of PANI, CoZIF and PANI-CoZIF as presented in Figure 4.6 - 4.8. The redox process on to the bare gold electrode (TBAP-DMSO) was observed at around −0.58 V [39]. The voltammogram of PANI indicated that the type of PANI synthesised is in the emeraldine state since it is half reduced and half oxidised [19]. The anodic peak at around -0.7 V was an oxidation peak owing to the polyleucoemarldine radical cation. The redox couple at approximately -0.7 V (Ep_a) and -0.6 V (Ep_c) corresponds to the change of PANI from the reduced leucoemeraldine (LE) state to the partly oxidised emeraldine state (EM). Further oxidation of PANI caused a change from (LE) state to pernigraniline (PE) redox state of PANI, giving rise to the redox couple at around 0.7 V (Ep_a) and 0.6 V (Ep_c) [38]. The ratio of maximum anodic current (Ip_a) and the maximum cathodic current observed are symmetrical hence equal to unity shown in Table 4.1. This is the characteristic of a reversible behavior [38,39]. The CoZIF showed the anodic and cathodic peaks located at 0.35 V and 0.15 V ascribed to the redox process of Co^{2+}/Co^{3+} redox couple in the framework [40]. The introduction of CoZIF to form the composite caused an increase in the conductivity as shown by the increase in current. This could be attributed to the increased electron density around PANI [24].

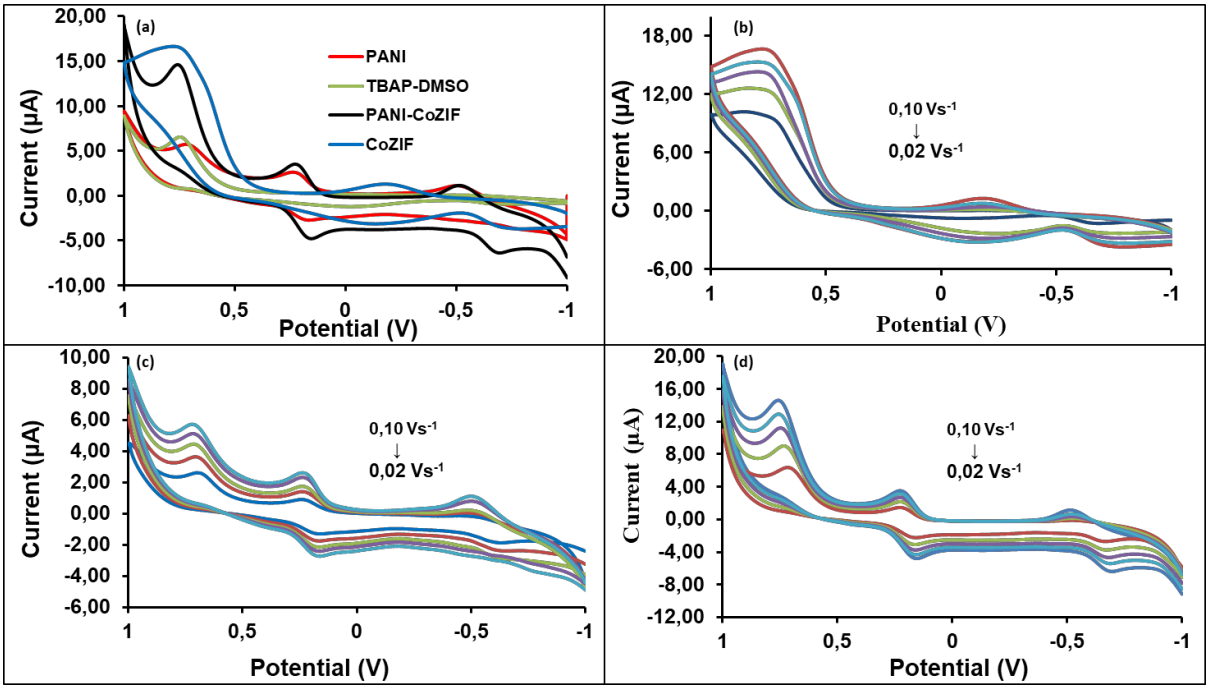

Figure 4.6: (a) CV curves of Blank, PANI, CoOZIF and PANI-CoZIF composite at 0.1 V.s-1 in 0.1 mol.L^{-1} TBAP-DMSO electrolyte on gold bare electrode. (b-d) COZIF, PANI and PANI-CoZIF respectively at various scan rates (0.02- 0.1 V.s^{-1}) in 0.1 mol.L^{-1} TBAP-DMSO.

Table 4.1: Experimental values of anodic and cathodic peak currents slope of log-log plot of the absolute value of the peak current vs scan rate, diffusion coefficients (*D*) and the anodic and cathodic peak current (Ip_a/Ip_c) ratios of CoZIF, PANI and PANI-CoZIF composite from CV and SWV.

Material	**Technique**	I_{p_a} **(A)**	I_{p_c} **(A)**	I_{p_a}/I_{p_c}	**Slope** **(A.V.s^{-1})**	***D*** **(cm^{2}.s^{-1})**	***Γ*** **(mol.cm^{-2})**
CoZIF	CV	1.29	3.9	0.33	0.31	9.92×10^{-5}	1.20×10^{-9}
	SWV	0.31	0.04	0.13	0.29	6.92×10^{-6}	3.76×10^{-6}
PANI	CV	2.65	2.62	1.00	0.35	1.55×10^{-5}	4.83×10^{-10}
	SWV	1.22	1.61	0.76	0.42	1.10×10^{-5}	8.55×10^{-7}
PANI-CoZIF	CV	4.28	3.48	1.20	0.36	8.67×10^{-5}	1.14×10^{-9}
	SWV	3.71	3.54	1.00	0.17	1.59×10^{-6}	6.10×10^{-7}

The SWV was utilised as the electrochemical analysis of the system owing to it being highly sensitive. It was used to support CV and confirm whether there were no hidden or additional redox couples on cyclic voltammetry. Therefore, as presented in Figure 4.7 (a-d) and 4.8 (a-d), it is clear that no additional redox couples are observed. Moreover, SWV confirmed reversibility of the redox couples. The effect of varying scan rates is presented in Figure 4.8 (b-d) for oxidation and Figure 4.7 (b-d) for reduction. There was an increase in current response as scan a rate increase which is in agreement with cyclic voltammetry results. PANI-CoZIF showed an enhancement in current as compared to the undoped PANI and the same findings were obtained from CV.

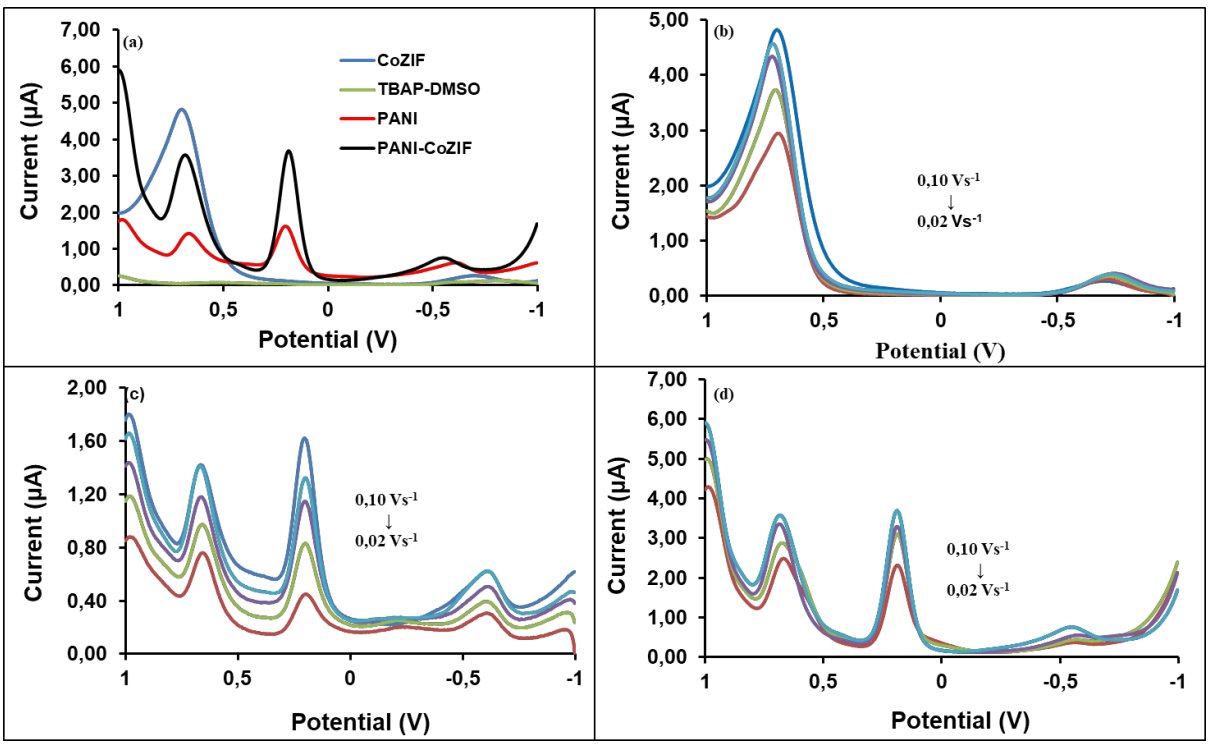

Figure 4.7: (a) SWV curves representing reduction for Blank (TBAP-DMSO), PANI, CoZIF and PANI-CoZIF composite at 0.1 $V.s^{-1}$ in 0.1 $mol.L^{-1}$ TBAP-DMSO electrolyte solution on Au electrode. (b-d) CoZIF, PANI and PANI-CoZIF respectively at various scan rates (0.02 - 0.1 $V.s^{-1}$) in 0.1 $mol.L^{-1}$ TBAP-DMSO.

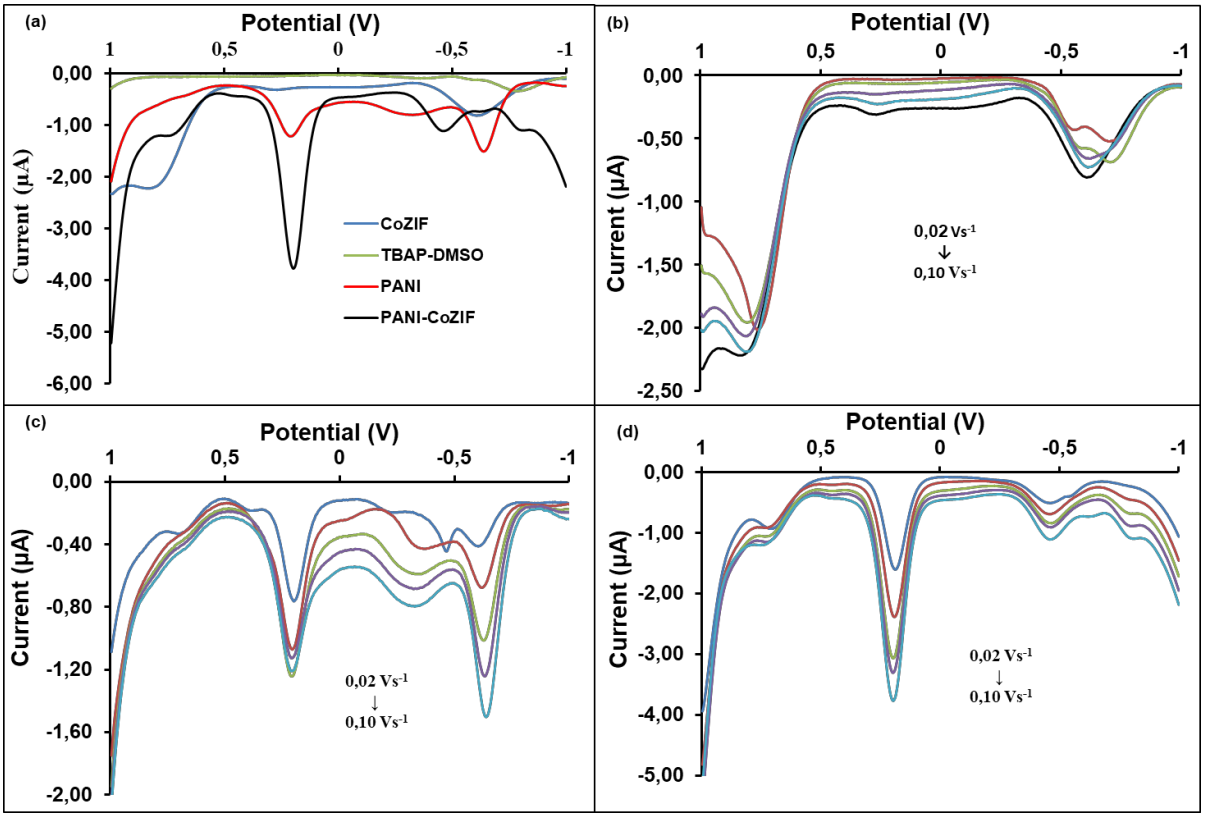

Figure 4.8: (a) SWV curves showing oxidation for TBAP-DMSO (blank), PANI, CoZIF and PANI-CoZIF composite at 0.1 $V.s^{-1}$ in 0.1 $mol.L^{-1}$ TBAP-DMSO electrolyte solution on Au electrode. (b-d) CoZIF, PANI and PANI-CoZIF respectively at various scan rates (0.02 - 0.1 $V.s^{-1}$) in 0.1 $mol.L^{-1}$ TBAP-DMSO.

The effect of scan rate on the electrochemical response of PANI, CoZIF and PANI-CoZIF composite was achieved in 0.1 M TBAP- DMSO electrolyte system and the multiscan voltammograms of the samples are shown in parts b-d of Figure 4.9, respectively. The higher the scan rates the higher the current response. The PANI-CoZIF composite showed an increase in current response in comparison to neat PANI and CoZIF at all scan rates. These results showed that both PANI and CoZIF structures in the composite were conductive and there was diffusion of electrons along the polymer chain [41]. All redox couples exhibited electrochemical reversibility. Unity of Ip_a/Ip_c ratios at all scan rates (Table 4.1) and the logarithm of the absolute value of the reductive peak current against the logarithm of the scan

rate Figure 4.9 (a,b) shows the slopes close 0.5 as an indicative of diffusion controlled characters [39] from both CV and SWV. The plot of current against the square root of scan rate was used to determine the diffusion coefficient of the materials. The diffusion coefficient, *D*, for electrocatalyst were obtained using SWV and CV following the Randles-Ševćik equation (Equation 4.3) [37].

$$Ip = (2.65x10^{5})n^{3/2}ACD^{1/2}v^{1/2} \quad (4.3)$$

The *D* values were determined to be 8.67×10^{-5}, 1.55×10^{-5} and 9.92×10^{-5} $cm^2.s^{-1}$ from CV and 6.92×10^{-6}, 1.10×10^{-6}, 1.59×10^{-6} $cm^2.s^{-1}$ from SWV for CoZIF, PANI and PANI-CoZIF, respectively (Table 4.1).

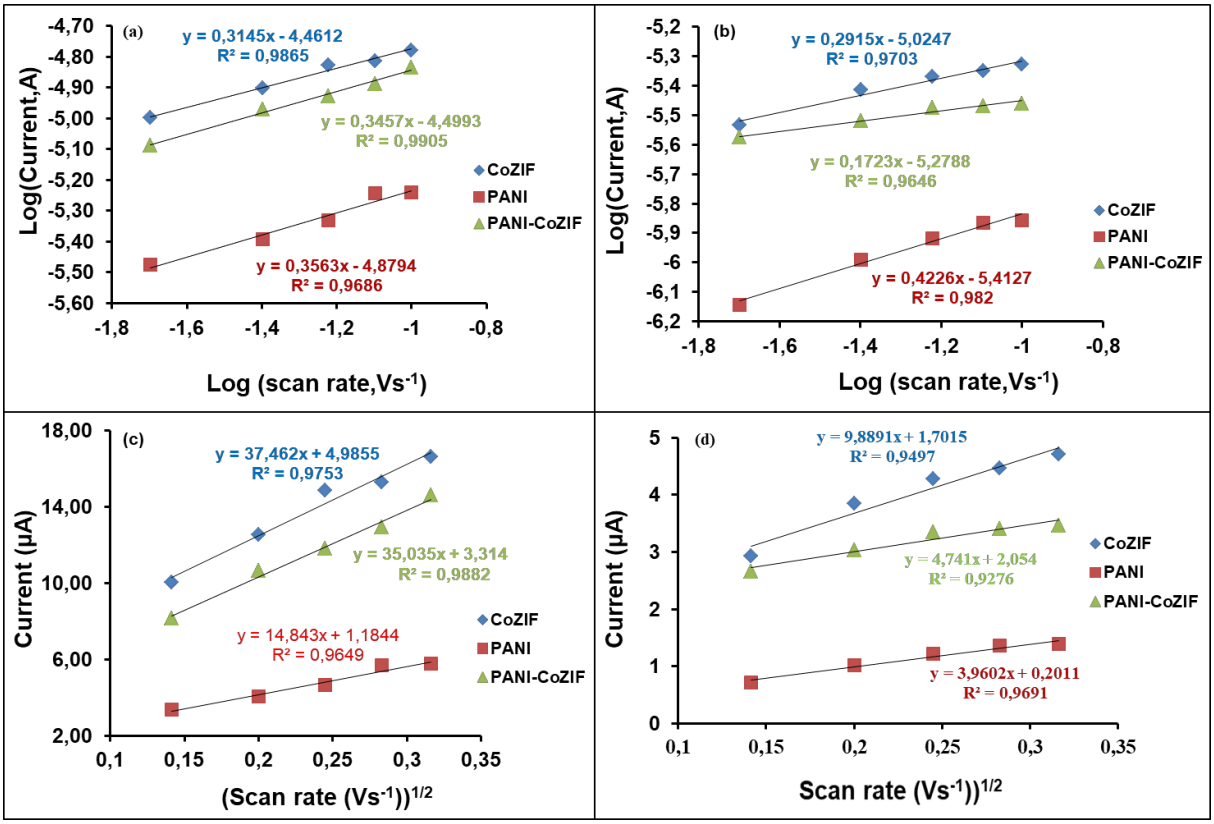

Figure 4.9: (a) CV and (b) SWV The log-log plot of the absolute value of the peak current vs scan rate and (c) CV and (d) SWV peak current against square root of scan rate on gold in 0.1 mol.L^{-1} TBAP-DMSO electrolyte system at varying scan rates (0.02– 0.10 V.s^{-1}) generated from CV and SWV respectively.

In addition, Figure 4.10 (a and b) displays the peak current as a function scan rate from cyclic voltammetry and square wave voltammetry. The peak currents are directly proportional to the scan rate, suggesting that the reaction is an adsorption- controlled [41]. The peak current were then directly related to the surface coverage (Γ) and the potential scan rate as given by Equation 4.4 [41].

$$Ip = \frac{n^2F^2\Gamma Av}{4RT} \qquad (4.4)$$

From the slope in Figure 9(a, b) the surface coverages for CoZIF, PANI and PANI-CoZIF were found to be 1.20×10^{-9}, 4.83×10^{-10} and 1.14×10^{-9} mol.cm^{-2}, respectively from CV and 3.76×10^{-6}, 8.55×10^{-7} and 6.10×10^{-7} mol.cm^{-2} from SWV (Table 4.1), which further confirm the adsorption of the material on the gold bare electrode and the process is surface controlled.

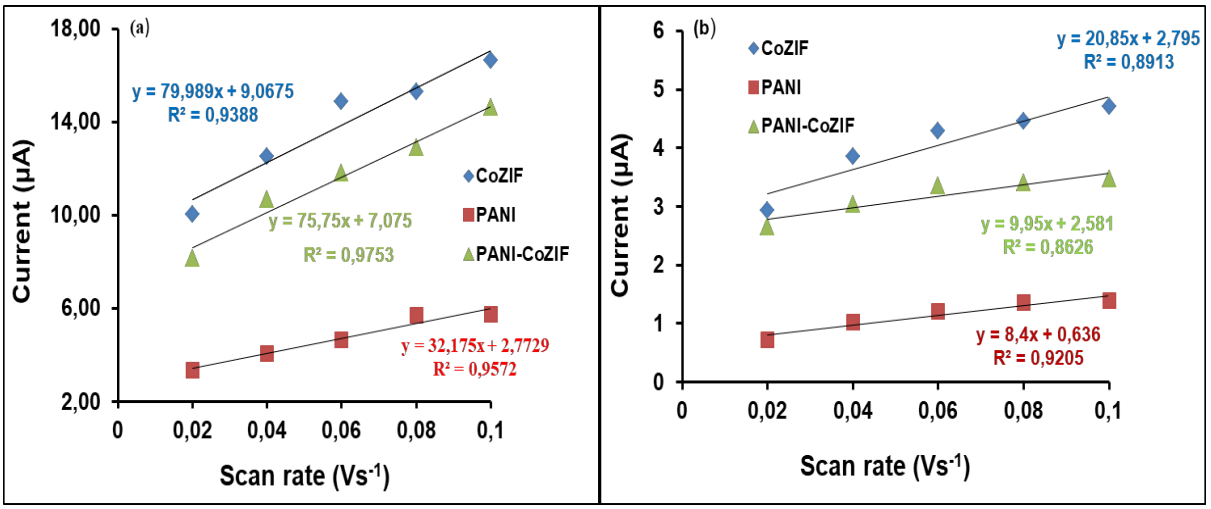

Figure 4.10: (a) CV (b) SWV peak current against scan rate for PANI, CoZIF and PANI-CoZIF on gold in 0.1 mol.L^{-1} TBAP-DMSO electrolyte system at varying scan rates (0.02 – 0.10 V.s^{-1}).

4.3.3.2. Hydrogen evolution studies

Electrocatalytic performance of PANI, CoZIF and PANI-CoZIF composites on HER was done in TBAP-DMSO electrolyte using sulphuric acid (H_2SO_4) as a hydrogen source and the findings are depicted in Figure 4.11. CV was used to determine the potential at which sulphuric acid is reduced to hydrogen gas. Hydrogen reduction peak was observed at approximately -0,9 V due to hydrogen evolution reaction [19] hence all chronoamperometric results were performed at this potential for hydrogen sensing. There is a relationship between the current intensities of the materials and the amount of hydrogen produced; thus the higher the current the larger the amount of hydrogen is produced [19]. Based on these findings the PANI-CoZIF composite

had higher current readings hence it is the best electrocatalyst for HER as compared to other materials.

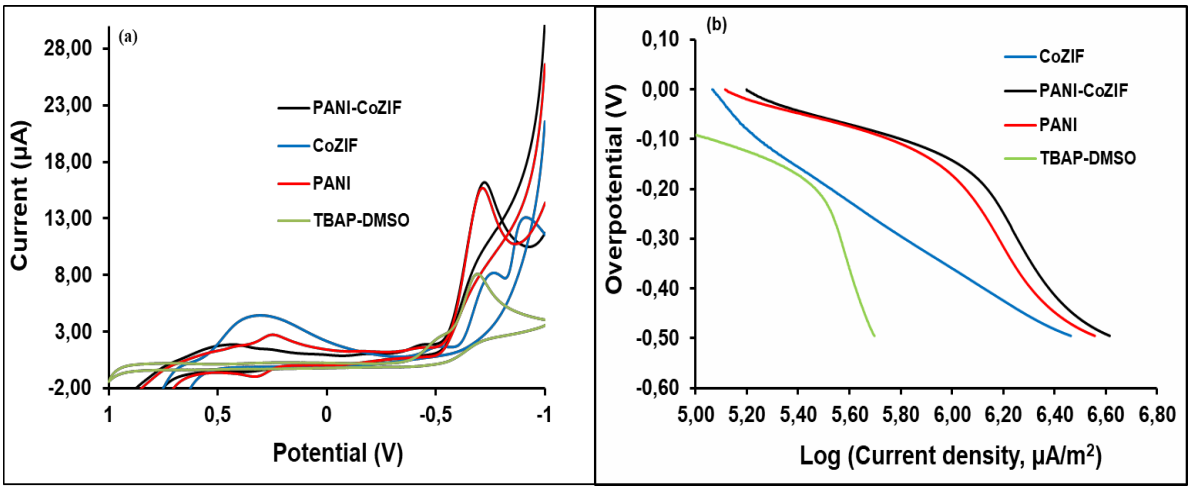

Figure 4.11: (a) CV curves (b) Tafel plots of TBAP-DMSO, CoZIF, PANI and PANI-CoZIF composite (~2.0 x 10^{-4} mol.L^{-1}) in the presence of 0.033 mol.L^{-1} H_2SO_4 at 0.10 V.s^{-1} scan rate on gold bare electrode in 0.1 mol.L^{-1} TBAP-DMSO electrolyte system.

Table 4.2: Experimental values of Tafel slope (*b*), charge transfer coefficient (1–*α*), exchange current density (i_0) and TOF of PANI, CoZIF and PANI-CoZIF composite.

Materials	**H_2SO_4 (mol.L^{-1})**	**Slope (*b*) (V.dec^{-1})**	**-*b* (mV.dec^{-1})**	**1-α**	**logi_0 (μA.m^{-2})**	**i_0 (A.m^{-2})**	**TOF (mol.H_2.s^{-1})**
Blank	0.033	-0.2414	242	0.25	5.9		
CoZIF	0.033	-03826	383	0.15	6.1	1.26	0.003
PANI	0.033	-0.1541	154	0.38	6.4	2.51	0.040
PANI-CoZIF	0.033	-0.1600	160	0.37	6.6	3.98	0.117
PANI/MOF [16]	0.075	−0.2393	239.3	0.247	0.50	3.162	-

In order to have a better understanding of a material‘s kinectics of HER and the electrochemical properties, the Tafel plots were utilised [40]. The Tafel slope value is used to convey information about the electrochemical reaction rate determining step [39]. The linear plot that displays the relationship between (overpotential) against log i_0 for blank electrode, CoZIF, PANI and PANI-CoZIF in acidic medium is presented in Figure 4.11. The Tafel plots were obtained from current density-potential data at 0.033 mol.L^{-1} acid concentration. The exchange current density, i_0 was determined from the intercept of the Tafel line with the current axis and it is related to the electrochemical surface area of the catalyst. The exchange current density i_0 gives very significant information about the performance of an electrocatalyst. In this work, the values of *b* and i_0 were estimated by linear polarisation curves and the results are shown in Table 4.2. The composite had higher exchange current density, thus the faster the reaction and better performance of this material as an electrocatalyst for HER. Moreover, Tafel plot gives information about reaction mechanism and it can be used to determine the cathodic transfer coefficient (1-α) [37]. The cathodic transfer

coefficient was calculated using region of high overpotential, wherein the Butler-Volmer equation simplifies to the Tafel equation and the Tafel slope, *b* is given by Equation 4.5:

$$b = \frac{-2.303RT}{(1-\alpha)F} \quad (4.5)$$

Previous reports explained that Tafel slopes between 105 - 150 mV.dec^{-1} indicate that Volmer is the rate determining step for HER [39]. In this communication, PANI- CoZIF composite possessed Tafel slope of 160 mV.dec^{-1} at 0.033 mol.L^{-1} H_2SO_4 as indicated in Table 4.2. From these findings it can be conferred that Volmer is the rate determining step of the composite. Furthermore, PANI showed lower Tafel slope values as compared to the composite. Moreover, the charge-transfer coefficient (α = 0.5), describes a mechanism where the rate determining step is the Volmer reaction or the Volmer reaction coupled with one of the other two reactions. Herein, the charge transfer coefficients for PANI and PANI-CoZIF composite are close to 0.5, hence Volmer is the rate determining step of HER on this work (Table 4.2). In addition, the Tafel plot gives an insight about the turnover frequency (TOF) which gives the information about the efficiency of electrocatalysts [42]. The TOF is defined as the mass of molecules reacting for a certain reaction per unit time [43] and calculated using Equation 4.6:

$$TOF = \frac{jM}{2Fm} \quad (4.6)$$

wherein *j* is the current density, M is mass percentage of materials, *F* is Faraday's constant, and m is the mass of per square centimetre of catalysts estimated from BET surface area of PANI (30.8 m^2.g^{-1}) [44] and CoZIF (413.0 m^2.g^{-1}) [45]. The TOF values for the synthesised materials are shown in the Table 4.2. The composite had higher TOF values as compared to its starting materials (Table 4.2) due to the enhancement of electronic density of the polymer backbone [16]. With all these findings, it can be concluded that PANI-CoZIF composite is a better electrocatalyst for HER and a suitable material for hydrogen sensing at -0.9 V hence the hydrogen

sensing ability of the materials was investigated using chronoamperometry at -0.9 V since it is the potential at which HER occurs and reported in Section 4.3.3.3.

4.3.3.3. Hydrogen sensing studies

The reduction kinetics of H_2SO_4 and hydrogen sensing capability of the materials were further investigated by means of chronoamperometry (CA) as depicted in Figure 4.12. Figure 4.12 (a) shows the CA curves of 0.1 $mol.L^{-1}$ TBAP-DMSO, CoZIF, PANI and PANI-CoZIF in the absence of H_2SO_4. It has been reported that CA shows better electrochemical properties of a material as compared to CV [25]. It was observed that PANI-CoZIF composite showed high current response with time as compared to neat PANI. These results are in agreement with the cyclic voltammetry
results. Figure 4.12 (b-d) display the CA curves of TBAP-DMSO, CoZIF, PANI and PANI-CoZIF in the presence of H_2SO_4 at applied potential of -0.9 V. They show that the current response increases with an increase in H_2SO_4 concentration. The current response of all the materials reaches a steady-state within 5 s, indicating the fast response [46] on hydrogen gas sensing. The composite showed high current response hence it can be concluded that the composite has better hydrogen sensing capability as compared to the undoped PANI.

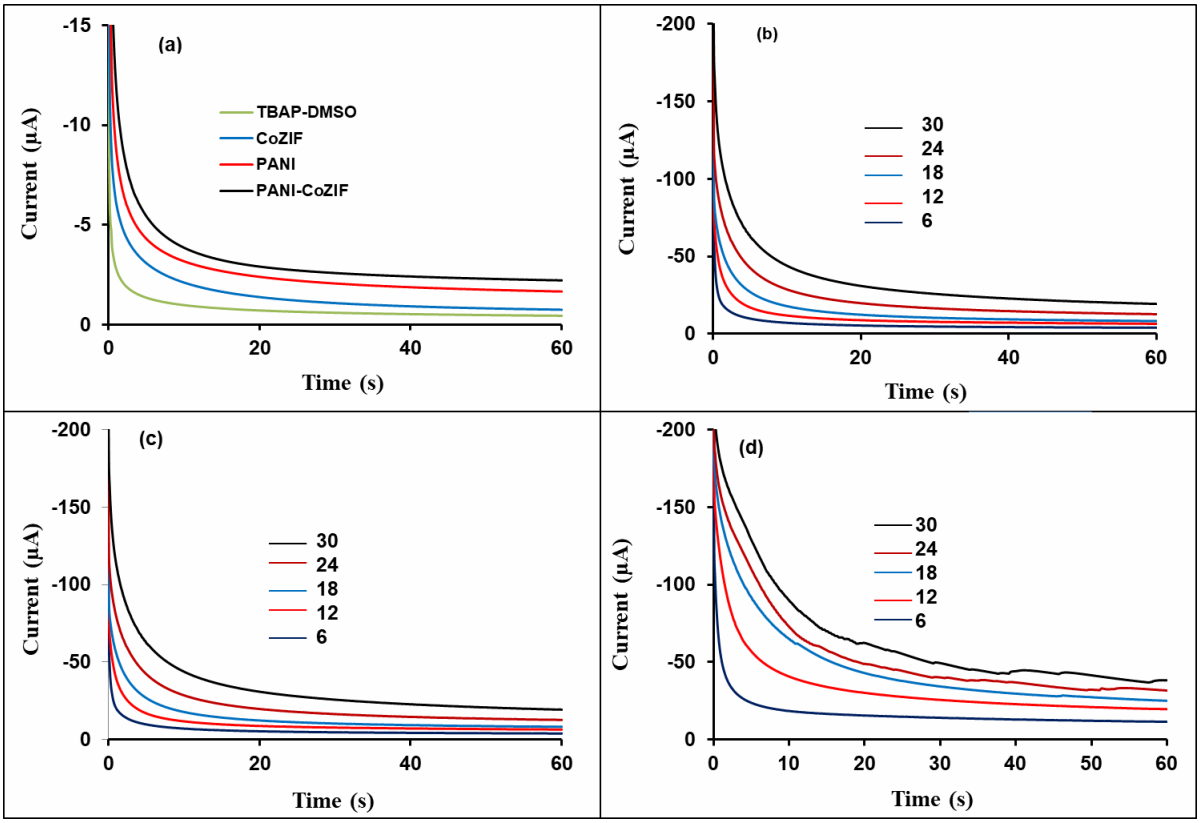

Figure 4.12: (a) Chronoamperograms for Blank, PANI, CoZIF and PANI-CoZIF composite at -0.9 V and (b-d) CoZIF, PANI and PANI-CoZIF respectively at different acid concentrations (6 – 30 $\times 10^{-4}$ mol.L^{-1}) in 0.1 mol.L^{-1} TBAP-DMSO electrolyte solution on Au bare electrode.

Figure 4.13 (a, b, c) shows current versus 1/square root of time, steady state current against PANI, CoZIF and PANI-CoZIF composites in different concentration of hydrogen source (6 – 30 $\times 10^{-4}$ mol.L^{-1} H_2SO_4) and ratio of current (presence/absence) of acid against the square root of time at -0,9 V on bare gold bare electrode in 0.1 mol.L^{-1} TBAP-DMSO as an electrolyte. Using the Cottrell Equation (Equation 4.7) [41].

$$I = nFACD^{1/2}P^{-1/2}t^{-1/2} \qquad (4.7)$$

In Figure 4.13 (a), the *D* values were found to be 0.60×10^{-4}, 1.18×10^{-4} and 2.24×10^{-4} $cm^2.s^{-1}$. From the slope of the linear plot of concentration as a function of current (Figure 4.13(b)), the sensitivity was found to be 5, 8 and 12 μAmM^{-1} for CoZIF, PANI and PANI-CoZIF respectively. Based on these results the composite showed better sensitivity, meaning it is very effective for hydrogen sensing application. The correlation coefficient (R^2) was found to be 0.95, 0.86 and 0.99 for PANI, CoZIF and PANI-CoZIF respectively. Using a signal-to-noise factor of 3 (S/N) = *LOD* (where N, S and *LOD* are the standard deviation, sensitivity and limit of detection, respectively [47], the *LOD* was calculated as 5.25, 5.19 and 5.27 µM for CoZIF, PANI and PANI-CoZIF, respectively. The limit of quantification (*LOQ* = 10×S/N) was calculated and found to be 17.5, 17.3 and 17.7 µM for CoZIF, PANI and PANI- CoZIF, respectively.

The catalytic rate constant (K_{cat}) of the materials can be calculated using Equation 4.8 [48]:

$$I_{cat}/I_L = \pi K_{cat} C_o t^{1/2} \qquad (4.8)$$

wherein I_{cat} and I_L are the catalytic and limiting currents of the materials in the presence and absence of H_2SO_4 respectively, K_{cat} is the catalytic rate constant and C_0 is the concentration of the substrate and t is the time elapsed [47]. Figure 4.13 (c) shows such plot of I_{cat}/I_L versus $t^{1/2}$ derived from the CA curves. The inset graph shows the linear region of the plot which was used to determine the K_{cat}. From the slope of I_{cat}/I_L against $t^{1/2}$, the values of K_{cat} were found to be 1.9×10^3, 6.4×10^3 and 11.9×10^3 $L.mol^{-1}s^{-1}$ for CoZIF, PANI and PANI-CoZIF respectively. PANI-CoZIF had larger catalytic constant than PANI due to a greater electrocatalytic H_2 sensitivity of the composite through HER mechanism [47].

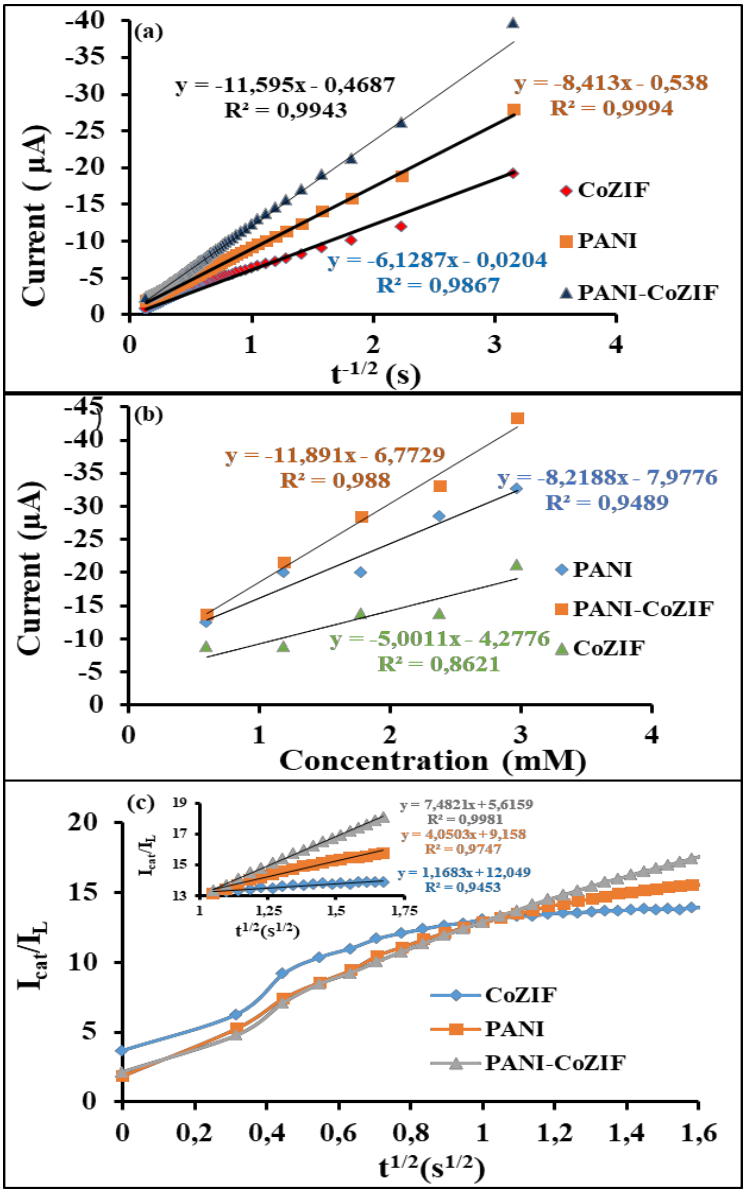

Figure 4.13: (a) Current against of 1/square root of time and (b) Steady state current against different concentrations (0.6 - 3.0 mmol.L^{-1}) of hydrogen source (H_2SO_4) and (c) calibration curve of I_{cat}/I_L versus $t^{1/2}$ at -0,9 V on gold bare electrode in 0.1 mol.L^{-1} TBAP-DMSO electrolyte system for PANI, CoZIF and PANI-CoZIF composites.

4.4. CONCLUSIONS

This workdemonstrated the synthesis of PANI-CoZIF by in-situ chemical oxidative polymerisation of PANI in the presence of CoZIF, which was employed for hydrogen sensing application through HER. FTIR and Raman spectra have proven the successful synthesis of CoZIF and PANI and PANI-CoZIF. Moreover, an increase in peak intensities upon composite formation on FTIR spectra has proven the successful synthesis of PANI-CoZIF composite. UV-Vis spectroscopy has shown the decrease in energy band gap of composite on irradiation ascribed to an increase in electron density on the polymer chains upon PANI-CoZIF composite formation. Thermal analysis revealed an enhancement in the thermal stability of PANI-CoZIF as compared to pure PANI. These results indicate that the composite can be used for high temperature application purposes. XRD study showed the amorphous structure of PANI, which is retained by the composite. Morphological characterisation using SEM and TEM revealed the grafting of CoZIF particles on the surface of PANI matrix. In addition, the composite exhibited better electrocatalytic performance for hydrogen production through HER in comparison to undoped PANI. This is due to an increase in electron density on the polymer backbone. Moreover, the Tafel slope and charge-transfer coefficients revealed that the rate determining step of Hydrogen evolution reaction on PANI-CoZIF composite is the Volmer reaction. Furthermore, the composite showed good sensitivity, fast response time and higher catalytic rate constant. These results proved that PANI-CoZIF based composite can be used as alternative electrocatalyst for hydrogen production through HER and it has a significant potential as a safety sensor during hydrogen production, storage and transportation.

4.5. REFERENCES

[1] S. Sharma and S. K. Ghoshal, “Hydrogen the future transportation fuel: From production to applications,” *Renew. Sustain. Energy Rev.*, vol. 43, pp. 1151–1158, 2015.

[2] J. Villatoro, D. Luna-Moreno, and D. Monzón-Hernández, “Optical fiber hydrogen sensor for concentrations below the lower explosive limit,” *Sens. Actuators B Chem.*, vol. 110 , pp. 23–27, 2005.

[3] G. Korotcenkov, S. Do Han, and J. R. Stetter, “Review of electrochemical hydrogen sensors,” *Chem. Rev.*, vol. 109, pp. 1402–1433, 2009.

[4] E. X. Chen, H. Yang, and J. Zhang, “Zeolitic imidazolate framework as formaldehyde gas sensor,” *Inorg. Chem.*, vol. 53, pp. 5411–5413, 2014.

[5] P. C. Chou., “Hydrogen sensing performance of a nickel oxide (NiO) thin film-based device,” *Int. J. Hydrogen Energy*, vol. 40, pp. 729–734, 2015.

[6] S. Nasirian and S. Yaser, “Hydrogen gas sensing performance of polyaniline/titania/nickel oxide nanocomposite at room temperature,” *Mater. Sci. Eng. B*, vol. 224, pp. 40–47, 2017.

[7] A. Z. Sadek and W. Wlodarski, “Doped and dedoped polyaniline nanofiber based conductometric hydrogen gas sensors,” *Sens. Actuators A*, vol. 139, pp. 53–57, 2007.

[8] A. M. More, H. J. Sharma, S. B. Kondawar, and S. P. Dongre, “Ag-SnO_2/Polyaniline composite nanofibers for low operating temperature hydrogen gas sensor,” *Mater. Nanosci.*, vol. 4, pp. 13–18, 2017.

[9] Y. Z. Long., “Recent advances in synthesis, physical properties and applications of conducting polymer nanotubes and nanofibers,” *Prog. Polym. Sci.*, vol. 36, pp. 1415–1442, 2011.

[10] S. Nasirian and H. Milani Moghaddam, “Hydrogen gas sensing based on polyaniline/anatase titania nanocomposite,” *Int. J. Hydrogen Energy*, vol. 39, pp. 630–642, 2014.

[11] H. J. Sharma, N. D. Sonwane, and S. B. Kondawar, “Electrospun

SnO_2/Polyaniline composite nanofibers based low temperature hydrogen gas sensor," *Fibers Polym.*, vol. 16, pp. 1527–1532, 2015.

[12] A. F. Mansour, A. Elfalaky, and F. A. Maged, "Synthesis, Characterization and optical properties of PANI/PVA blends," *IOSR J. Appl. Phys.*, vol. 7, pp. 37–45, 2015.

[13] G. Lu and J. T. Hupp, "Metal Organic Franeworks as Sensors A ZIF-8 Based Fabry Perot Device as a Selective Sensor for Chemical Vapours and Gases," *J. Am. Chem. Soc.*, vol. 132, pp. 7832–7833, 2010.

[14] Q. Li and H. Kim, "Hydrogen production from NaBH 4 hydrolysis via Co-ZIF-9 catalyst," *Fuel Process. Technol.*, vol. 100, pp. 43–48, 2012.

[15] B. Assfour, S. Leoni, S. Yurchenko, and G. Seifert, "Hydrogen storage in zeolite imidazolate frameworks. A multiscale theoretical investigation," *Int. J. Hydrogen Energy.*, vol. 36, pp. 6005–6013, 2011.

[16] K. E. Ramohlola, G.R Monanaa, M.J. Hato, K.D. Modibane, K.M. Molapo, M. Masikini, S.B. Mduli, E. I. Iwuoha , "Polyaniline-metal organic framework nanocomposite as an effi cient electrocatalyst for hydrogen evolution reaction," *Compos. Part B*, vol. 137, pp. 129–139, 2018.

[17] J. Qian, F. Sun, and L. Qin, "Hydrothermal synthesis of zeolitic imidazolate framework-67 (ZIF-67) nanocrystals," *Mater. Lett.*, vol. 82, pp. 220–223, 2012.

[18] S. Patra and N. Munichandraiah, "Insoluble poly(anthranilic acid) confined in Nafion membrane by chemical and electrochemical polymerization of anthranilic acid," *Synth. Met.*, vol. 150, pp. 285–290, 2005.

[19] K. E. Ramohlola, M. Masikini, S.B. Mdluli, G.R. Monama, M.J. Hato, K.M. Molapo, E.I. Iwuoha, K.D. Modibane, "Electrocatalytic hydrogen production properties of polyaniline doped with metal-organic frameworks," *Electrochim. Acta.*, pp. 373–389, 2017.

[20] Y. Huang, D. Liu, Z. Liu, and C. Zhong, "Synthesis of zeolitic imidazolate framework membrane using temperature-switching synthesis strategy for gas separation," *Ind. Eng. Chem. Res.*, vol. 55, pp. 7164–7170, 2016.

[21] A. Abdolahi, E. Hamzah, Z. Ibrahim, and S. Hashim, "Synthesis of uniform

polyaniline nanofibers through interfacial polymerization," *Materials (Basel).*, vol. 5, pp. 1487–1494, 2012.

[22] M. Trchová, Z. Morávková, M. Bláha, and J. Stejskal, " Raman spectroscopy of polyaniline and oligoaniline thin films," *Electrochim. Acta*, vol. 122, pp. 28–38, 2014.

[23] G. M. Nascimento, J. E. P. Silva, S. I. Co, and D. Torresi, "Comparison of secondary doping and thermal treatment in poly(diphenylamine) and polyaniline monitored by resonance Raman spectroscopy," *Macromolecules,* pp. 121–125, 2002.

[24] K. A. Ibrahim, "Synthesis and characterization of polyaniline and poly (aniline-co-o-nitroaniline) using vibrational spectroscopy," *Arab. J. Chem.*, vol. 10, pp. 2668–2674, 2017.

[25] M. Grzeszczuk, A. Grańska, R. Szostak, and F. Chemistry, "Raman spectroelectrochemistry of polyaniline synthesized using different electrolytic regimes – multivariate analysis," *Int. J. Electrochem. Sci*., vol. 8, pp. 8951– 8965, 2013.

[26] S. Tharani and S. C. Vinayagam, "Synthesis of novel cerium doped polyaniline multiwalled carbon nanotubes and their optical and electrochemical properties for supercapacitor applications," *Phys. Rev*., vol. 3, pp. 810–822, 2015.

[27] J. Li, D. Luo, C. Yang, S. He, S. Chen, and J. Lin, "Copper (II) imidazolate frameworks as highly effi cient photocatalysts for reduction of CO_2 into methanol under visible light irradiation," *J. Solid State Chem.*, vol. 203, pp. 154–159, 2013.

[28] H. S. Abdulla and A. I. Abbo, "Optical and Electrical Properties of Thin Films of Polyaniline and Polypyrrole," I*nt. J. Electrochem. Sci.*, vol. 7, pp. 10666– 10678, 2012.

[29] K. T. Butler, S.D. Worrall, C.D. Molloy , C.H. Hendon, M.P. Attfield , R.A. W. Dryfe and A. Walsh , "Electronic structure design for nanoporous , electrically conductive zeolitic imidazolate frameworks ," *J. Mater. Chem.*, vol. 5, pp. 7726–7731, 2017.

[30] S. Yan, S. Ouyang, H. Xu, M. Zhao, X. Zhanga and J. Ye, "Co-ZIF-9/TiO_2

nanostructure for superior CO_2 photoreduction activity," *J. Mater. Chem*., vol. 4, pp. 15126–15133, 2016.

[31] S. M. Hu, H.L Niu, L.G. Qiu, Y.P. Yuan, X. Jiang, A.J. Xio, Y.H,Shen and J.F. Zhu, "Facile synthesis of highly luminescent nanowires of a terbium-based metal-organic framework by an ultrasonic-assisted method and their application as a luminescent probe for selective sensing of organoamines," *Inorg. Chem. Commun.*, vol. 17, pp. 147–150, 2012.

[32] A. Singhania, V. V. Krishnan, A. N. Bhaskarwar, B. Bhargava, and D. Parvatalu, "Hydrogen-iodide decomposition over Pd–CeO_2 nanocatalyst for hydrogen production in sulfur-iodine thermochemical cycle," *Int. J. Hydrogen Energy*, vol. 43, pp. 3886–3891, 2018.

[33] L. T. L. Nguyen, K. K. A. Le, H. X. Truong, and N. T. S. Phan, "Metal–organic frameworks for catalysis : the Knoevenagel reaction using zeolite imidazolate framework ZIF-9 as an efficient heterogeneous catalyst,"*Catal.Sci.Technol*, vol. 2, pp. 521–528, 2012.

[34] J. E. P. Silva, D. L. A. De Faria, S. I. Co, and D. Torresi, "Influence of thermal treatment on doped polyaniline studied by resonance Raman spectroscopy," *Macro. Lett*., vol. 33, pp. 3077–3083, 2000.

[35] J. Bhadra, N. J. Al-thani, S. Karmakar, and N. K. Madi, "Photo-reduced route of polyaniline nanofiber synthesis with embedded silver nanoparticles," *Arab. J. Chem.*, vol 36, pp. 1–13, 2016.

[36] J. Dai, S. Xiao, J. Liu, J. He, J. Lei, and L. Wang, "Fabrication of ZIF-9@super-macroporous microsphere for adsorptive removal of Congo red from water ," *RSC Adv.*, vol. 7, pp. 6288–6296, 2017.

[37] K. E. Ramohlola, M. Masikini, S. B. Mdluli, and G. R. Monama, M. J. Hato, K. M. Molapo, E.I. Iwuoha, K.D. Modibane "Electrocatalytic Hydrogen Production Properties of Poly (3-aminobenzoic acid) doped with Metal Organic Frameworks," *Int. J. Electrochem. Sc*i, vol. 12, pp. 4392–4405, 2017.

[38] D. K. Mahla, S. Bhandari, and M. Rahaman, "Morphology and cyclic voltammetry analysis of in situ polymerized polyaniline / graphene composites," *J. Electrochem .Sci. Eng*, vol. 3, pp. 157–166, 2013.

[39] G. R. Monama, S.B. Mdluli , G. Mashao, M.D. Makhafola, K.E. Ramohlola, K.M. Molapo , M.J. Hato , K. Makgopa , E.I. Iwuoha , K.D. Modibane., “Palladium deposition on copper (II) phthalocyanine / metal organic framework composite and electrocatalytic activity of the modifi ed electrode towards the hydrogen evolution reaction,” *Renew. Energy*, vol. 119, pp. 62–72, 2018.

[40] D. Zhang, J. Zhang, H. Bai, R. Zhang, H. Shi, and B. Yuan, “ZIF-9 with Enhanced Surpercapacitor and Electrocatalytic for Oxygen Evolution Reaction Performances in Alkaline Electrolyte,” *Int. J. Electrochem. Sci.*, vol. 11, pp. 7519–7526, 2016.

[41] H. R. Zare, N. Nasirizadeh, and M. M. Ardakani, “Electrochemical properties of a tetrabromo- p -benzoquinone modified carbon paste electrode . Application to the simultaneous determination of ascorbic acid , dopamine and uric acid,” *J. Electroanal. Chem.,* vol. 577, pp. 25–33, 2005.

[42] J. Zakzeski, D. Agnieszka, P. C. A. Bruijnincx, and B. M. Weckhuysen, “General Catalytic oxidation of aromatic oxygenates by the heterogeneous catalyst,” *Appl. Catal* ., vol. 394, pp. 79–85, 2011.

[43] C. Costentin, S. Drouet, M. Robert, and J. Save, “Turnover Numbers, Turnover Frequencies, and Overpotential in Molecular Catalysis of Electrochemical Reactions. Cyclic Voltammetry and Preparative-Scale Electrolysis,” *J. Am.Chem*. Soc., vol. 134, pp. 11235-11242, 2012.

[44] M. V Lebedeva, A. B. Ayupov, P. M. Yeletsky, and V. N. Parmon, “Rice Husk Derived Activated Carbon / Polyaniline Composites As Active Materials For Supercapacitors,” I*nt. J. Electrochem. Sci.*, vol. 13, pp. 3674–3690, 2018.

[45] J. Dai, S. Xiao, J. Liu, J. He, J. Lei, and L. Wang, “Synthesis of novel microporous nanocomposites of ZIF-8 on multiwalled carbon nanotubes for adsorptive removing benzoic acid from water” *J. Chem. Eng*, vol. 331, pp. 64-74, 2017.

[46] M.H.P. Azar, H.R. Nerbin, “Electrocatalytic characteristics of ascorbic acid oxidation at nickel plated aluminum electrodes modified with nickel pentacyanonitrosylferrate films,” *J. Electroanal. Chem.,* vol. 488, pp. 17–24,

2000.

[47] D. Yin, J. Liu, X. Bo, M. Li, and L. Guo, “Porphyrinic metal-organic framework / macroporous carbon composites for electrocatalytic applications,” *Electrochim. Acta*, vol. 247, pp. 41–49, 2017.

[48] A. S. Adekunle, O. S. Oluwafemi, V. Ncapayi, and R. E. Sadiku, “Ethanol Sensor Based On Platinum-MWCNT-NiO Nanoparticles Platform Electrode,” *Int. J. Electrochem. Sci.*, vol. 7, pp. 2695–2709, 2012.

CHAPTER FIVE

FABRICATION OF POLYANILINE DECORATED WITH ZINC BASED ZEOLITIC BENZIMIDAZOLATE FRAMEWORK NANOCOMPOSITE AS AN EFFECTIVE ELECTROCATALYST FOR HYDROGEN GAS SENSING APPLICATION

This chapter was submitted for possible publication in *Materials Chemistry and Physics (revised manuscript is under review with provisional acceptance).*

CHAPTER SUMMARY

Herein, we report on the *in-situ* chemical polymerisation of PANI doped with zinc based zeolitic benzimidazolate framework denoted as PANI-ZnZIF (ZIF-7) composite for electrochemical hydrogen gas sensing. Both FTIR and Raman studies of PANI- ZnZIF composite revealed the presence of functional groups corresponding to both ZnZIF and PANI. XRD and STA analyses showed the co-existence of both PANI and ZnZIF in the composite supported by the decrease in crystallite size and the improvement in the thermal stability, respectively. The SEM/EDX, TEM/EDS, HR- TEM/SAED revealed that PANI nanofibers are wrapping the cube nanofiber-like structures of ZnZIF. The SWV, CV and CA presented good electrochemical performance indicated by an increase in current response with 3.6 wt.% loading of ZnZIF. The high electrochemical current response is due to extraordinary specific surface area, more accessible active sites available for the electrolyte provided by ZnZIF and high conductivity supplied by PANI. Moreover, Tafel parameters and TOF values derived from CV showed an improvement in the catalytic hydrogen evolution of PANI-ZnZIF composite. The resulting PANI-ZnZIF composite was found to be highly responsive to hydrogen gas indicated by higher current response and sensitivity (10.8 $\mu A.mmol.L^{-1}$ H_2), faster steady state response time (4 s) accompanied by lower detection limit (5.27 $\mu mol.L^{-1}$) as compared to pure PANI.

Therefore, the composite has a potential as an electrocatalyst for hydrogen gas sensing application.

5.1. INTRODUCTION

Exploring hydrogen as an energy carrier to replace traditional fossil fuel- based energy sources has been a hot topic over the past years owing to its renewability, recyclability, and free pollution [1,2]. However, during utilisation, hydrogen gas can be easily ignited if its concentration in air is above 4 wt.% [2]. Thus, hydrogen safety sensors are vital to guarantee safety of people in the hydrogen infrastructure [3]. A broad range of sensing methods exist to detect hydrogen gas which include thermal conduction, electrochemical and catalytic technologies [3]. An effective sensing method to reach the target set by Department of Energy of the United States is required. They set a target that the sensor must have the measuring range between
0.1 to 10%, operating temperature of -30 to 80 °C and response time of less than 1s [4]. Among the above mentioned methods, electrochemical gas sensors demonstrated the capability to sense low concentration (ppm level) of hydrogen gas and does not require heating [5].

As mentioned in the previous chapters, a number of conducting polymers including PANI have been studied extensively for gas sensing applications due to their fascinating properties [6,7]. Some of these polymers such as PPY have some suffers from longer response time, lack of adsorption-desorption reversibility and poor sensitivity which can hamper its wide application as a gas sensing material [7]. Thus, PANI particularly as half-reduced emeraldine form has been exploited as an excellent tool for hydrogen gas sensing application due to its exceptional electrical conducting, environmental stability and unique acid/base doping process as compared to other CPs [5,8]. However, its wide application in H_2 sensing is limited due to its insoluble nature in most organic solvents [9], poor sensitivity and selectivity towards gas species as compared to metals and metal oxides [5]. Onn the other hand, it was reported that hybridisation or composite formation of polyaniline with other materials such as metals, carbonaceous materials and metal oxide semiconductors can improve selectivity, sensitivity as well as processibility [3,6,10]. For example, Willis and Haron [5] fabricated a hydrogen gas sensor based on PANI/ZnO composite doped with Pd wherein this metal was used to enhance the selectivity of the composite towards hydrogen gas. In another report by Al-mashat *et*

al. [11] graphene/PANI nanocomposite was designed for hydrogen sensing and the composite showed better sensitivity (i.e. 16.57%) towards 1% of hydrogen as compared to graphene sheets and PANI nanofibers alone. Furthermore, Do and the co-authors [3] designed an amperometric hydrogen gas sensor (10-10,000 ppm H_2) based on Nafion®(5.7 µm)/Pt/nsPANi/Au/Al_2O_3 sensing electrode with a Pt loading of 1.87 mg and obtained response time and specific sensitivity of 100-250 s and 338.50 mA ppm^{-1} g^{-1}, respectively. Recently, Yuan and Liu [12] incorporated ZIF-8 into PANI backbone to produce a novel nanocomposite for electrochemical determination of dopamine. The nanocomposite exhibited better electrocatalytic performance towards dopamine due to excellent electrocatalytic activity and larger surface area of ZIF-8 and exceptional electric conductivity of PANI [12,13]. ZIF has ultrahigh surface area, high crystallinity, abundant functionalities and exceptional thermal and chemical stabilities which have led to its usage in a wide range of potential applications such as gas separation, catalysis, sensing and drug delivery in the past years [13,14]. Motivated by previously reported literature, this work reports for the first time the synthesis and characterisation of PANI based zinc benzimidazolate framework composite nanofiber denoted as PANI-ZnZIF (ZIF-7) for electrochemical hydrogen gas. The prepared PANI-ZnZIF nanofiber demonstrated to possess good electrochemical behavior towards hydrogen gas detection through hydrogen evolution reaction with high sensitivity, fast response time, low detection limit and high diffusion coefficient.

5.2. EXPERIMENTAL SECTION

5.2.1. Materials

Methanol (CH_3OH), absolute ethanol (C_2H_5OH), zinc chloride ($ZnCl_2$), tetrabutylammonium percholate (TBAP) and benzimidazole ($C_7H_6N_2$) (BIZ) were all procured from Merck. Ammonium persulfate (APS) and iron chloride ($FeCl_3$) were purchased from Riedel-de Haen and Educhem, respectively. Aniline was acquired from Sigma Aldrich and it was distilled before use. Hydrochloric acid (HCl), dimethyl sulfoxide (DMSO) and sulphuric acid (H_2SO_4) were obtained from Rochelle

chemicals. Sulphuric acid was used to prepare standard solutions, prepared in DMSO solution and 0.1 mol.L^{-1} TBAP as a supporting electrolyte system.

5.2.2. Methods

5.2.2.1. Synthesis of PANI, ZnZIF and PANI-ZnZIF composite

PANI was synthesised as per discussion given in chapter 4 [15] (see supporting information). ZnZIF (ZIF-7) was synthesised as described by Quan *et al*. [16] (see supporting information) with some a modification wherein methanol and benzimidazole (BIZ) were used as a solvent and linker, respectively. PANI-ZnZIF composite was prepared by following a reported procedure by Ramohlola *et al*. [15] with some modification, whereby MOF was replaced by ZnZIF .

5.2.2.2. Characterisations

The functional group determination and composite formation in the wave number range between 400-4500 cm^{-1} were achieved at room temperature using Spectrum II Perkin-Elmer and about 32 scans were collected at a resolution of 4 cm^{-1}. Raman spectroscopy measurements were achieved with a Horiba Jobin-Yvon Labram HR 2000 confocal using a clean SiO_2/Si substrate. The synthesised materials were characterised by X-ray diffraction (XRD) using a system XRD Phillip (CuK_α radiation, λ = 1.5406 Å) operated at 1830 W power. The STA thermal analysis measurements of samples ranging from 1 - 4 mg at a heating temperature (30-500 °C) and heating rate (20 °C.$min^{-1)}$ under inert atmosphere were performed by employing STA Perkin-Elmer 6000 model adsorption analyser. Transmission electron microscopy (TEM) coupled with EDX and Scanning Electron Microscopy (SEM) coupled EDS were recorded with FEI Tecnai G2 20 transmission electron microscope at 200 kV and Auriga Field Emmision Scanning Electron Microscope. Electrochemical experiments were conducted on EPSILON electrochemical workstation containing three-electrodes: a Pt electrode and gold electrode with the diameter of 3 mm and area of 0.071 cm^2 as the working and auxiliary electrodes, respectively, and Ag/AgCl electrode as the reference electrode. Electrochemical analysis were measured at 22

± 2 °C controlled by water bath. The multiscans of solutions of the synthesised materials (2.0×10^{-4} mol.L^{-1}) in 10 mL of 0.1 mol.L^{-1} TBAP-DMSO electrolyte were obtained at a potential window in the range between -1.0 to 1.0 V and scan rate of 0.02 - 0.10 V.s^{-1}. Hydrogen evolution reaction and hydrogen gas sensing were conducted in TBAP-DMSO electrolyte using ZnZIF, PANI and PANI-ZnZIF (2.0×10^{-4} mol.L^{-1}) as electrocatalysts or sensing electrode and 0.033 mol.L^{-1} of H_2SO_4 (HER) and 0.6 to 3.0×10^{-3} mol.L^{-1} H_2SO_4 (hydrogen sensing) as the proton source.

5.3. RESULTS AND DISCUSSION

5.3.1. Spectroscopic and physical characterisations

Figure 5.1 shows the FTIR, Raman, XRD pattern and STA curves (TGA and DSC) of the synthesised materials. FTIR was recorded to compare the as-synthesised ZnZIF (ZIF-7) results and its precursors ($ZnCl_2$ and benzimidazole, BIZ), as shown in Figure 5.1 (a), the BIZ ligand showed vibrations at about 1200, 1640 and 3050 cm^{-1} corresponding to C-N, C=C and C-H, respectively. It was shown by Huang *et al*. [17] that BIZ organic ligand possesses the C-H vibration stretch at about 3100-3000 cm^{-1}, C=C stretch at around 1600-1500 cm^{-1} and a strong N-H peak at approximately 3500-2500 cm^{-1}. The broad peak resonating at 3200 cm^{-1} was ascribed to N-H of the ligand and this peak disappeared when ZnZIF was formed. Meanwhile, the FTIR spectra of ZnZIF displayed the characteristic Zn−N peak at around 3050 cm^{-1}. These results show that BIZ organic ligand was entirely deprotonated upon crystallisation and it signifies the successful synthesis of ZnZIF [17].

In order to confirm composite formation, the FTIR spectra of PANI, ZnZIF and PANI-ZnZIF are presented in Figure 5.1(b). PANI and PANI-ZnZIF exhibit characteristic peaks at 780 and 1000 cm^{-1} corresponding to C-H out of plane bending vibration and C-H in-plane bonding of the para-disubstituted benzene rings, respectively [18]. The peaks at 1300 and 2000 cm^{-1} were assigned to C-N stretch of benzenoid and quinoid rings, respectively [18]. Furthermore, the bands at 2550 and 3350 cm^{-1} were attributed to the C-H stretch and N-H bonding of polyaniline which are in agreement with Geng *et al*. [19]. The existence of benzenoid and quinoid peaks indicates clearly

that the synthesised PANI consists of amine and imine units thus this PANI is in its emeraldine form [15,20]. Furthermore, to reveal the type of interaction between PANI and ZnZIF, we discuss the changes of the spectrum of pure PANI and ZnZIF upon forming the composite. The resultant PANI-ZnZIF composite retained PANI characteristic peaks and presented an increase in the aromaticity, which proved that both ZnZIF and PANI are co-existing in the composite.

The co-existence of PANI and ZnZIF in the composite was further analysed by employing Raman spectroscopy as shown in Figure 5.1(c). The main contributions of the ZnZIF spectrum primarily come from the vibrational modes of the benzimidazole organic linker [21]. ZnZIF spectrum exhibited organic linker prominent peak at about 1210 cm^{-1} attributed to C=C bond of the benzene ring [21]. Moreover, the C-H bending vibrations of the ring resonated at around 611 and 812 cm^{-1}. Tanaka *et al*.

[22] assigned the peak which appears at approximately 282 cm^{-1} to Zn-N using methyl imidazole as the organic linker. However, in this work the peak shifted to 500 cm^{-1} which might be due to the presence of benzimidazole linker instead of methyl imidazole. Spectrum of PANI exhibited a peak at about 1001 cm^{-1} as an indicative of a successful synthesis of conductive PANI [23]. The spectrum of PANI- ZnZIF confirmed the incorporation of ZnZIF indicated by the presence of Zn-N peak at approximately 551 cm^{-1} [22]. Furthermore, there was a drastic enhancement in the peak intensities upon composite formation.

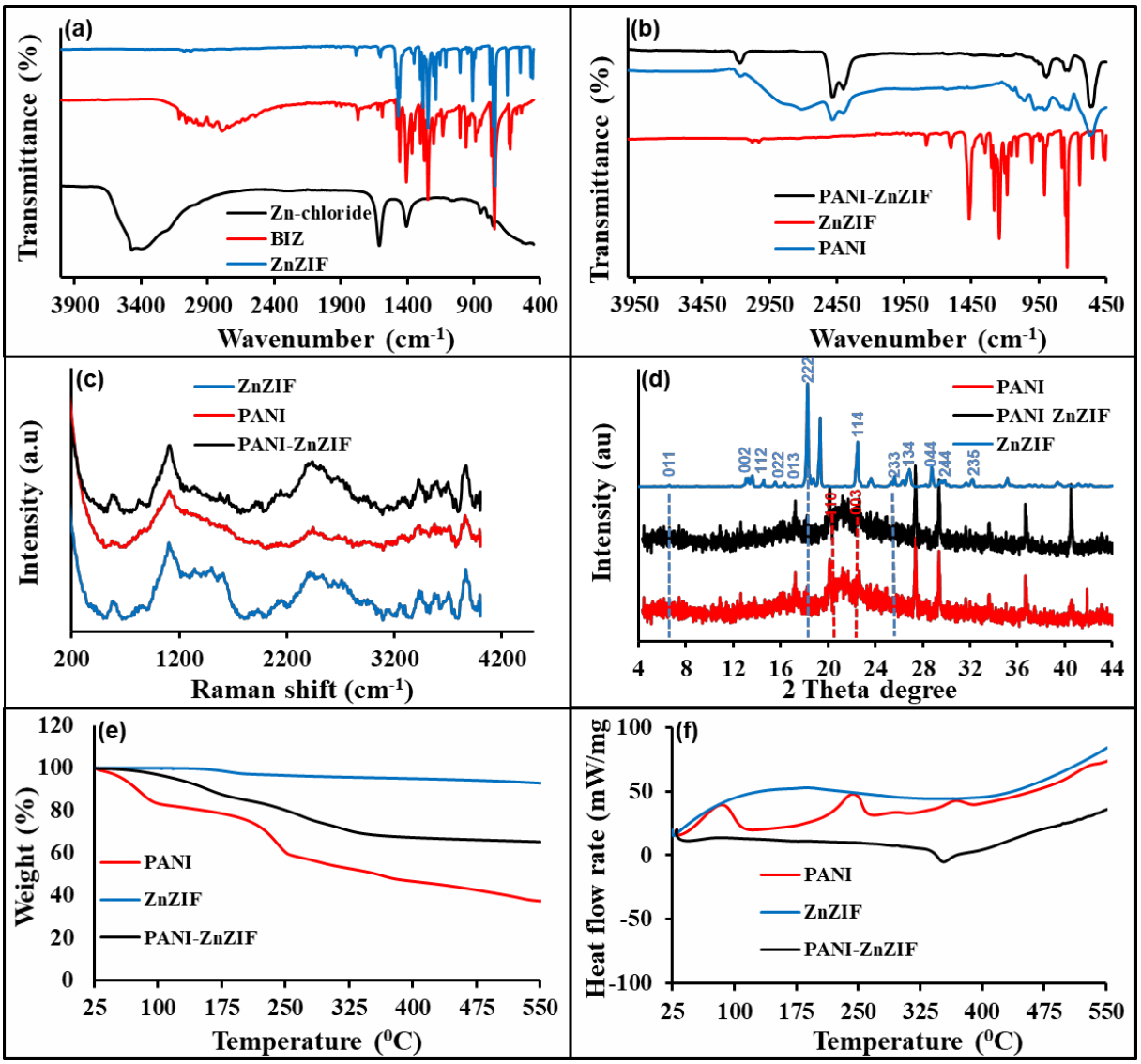

Figure 5.1: (a) FTIR spectra of $ZnCl_2$, BIM and as synthesised ZnZIF (b) FTIR, (c) Raman spectra (d) XRD pattern (e) TGA and (f) DSC thermograms for PANI, ZnZIF, and PANI-ZnZIF composite

XRD was employed to examine the diffraction phases and interplaner *d*-spacing of the synthesised PANI, ZnZIF and PANI-ZnZIF composite, and the results are depicted in Figure 5.1(d). The recorded pattern for ZnZIF matches well with reported data by Li *et al*. [24] The XRD shows pure ZnZIF phases which are crystalline [25]. The diffraction peak that appeared at 2θ angle values of 6.88° for ZnZIF, which accounts for the reflection (011), was used to determine the interplanar *d*-spacing value of 1.28 nm (estimated using Bragg's equation: $n\lambda = 2d\sin\theta$ [26] where n, λ and θ are the integer, wavelength and Bragg's angle, respectively).

The XRD pattern of PANI displays broad peaks at around 2θ = 21 and 23° corresponding to (100) and (110) reflections of polyaniline, respectively [19,20]. These results show that PANI was synthesised in its amorphous state and the results are in accordance with the previous reports in JCPDS file no 53-1717 [23]. The *d*-spacing of PANI was found to be 0.4 nm at 2θ angle of 21° accounting for
(100) reflection. The crystallite size of PANI was calculated from the peak width using Debye Scherrer's equation [27] (Equation 5.1), given by

$$D = \frac{k\lambda}{\beta \cos\theta} \quad (5.1)$$

Wherein, k = 0.9, λ is the CuK_α radiation wavelength (1.5406 A), β is the full width at half maximum in radians, θ is the Bragg's angle [20]. From the above mentioned equation the crystallite size was found to be 3.22 nm at 2θ angle of 21°.

Bhanvase *et al.* studied the XRD phases of PANI/$ZnMoO_4$ (ZM) nanocomposite prepared by ultrasound assisted synthesis to improve PANI anticorrosion and physico-chemical properties [20]. The diffraction peaks of PANI in the PANI/ZM nanocomposite shifted slightly and broadened as compared to neat PANI upon the incorporation of ZM nanoparticles [20]. In our work , in situ oxidative polymerisation of PANI in the presence of ZnZIF caused a shift in the diffraction peaks of PANI, thus revealing the coexistence of both PANI and ZnZIF in PANI-ZnZIF composite. Furthermore, the XRD patterns of PANI-ZnZIF composite show amorphous structure evidenced by a broad peak at around 2θ = 21 and 23° even after doping with ZnZIF indicating that the PANI structure has been preserved. It was seen that PANI-ZnZIF nanofiber possessed the average crystallite size of 2.58 nm which was smaller than that of undoped PANI confirming successful composite formation. The smaller the crystallite size of a material, the higher the surface to volume ratio leading to greater response towards gas species [28].

STA (TGA and DSC) is an important technique used to examine the thermal stability and different sample transitions of solid materials when subjected to elevated temperatures. Furthermore, it can be used to check the precise weight ratio of each component in solid samples. TGA thermograms and DSC curves of PANI, ZnZIF and PANI-ZnZIF composite under heating rate of 10 ^{0}C/min areshown in Figure 5.1(e and f), respectively. The TGA thermograms of ZnZIF (Figure 5.1e) consists of two

important degradation step from 25 to 550 °C. The first 2.0% weight loss step observed at about 25-175 °C resulted from the removal of trapped guest molecules and unreacted species such as solvent and moisture within the porous cavities of ZnZIF structure [24]. The degradation step of about 8 wt.% observed at around 225 - 525 °C was due to the thermal decomposition of ZnZIF [25]. At this degradation step about 93 wt.% of the starting material remained. The remaining 93 wt.% shows that the BIZ organic linker was not pyrolysed hence ZnZIF was still intact and thermally stable at temperature up to 525 °C. Similar results were obtained in the study conducted by Lien et.al, when they studied the heterogeneous catalyst based on ZIF-9 [29]. On the other hand, TGA results of PANI displayed three thermal degradation steps at about 98, 250 and 400 °C, mainly attributed to the removal of moisture present in the structure of polyaniline, phase transition or cross- linking and collapse of polyaniline chains, respectively [20]. Furthermore, the TGA results of PANI, ZnZIF and PANI-ZnZIF composite exhibited an overall weight loss of around 60%, 10% and 30%, respectively. PANI-ZnZIF composite exhibited lower weight loss at higher temperature as compared to undoped PANI indicating the enhancement in the thermal stability upon forming the composite. The improvement in the thermal stability indicates a successful incorporation of ZnZIF in PANI structure supporting the observed analysis above in XRD and FTIR.

Figure 5.1(e) shows the DSC results of the synthesised solid materials. The DSC thermograph of PANI displayed three exothermal peaks at around 98, 250 and 400 °C. The peak at 98 °C can be ascribed to the loss of moisture present in polymer backbone [30]. The exothermal peak at 252 °C may be due to the cross-linking or oxidation of polyaniline, while the small exothermic peak at about 400 ^{0}C attributed to the degradation temperature of PANI [30]. PANI-ZnZIF composite presents two endothermal peaks corresponding to the crystallisation transition (at 55 °C) and melting transition (at 350 °C) in the composite. These transitions may be due to the dehydration of the composite and the absorption of heat by the composite as it experiences the change from solid to liquid phase (endothermic phase transition) [15]. PANI and ZnZIF have higher heat flow rates as compared to PANI-ZnZIF. All DSC transition results of ZnZIF, PANI and PANI-ZnZIF were found to correlate well with the degradation steps observed in TGA.

5.3.2. Morphological characterisations

Morphological characterisation of the synthesised materials is very essential to evaluate different shape, structure and elemental composition of the precursor materials and also to confirm the success in synthesising the composite material. Figure 5.2 ((a, c and e)) shows SEM images of ZnZIF, PANI and PANI-ZnZIF composite nanofibers, respectively, and indicated that they consists of pores and voids, cubic structure and nanofiber like shaped crystals, which are consistent with the previous literature reports [24,25]. The corresponding EDS of ZnZIF (Figure 5.2b) confirmed the existence of zinc (Zn), nitrogen (N), chlorine (Cl) and carbon atoms (C) with the elemental composition of 63, 11 and 26% for C, Zn and N, respectively. The little impurity of Cl is from the starting material $ZnCl_2$. SEM image of PANI (Figure 5.2(c)) show some agglomerates of interconnected tubules and the nanofiber rod like structures which may be attributed to soft template assisted development of PANI [23,31]. The EDS results (Figure 5.2d) showed the presence of C, N, iron (Fe), Cl, oxygen (O) and Sulphur (S) which comes from dopant (HCl), oxidising agents (APS, $FeCl_2$) and the aniline monomer used during the synthesis. The elemental compositions were found to be 68 and 32% for C and N respectively, corresponding to the empirical formula of aniline. The SEM image of PANI-ZnZIF (Figure 5.2(e)) revealed that PANI nanofibers were wrapping the cubic structures of ZnZIF suggesting the electrostatic interaction. Meanwhile the EDS (Figure 5.2f) of the composite presented an increase in the percentage of C and N atoms which confirms successful composite formation. The percentage composition with respect to aniline monomer is 53% and 47% for C and N, respectively.

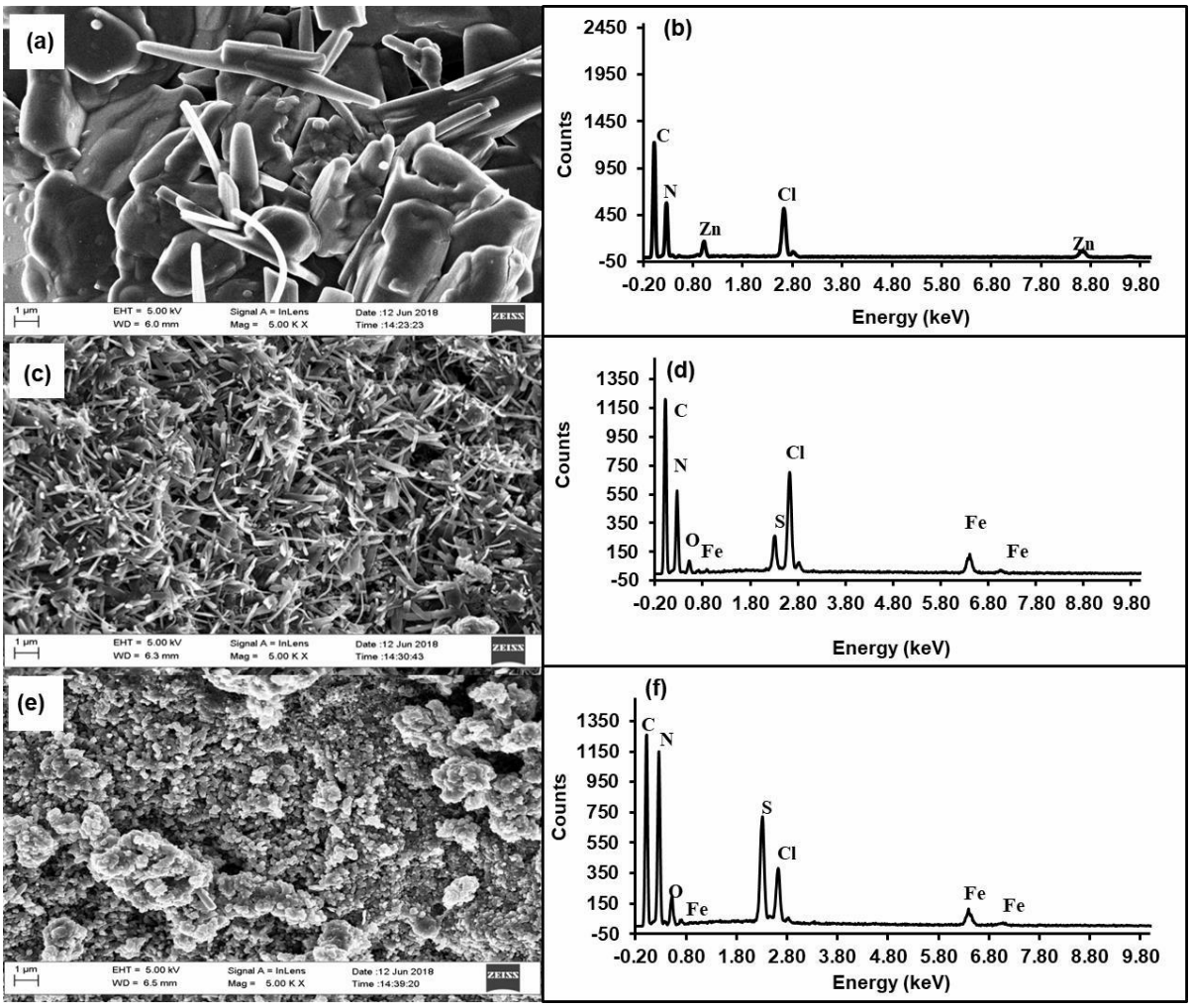

Figure 5.2: SEM images of (a) ZnZIF, (c) PANI and (e) PANI-ZnZIF; composite and EDS spectrum of (b) ZnZIF, (d) PANI and (f) PANI-ZnZIF composite.

The TEM micrograph of the synthesised materials are presented in Figure 5.3(a, c and e). The synthesised ZnZIF possessed porous rectangular or cube like structures (Figure 5.3(a)). The EDX spectrum of ZnZIF constitutes of copper (Cu), Zn and C. These elements are due to the copper grid used, metal center ($ZnCl_2$) and benzimidazole organic material. On the other hand, PANI (Figure 5.3(c)) displayed twisted fiber like structure with some agglomerate or clusters of particles. The corresponding EDX of PANI (Figure 5.3(d)) consists of elements such as C, N, Fe, S, O, Cl and Cu [32]. The impurities of S, Cl, O, Fe and Cu are due to dopant, oxidants and copper grid [23]. The micrograph of PANI-ZnZIF (Figure 5.3(e)) showed the modification of PANI morphology with the intertwinement of ZnZIF and PANI morphology. The corresponding EDX of PANI-ZnZIF (Figure 5.3(f)) showed an

increase in nitrogen percentage proving the co-existence of nitrogen coming from benzimidazole in ZnZIF and aniline in polyaniline

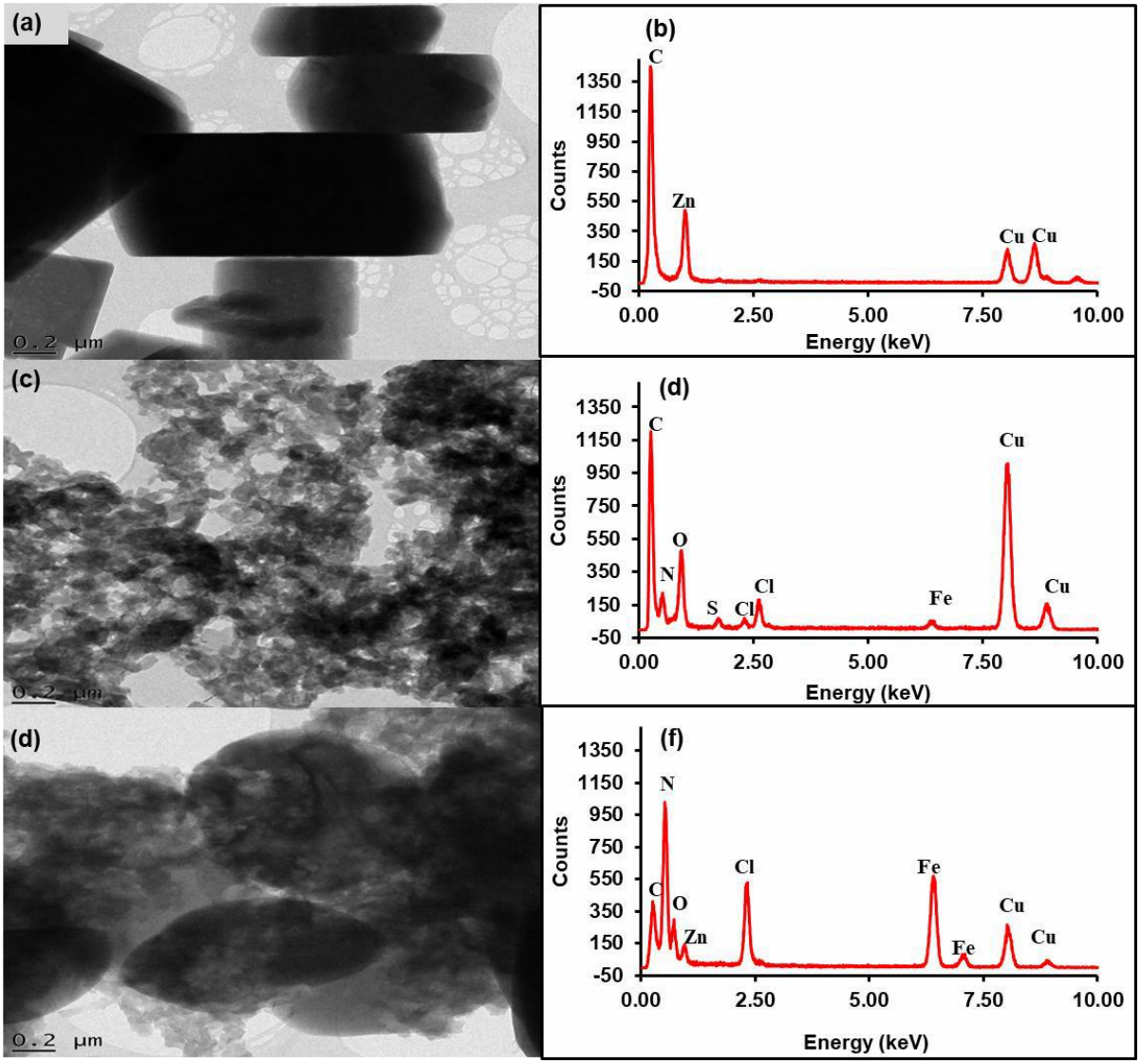

Figure 5.3: TEM images of (a) ZnZIF, (c) PANI and (e) PANI-ZnZIF composite and EDX spectrum of (b) ZnZIF, (d) PANI and (f) PANI-ZnZIF composite

Figure 5.4 shows the HRTEM images of PANI, ZnZIF and PANI-ZnZIF composite; and their corresponding SAED patterns. The HRTEM and SAED results of PANI shows nanofibrous morphology and no indication of any clear rings meaning it is amorphous as shown in both Figure 5.4(a and b). The d-spacing of PANI using SAED image was found to be 0.733 nm (7.3 Å) which is closer to 0.4 nm (4 A) from XRD results at 2 θ angle of 21° accounting for (100) reflection. HRTEM results for

ZnZIF (Figure 5.4(c)) showed porous nanofibers and crystalline structures. The corresponding SAED (Figure 5.4(d)) showed clearly visible crystalline diffraction spots as conferred by XRD. Using the SAED image, the d-spacing was determined to be 1.26 nm (12 Å) which is closer to 1 nm (10 A) obtained from XRD using Bragg's law. Based on the HRTEM studies, the surface of the PANI sample closely resemble that of PANI-ZnZIF as shown in Figure 5.4(e and f) and a slight morphology change is caused by introducing ZnZIF. Upon composite formation both nanofibrous and tubular like structures of ZnZIF and PANI are visible as shown in Figure 5.4(e). The d-spacing of PANI-ZnZIF using SAED (Figure 5.4f) was found to be 0.710 nm (7.1 Å) which was lower than that of PANI which is in accordance with previous reports [15].

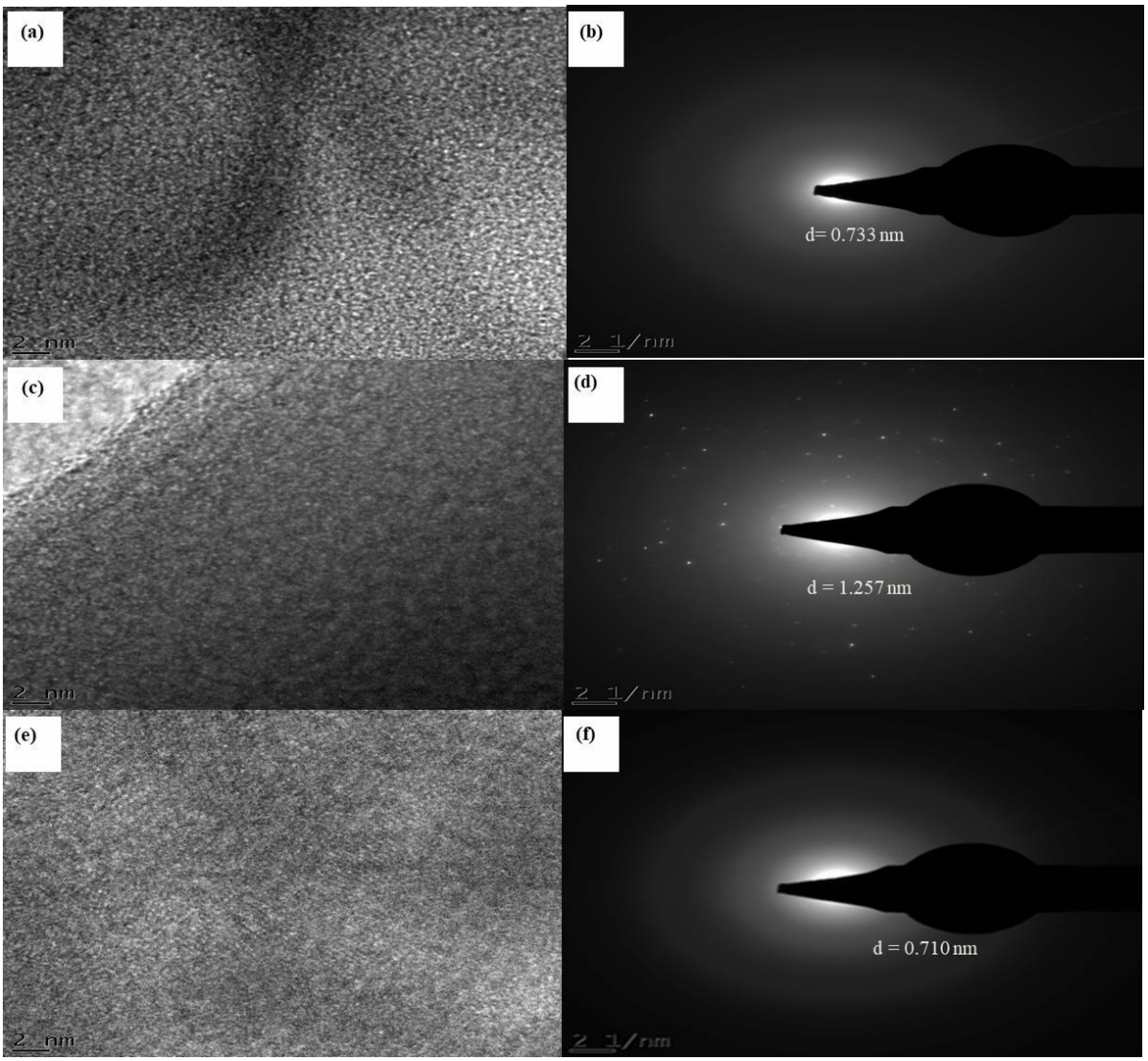

Figure 5.4: HRTEM images of (a) ZnZIF, (c) PANI and (e) PANI-ZnZIF composite; and SAED images of (b) ZnZIF, (d) PANI and (f) PANI-ZnZIF composite.

5.3.3. Electrochemistry

5.3.3.1 *Electrochemical characterisation*

Figure 5.5(a) shows the cyclic voltammograms overlay of the blank (TBAP-DMSO), ZnZIF, PANI and PANI-ZnZIF. The bare gold electrode in TBAP-DMSO electrolyte system showed current response with a redox behavior at about 0.6 V due to the oxidation and reduction of gold. Furthermore, cyclic voltamogram was used to evaluate the electrochemical performance and redox states of PANI as shown in Figure 5.5(a) to. CV was used to interpret the structural formula of PANI as it

undergoes reduction and oxidation processes. As documented in Figure 5.5(a), the CV results of polyaniline shows two sets of distinctive redox processes shown by the appearance of two redox couples (cathodic and anodic peaks). The redox couple at about -0.7 and -0.6 V) is related with the change of the fully reduced base (leucoemeraldine) to the partly oxidised base (emeraldine) form of polyaniline [7]. The other redox pair appearing at around 0.7 and 0.6 V is associated to the alteration of emeraldine to the fully oxidised base (pernigraniline) form of polyaniline [7]. The presence of both leucoemeraldine and pernigraniline components on the CV of the synthesised PANI suggest that PANI consists of both amine and imine groups, thus polyaniline is synthesised in its emeraldine form [7]. The emeraldine form is known to be highly conductive as compared to other forms of PANI which is essential in electrochemical sensing application [12,33,34]. PANI presented a distinctive reversible character wherein the ratio of peak height current at the anode and cathode (I_a/I_c) equals to unity. Cyclic voltammogram of ZnZIF exhibited anodic peak at around -0.2 V and cathodic peak at about -0.4 V pertaining to the change in oxidation state of Zn^{2+} to Zn^{3+} (Zn^{2+}/Zn^{3+}) in the structure [35]. The resultant composite presented higher electrical conductivity as compared to the precursor materials PANI and ZnZIF. The higher electrical conductivitywas witnessed by higher current response (see Figure 5.5 a),due to the synergy between the PANI and ZnZIF. The observed drastic increase in current response is due to an increase in electron density around polymer matrix [23].

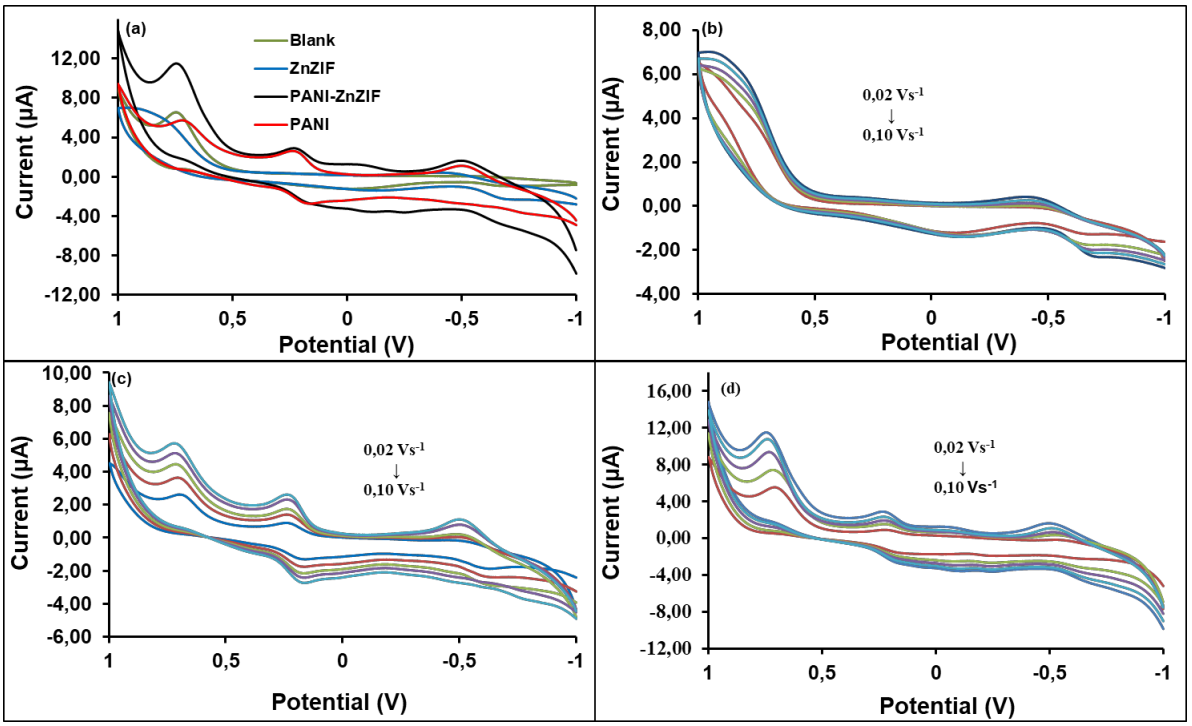

Figure 5.5: (a) Overlaid cyclic voltammograms of (a) Blank, PANI, ZnZIF and PANI-ZnZIF composite at the scan rate of 0.1 $V.s^{-1}$ in 0.1 $mol.L^{-1}$ TBAP-DMSO electrolyte solution on Au electrode, (b-d) ZnZIF, PANI and PANI-ZnZIF, respectively, in 0.1 $mol.L^{-1}$ TBAP-DMSO at different scan rates (0.02 - 0.1 $V.s^{-1}$), in 0.1 $mol.L^{-1}$ TBAP-DMSO electrolyte solution using Au as current collector.

Table 5.1: Experimental values of anodic and cathodic peak currents slope of log-log plot of the absolute value of the peak current vs scan rate, diffusion coefficients (*D*) and the ratio of anodic and cathodic peak current I_{pa}/I_{pc} ratios of ZnZIF, PANI and PANI-ZnZIF composite from CV and SWV.

Material	**Technique**	I_{p_a} **(A)**	I_{p_c} **(A)**	I_{p_a}/I_{p_c}	**Slope (A.V.s^{-1})**	D **(cm^2 .s^{-1})**	Γ **(mol.cm^{-2})**
ZnZIF	CV	1.30	0.27	4.81	0.23	8.90×10^{-7}	1.12×10^{-9}
	SWV	0.31	0.04	0.13	0.29	6.92×10^{-6}	3.76×10^{-6}
PANI	CV	2.65	2.62	1.00	0.35	1.55×10^{-5}	4.83×10^{-10}
	SWV	1.22	1.61	0.76	0.42	1.10×10^{-50}	8.55×10^{-70}
PANI-ZnZIF	CV	2.37	2.90	0.82	0.5	9.55×10^{-50}	1.17×10^{-10} 0
	SWV	1.33	0.40	3.32	0.34	5.17×10^{-5}	2.77×10^{-10}

Figure 5.6 and 5.7 shows the overlaid square-wave voltammograms (SWV) indicating the reduction and oxidation results, respectively, of the blank, ZnZIF, PANI and PANI-ZnZIF. SWV was used as an analytical probe to support CV and check whether there are no additional redox processes that are not shown by CV. The results show that there are no additional peaks, hence the results observed from the SWV complement the one observed from CV. From both Figure 5.6(a) and 5.7(a), it was found that the PANI-ZnZIF composite with 3.6 wt.% loading of ZnZIF had higher electrochemical properties such as current response than its starting materials. This increase in current response is ascribed to the increase in electron density on the polymer chains caused by high specific surface area and pore volume [15,36] of ZnZIF. Introduction of ZnZIF makes it possible for all interior active sites to be accessible to the electrolyte, thus electron diffusion increases as witnessed by increase in the diffusion coefficient (Table 5.1) [36]. Similar results were also obtained when studying the electrochemical behavior of the composite using CV.

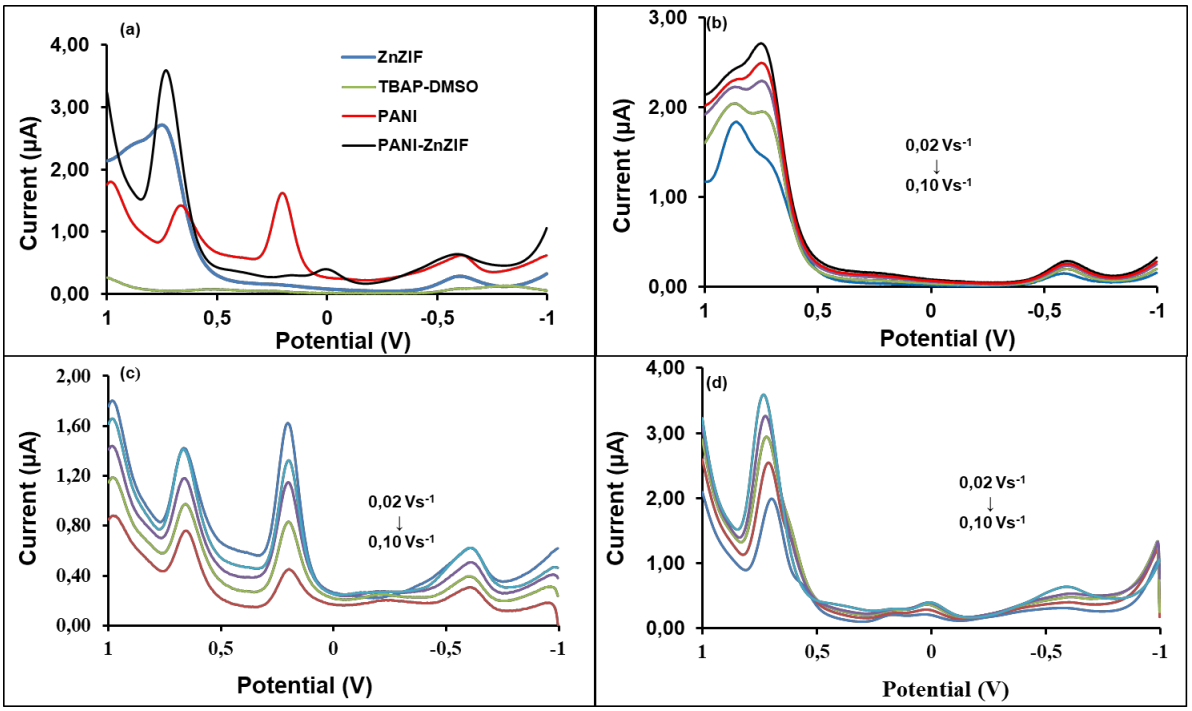

Figure 5.6: (a) Overlaid square-wave voltammograms (SWV) showing reduction for Blank (TBAP-DMSO), PANI, ZnZIF and PANI-ZnZIF composite at 0.1 $V.s^{-1}$, (b-d) ZnZIF, PANI and PANI-ZnZIF respectively,at different scan rates (0.02-0.1 $V.s^{-1}$) in 0.1 $mol.L^{-1}$ TBAP-DMSO electrolyte using Au as current collector.

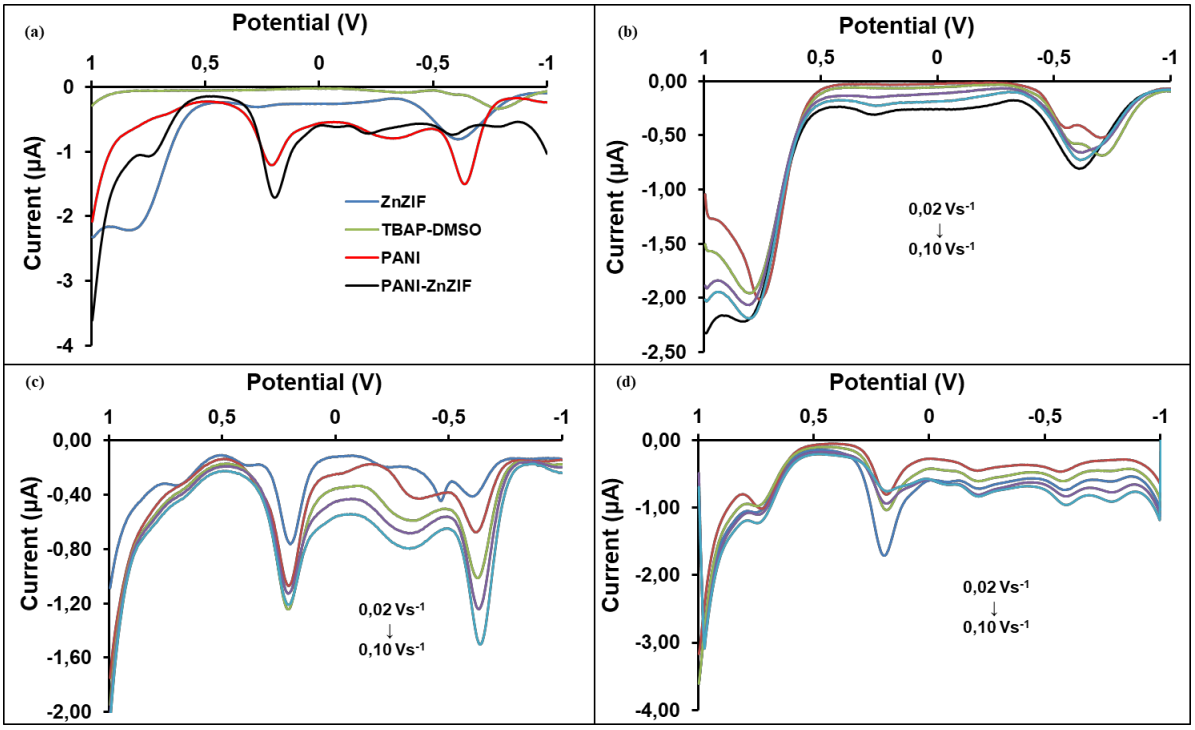

Figure 5.7: (a) Overlaid square-wave voltammograms showing oxidation for TBAP-DMSO (blank), PANI, ZnZIF and PANI-ZnZIF composite at 0.1 $V.s^{-1}$, (b-d) ZnZIF, PANI and PANI-ZnZIF, respectively, at different scan rates (0.02-0.1 $V.s^{-1}$) in 0.1 $mol.L^{-1}$ TBAP-DMSO electrolyte using Au as current collector.

The multiscan voltammograms derived from both CV (Figure 5.5(b-d)) and SWV ((Figure 5.6(b-d) and 5.7(b-d)) were conducted to evaluate the effect of scan rates on the current response of the synthesised PANI, ZnZIF and PANI-ZnZIF composite nanofiber. In both cyclic and square-wave, voltammograms, there was a direct proportionality between current responses and increasing scan rates. The multiscan voltammograms further revealed that PANI-ZnZIF possesses higher current response due to the synergistic effect resulting from the conductive structures of both ZnZIF and PANI. The rise in electrochemical performance of the composite indicates the easiness in diffusion of electrons around the polymer matrix. The redox pairs in all multiscan voltamograms displayed electrochemical quasi-reversible process at different peak potentials (ΔEp). Additionally, Ip_a/Ip_c values (Table 5.1) at different scan rates displayed a quasi-reversible character for both PANI and PANI- ZnZIF composite. The slope of the plot of logarithm of the absolute value of the cathodic peak current versus the logarithm of the scan rate (Figure 5.8(a and b))

showed the slope of about 0.5, signifying electron transfer limited process. This redox processes involves the diffusion of electrons and thus known as diffusion controlled process [1].

Since all the multiscan voltammograms indicated a diffusion controlled process, the diffusion coefficient of the materials were determined using the plot of current versus the square root of scan rates ($v^{1/2}$) shown in Figure 5.8(c and d). It was observed that there was a direct proportionality between current and $v^{1/2}$. The *D* values were derived from both CV and SWV using the Randles-Sevcik equation (Equation 5.2) given as follows [1]

$$I_p = (2.65x10^5)n^{3/2}ACD^{1/2}(v)^{1/2} \quad (5.2)$$

wherein, *n* is the number of transferred electrons, *A* is the area of the electrode (cm^2), *D* is the diffusion coefficient ($cm^2.s^{-1}$), *C* is the concentration of catalyst ($mol.cm^{-3}$) and v is scan rate ($V.s^{-1}$) [1].

PANI, ZnZIF and PANI-ZnZIF possessed the *D* values (Table 5.1) of 8.90×10^{-7}, 1.55×10^{-5} and 9.55×10^{-5} $cm^2.s^{-1}$ from CV and 1.20×10^{-6}, 1.10×10^{-5} and 5.17×10^{-5} $cm^2.s^{-1}$ from SWV for ZnZIF, PANI and PANI-ZnZIF, respectively. These results showed that PANI-ZnZIF is a good electrocatalyst as compared to its precursor materials. Furthermore, the peak currents were related to the scan rates and a linear relationship between them was observed. The peak current increased with an increase in scan rates as an indication of an adsorption controlled process [12]. The peak currents were then linked with the surface coverage of the synthesised materials using the following equation of Laviron [12] (Equation 5.3)

$$Ip = \frac{n^2 F^2 A v \Gamma}{4RT} \quad (5.3)$$

Using the slopes of graphs in the Figure (5.8e and f), the surface coverage values (Γ) were found to be 1.12×10^{-9}, 1.10×10^{-10} and 4.83×10^{-10} from CV and 1.33×10^{-10}, 1.17×10^{-10} and 2.77×10^{-10} $mol.cm^{-2}$ from SWV for ZnZIF, PANI and PANI-ZnZIF, respectively (Table 5.1). From these results it was observed that the composite exhibited higher surface coverage as compared to neat PANI and ZnZIF

which further confirm the adsorption of the material on the gold bare electrode and the process is adsorption controlled process [12].

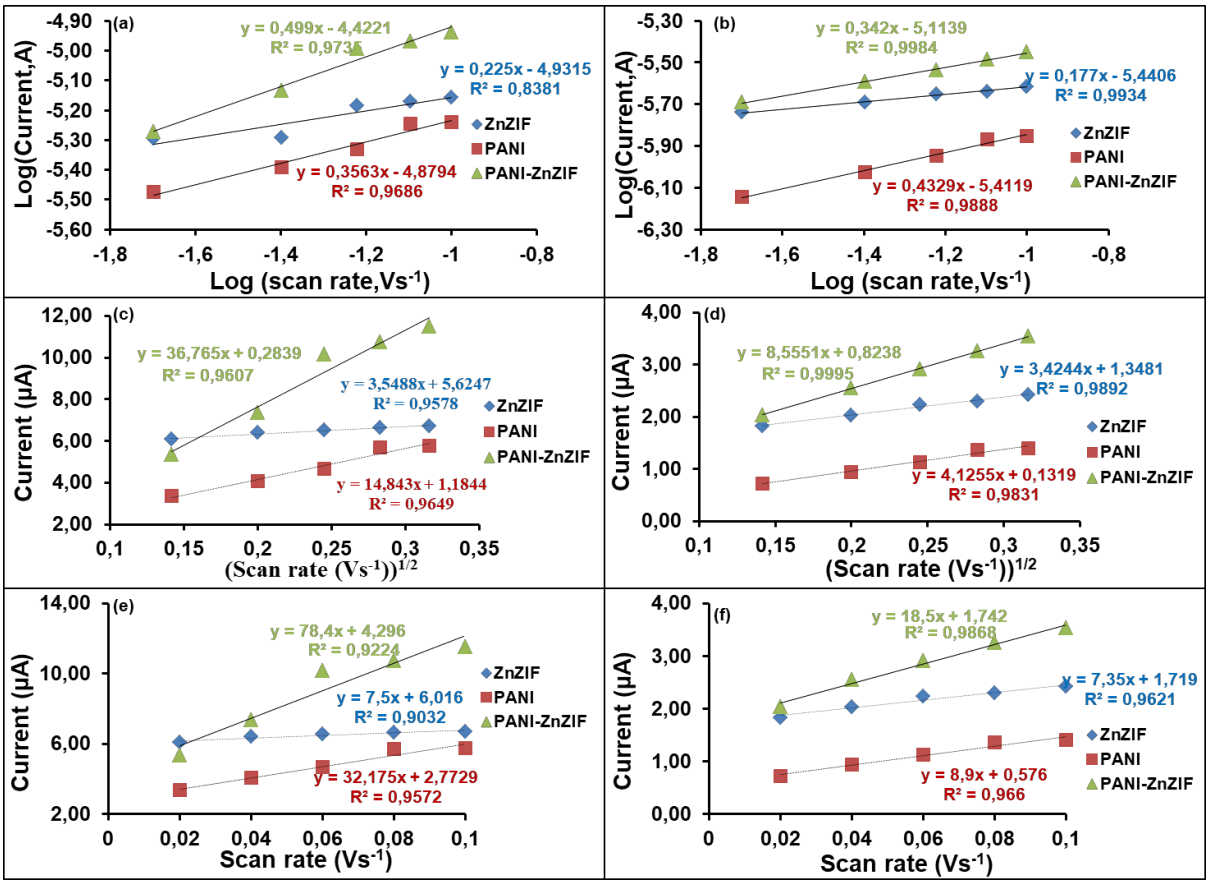

Figure 5.8: The log-log plot of the absolute value of the peak current vs scan rate from CV (a) and SWV (b); peak current as a function of square root of scan rate from CV (c) and SWV (d) and peak current as a function of scan rate from CV (e) and SWV (f) for PANI, ZnZIF and PANI-ZnZIF on gold in 0.1 mol.L^{-1} TBAP-DMSO electrode system at different scan rates (0.02– 0.10 $V.s^{-1}$).

5.3.3.2. *Hydrogen evolution studies*

Since it was observed from the previous results that PANI-ZnZIF composite exhibited good electrocalytic behavior, the studies on electrocatalytic performance of PANI, ZnZIF and PANI-ZnZIF towards hydrogen evolution reaction (HER) were further investigated by using CV in 0.1 M TBAP-DMSO electrolyte solution and H_2SO_4 as hydrogen source. The results are shown in Figure 5.9(a). The cathodic

peak potential corresponding to reduction of H_2SO_4 was observed at around -0.9 V similar to other reports [1]. High current response observed signifies more hydrogen produced [15]. PANI-ZnZIF showed better hydrogen production capability indicated by high current response thus it can be considered as a good electrocatalyst for HER as compared to pure PANI and ZnZIF. Tafel curve was employed to study the kinetics of HER using PANI, ZnZIF and PANI-ZnZIF composite nanofiber and the results are shown in Figure 5.9(b). The curves of overpotential versus log i_0 at 0.033 mol.L^{-1} H_2SO_4 were used to determine electrochemical parameters such as Tafel slope (b) and exchange current density i_0 which are essential to probe the performance of an electrocatalyst. The Tafel slope gives an insight about the electrochemical rate determing step [9]. Monama *et al.* [1] have reported that the Tafel slope, *b* can tell if HER is through Heyrovsky, Volmer or Tafel in a multi-step proton transfer process. Furthermore, it was previously reported that for HER on platinum electrode in acidic solutions, the reactions show the Tafel slope values of 120 mV, 40 mV and 30 mV for the Volmer, the Heyrovsky and the Tafel, respectively [23]. In the present study, *b* was found to be 544, 154 and 246 mV.dec^{-1} for ZnZIF, PANI and PANI-ZnZIF composite, respectively. From these results it can be noted that Volmer is the rate determing step for PANI, however, introduction of ZnZIF caused an increase in Tafel slope. The exchange current density, i_0 was determined from the Tafel plot were it cuts the x-axis and it conveys information about electrocatalyst performance [15]. It can be related to the electrochemical active surface area of the catalyst [15]. PANI-ZnZIF composite exhibited higher exchange current density (5.01 A.m^{-2}) as compared to pristine ZIF (0.32 A.m^{-2}) and homopolymer PANI (2.51 A.m^{-2}) indicating the large surface area, fast electron transfer rate, and favorable HER kinetics [37].

Cathodic transfer coefficient (1-α) is another important electrochemical parameter which can be evaluated using Tafel plot [9]. It can be calculated using region of high overpotential, whereby Butler-Volmer equation simplifies to the Tafel equation (Equation 5.4) and Tafel slope is given by [9].

$$b = \frac{-2.303\,RT}{(1-\alpha)F} \tag{5.4}$$

As displayed in Table 5.2, the cathodic transfer coefficients values for PANI and PANI-ZnZIF composite were found to be close to 0.5. Therefore, the rate

determining step of HER on these materials may possibly be the Volmer reaction or the Volmer reaction coupled with Heyrovsky or Tafel as described by Ramohlola *et al.* [23].

Turnover frequency (TOF) which is described as mass of molecules reacting for a certain reaction per unit time was further used to evaluate the efficiency of the electrocatalysts [38]. The TOF given by Equation 5.5 below [39].

$$\mathrm{TOF} = \frac{jM}{Fm} \tag{5.5}$$

where j represent current density at a given potential, M is mass percentage of materials, F is Faraday's constant, and m is the mass per square centimeter of catalysts [39]. From the BET surface area of ZnZIF (312 $m^2.g^{-1}$) [25] and PANI (30.8 $m^2.g^{-1}$), PANI and PANI-ZnZIF composite possessed the estimated TOF values of 0.04 and 0.45 mol $H_2.s^{-1}$ as depicted in the Table 5.2. From these results it was observed that the synthesised PANI-ZnZIF composite exhibited displayed higher TOF value using 0.033 $mol.L^{-1}$ H_2SO_4 as compared to pure PANI owing due to an increase in electronic density of polymer backbone [23]. All Tafel parameters determined in this study shows that PANI-ZnZIF has a potential as an electrocatalyst for HER in hydrogen sensing technology.

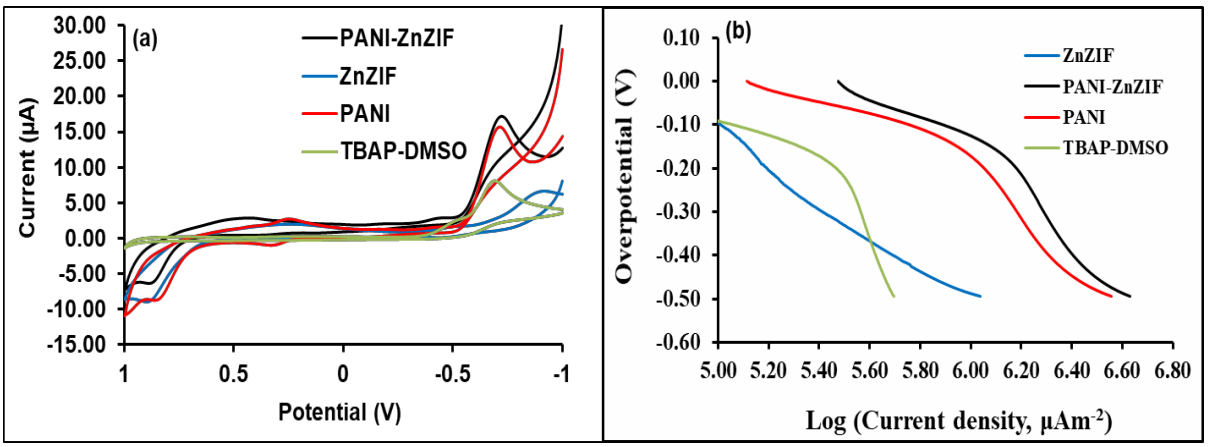

Figure 5.9: (a) CV curves (b) Tafel plots of TBAP-DMSO, ZnZIF, PANI and PANI-ZnZIF composite (~$2.0x10^{-4}$ $mol.L^{-1}$) in the presence of 0.033 $mol.L^{-1}$ H_2SO_4 in 0.1 $mol.L^{-1}$ TBAP-DMSO electrode system on Au electrode at 0.10 $V.s^{-1}$ scan rate.

Table 5.2: Experimental values of Tafel slope (*b*), charge transfer coefficient (1–*α*), exchange current density (i_0) and TOF of PANI, ZnZIF and PANI-ZnZIF composite.

Materials	H_2SO_4 (mol.L^{-1})	Slope (*b*) (V.dec^{-1})	-*b* (mV.dec^{-1})	1-α	logi_0 (μA.m^{-2})	i_0 (A.m^{-2})	TOF (mol.H_2.s^{-1})
Blank	0.033	-0.241	241	0.25	5.90	0.79	
ZnZIF	0.033	-0.544	544	0.11	5.50	0.32	0.05
PANI	0.033	-0.154	154	0.38	6.40	2.51	0.04
PANI-ZnZIF	0.033	-0.246	246	0.24	6.70	5.01	0.45
PANI/MOF [40]	0.075	−0.239	239	0.247	0.50	3.162	0.28

5.3.3.3 *Electrochemical hydrogen gas sensing studies*

The electrochemical gas sensing behaviour of PANI doped with ZnZIF was examined to grasp a better understanding of its sensing capability. Figure 5.10(a-d) reports on the plot of current response against time (Chronoamperometry, CA) of PANI, ZnZIF and PANI-ZnZIF sensors in the absence and present of H_2SO_4 concentration at room temperature. The synthesised PANI-ZnZIF composite exhibited higher current response (Figure 5.10(a)) as compared to PANI homopolymer, as time progresses from 0 to 60 s. The increase in current response was also conferred by both CV (Figure 5.5) and SWV (Figure 5.6) in the absent of hydrogen source. In case of the synthesised PANI-ZnZIF composite, the presence of hydrogen source caused drastic improvement in the electrochemical current response (Figure 5.10(d)) as compared to PANI (Figure 5.10(c)) and ZnZIF (Figure 5.10(b)). This sudden increase in current response is due to the absorption of

hydrogen gas on PANI-ZnZIF composite which resulted in the deprotonation of N^+–H sites (emeraldine salt) of polyaniline to form NH_4^+ [41]. The deprotonation of PANI-ZnZIF might have caused a change in conductivity [41] of the composite leading to

better electrochemical properties of the composite for hydrogen gas sensing. The observed high current response is attributed to high conductivity of polyaniline in acidic medium [34]. From these findings, it can be deduced that the leading sensing mechanism of PANI-ZnZIF composite is due to deprotonation of PANI. Similar gas sensing mechanism was reported by Lim *et al.* [41]. Furthermore, it was observed that current increases with an increasing concentration (Figure 5.10(b-d)). At high acid concentrations, movement and number of hydrogen gas molecules reaching the electrode surface increases thus stimulating fast achievement of steady-state [42].

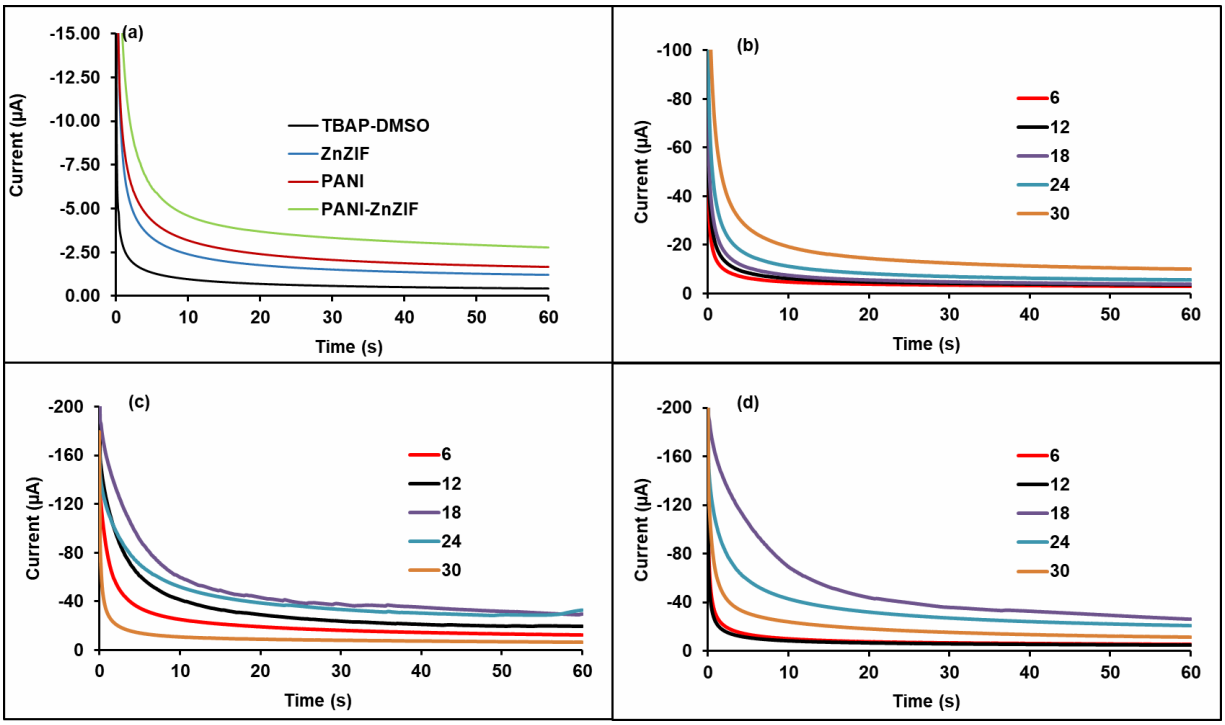

Figure 5.10: (a) Chronoamperometric results for (a) TBAP-DMSO, PANI, ZnZIF and PANI-ZnZIF composite at -0.9 V in 0.1 mol.L^{-1} TBAP-DMSO electrolyte solution on gold bare electrode. (b-d) ZnZIF, PANI and PANI-ZnZIF respectively at different H_2SO_4 concentrations in 0.1 mol. L^{-1} TBAP-DMSO.

Figure 5.11(a) reports the linear plot of steady state current response of PANI-ZnZIF sensors against different concentrations ($6.0 \times 10^{-4} – 30 \times 10^{-4}$ mol.L^{-1}) of H_2SO_4. PANI-ZnZIF composite possessed a lower detection limit (*LOD* = 3 × S/N) of 5.27 μmol.L^{-1} towards H_2, in which the *LOD* is the concentration which gives a signal-to-noise ratio of at least 3 [40]. PANI and ZnZIF gave higher detection limit as compared to the composite which indicates poor gas sensing performance [40]. The

limit of quantification (*LOQ* = 10 × S/N) was found to be 17.3, 17.6 and 17.5 µmol.L^{-1} for PANI, PANI-ZnZIF and ZnZIF, respectively. The synthesised materials were found to possess the correlation coefficient values (R^2) of 0.86, 0.95 and 0.98 for ZnZIF, PANI and PANI-ZnZIF composite, respectively. Moreover, PANI-ZnZIF composite showed a linear relationship between current response and hydrogen source at concentrations from 6.0 x 10^{-4} – 30 × 10^{-4} mol.L^{-1} with the sensitivity of about 10.8 µAmmol.L^{-1} H_2, which is much larger than 8.22 and 5 µA.mmol.L^{-1} H_2 sensitivity values for PANI and ZnZIF, respectively. The steady state response time was found to be approximately 4 s.

Figure 5.11(b) shows linear relationship between current and 1/square root of time ($t^{-1/2}$) at -0.9 V on bare gold electrode using 0.1mol.L^{-1} TBAP-DMSO as an electrolyte. Using Figure 5.11(b) and Cottrell Equation (Equation 5.6) given by [43]

$$I = nFACD^{1/2}P^{-1/2}t^{-1/2} \tag{5.6}$$

The diffusion coefficient values of PANI, ZnZIF and PANI-ZnZIF were found to be 1.184×10^{-4}, 1.23×10^{-4} and 2.72×10^{-4} cm^2.s^{-1}, respectively. The composite showed an increase in diffusion coefficient attributed to greater mobility of polymer electrons caused by the presence of ZnZIF in the polymer backbone thus increasing the sensing performance [44].

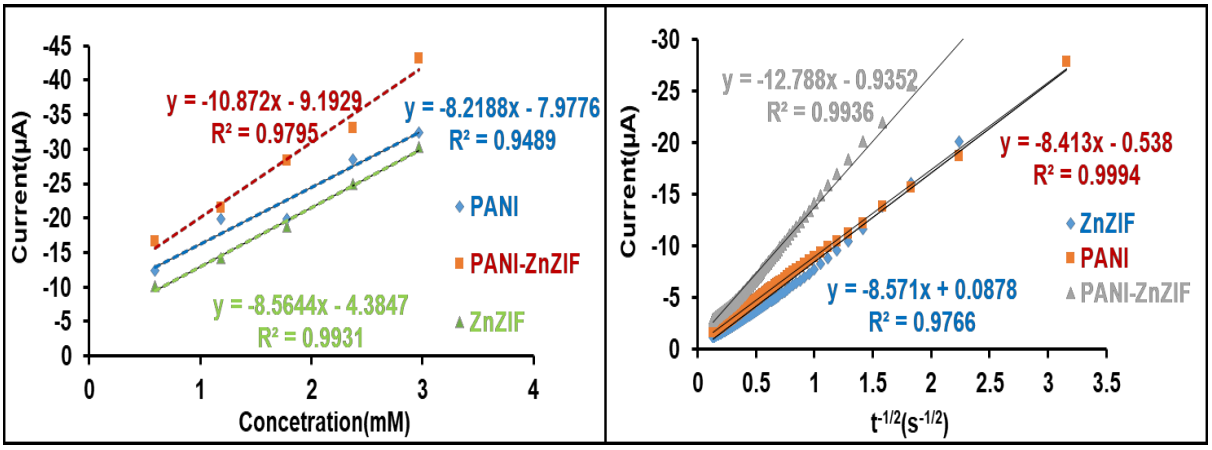

Figure 5.11: (a) steady state current versus different proton source (H_2SO_4) concentrations (0.6 - 3.0 mmol.L^{-1}) and (b) current versus of 1/square root of time

for PANI, ZnZIF and PANI-ZnZIF composites at -0.9 V on bare Au electrode in 0.1 mol.L^{-1} TBAP-BMSO electrolyte system.

5.4. CONCLUSION

This work studied the in-situ chemical polymerisation of polyaniline doped with zinc zeolitic benzimidazolate framework (PANI-ZnZIF composite) for electrochemical hydrogen gas sensing application. The FTIR and Raman spectroscopy analyses revealed the successful incorporation of ZnZIF on PANI. XRD and Simultaneous thermal analysis (STA) displayed the co-existence of both PANI and ZnZIF observed by the decrease in crystallite size and the improvement in the thermal properties upon loading of ZnZIF, thus making it an attractive material for high temperature application purposes. SEM/EDS, TEM/EDX, and HR-TEM/SAED revealed that PANI nanofibers are wrapping the cube like nanofiber particles of ZnZIF suggesting electrostatic interaction. This behavior might be due to the interaction between the partially positive ZnZIF and partially negative polyaniline. SWV, CV and CA results presented higher electrochemical properties HER and hydrogen sensing properties, indicated by an increase in current response with loading of ZnZIF. These results may be owed to high specific surface area of ZnZIF and high conductivity of PANI. Furthermore, the resulting PANI-ZnZIF composite exhibited exceptional electrochemical hydrogen gas sensing performance indicated by high current response and sensitivity (10.8 µAmmol.L^{-1} H_2), faster steady state response time (4 s) accompanied by lower detection limit (5.27 µmol.L^{-1}) as compared to pure PANI. Therefore, the composite has a potential as an electrocatalyst for hydrogen gas sensing application induced by hydrogen evolution reaction.

5.5. REFERENCES

[1] G. R. Monama, S. B. Mdluli, G. Mashao, M. D. Makhafola Mdluli, K.E. Ramohlola, K.M. Molapo, M.J. Hato, K. Makgopa, E.I. Iwuoha, and K.D. Modibane, “Palladium deposition on copper(II) phthalocyanine/metal organic framework composite and electrocatalytic activity of the modified electrode towards the hydrogen evolution reaction,” *Renew. Energy*, vol. 119, pp. 62–72, 2018.

[2] P. Soundarrajan and F. Schweighardt, *Hydrogen Sensing and Detection*, *Hydrog. Fuel Prod. Transp. Storag.*, vol.13, pp. 495-500, 2016.

[3] J. Do, Y. Chen, and M. Tsai, “Planar solid-state amperometric hydrogen gas sensor based on Nafion®/Pt/nano-structured polyaniline/Au/Al_2O_3 electrode,” *Int. J. Hydrogen Energy*, vol. 43, pp. 14848–14858, 2018.

[4] W. J. Buttner, M. B. Post, R. Burgess, and C. Rivkin, *“An overview of hydrogen safety sensors and requirements*,” *Int. J. Hydrogen Energy*, vol. 36, pp. 2462–2470, 2010.

[5] A. G. Willis and S. Haron, *“Synthesis and characterization of composite polyaniline as hydrogen gas detector,” Malaysian J. Fundam. Appl. Sci.*, vol. 13, pp. 559–562, 2017.

[6] X. Liu, “A Survey on Gas Sensing Technology,” *Eng. Inf.*, vol. 12, pp. 9635–9665, 2012.

[7] E. Song and J. Choi, “Conducting Polyaniline Nanowire and Its Applications in Chemiresistive Sensing,” vol. 53, pp. 498–523, 2013.

[8] A. Z. Sadek and W. Wlodarski, “Doped and Dedoped Polyaniline Nanofiber Based Conductometric Hydrogen Gas Sensors,” *Sens Actuators A*, vol. 139, pp. 53–57, 2007.

[9] K. E. Ramohlola, M. Masikini, S. B. Mdluli, G. R. Monama1, M. J. Hato, K. M. Molapo, E. I. Iwuoha, and K. D. Modibane “Electrocatalytic Hydrogen Production Properties of Poly(3- aminobenzoic acid) doped with Metal Organic Frameworks,” *Int. J. Electrochem. Sci.*, vol. 12, pp. 4392–4405, 2017.

[10] H. Bai and G. Shi, “Gas Sensors Based on Conducting Polymers,” *Sensors*, vol. 7, pp. 267–307, 2007.

[11] L. Al-mashat, K. Shin, and K. Kalantar-zadeh, “Graphene/Polyaniline Nanocomposite for Hydrogen Sensing,” *J. Phys. Chem. C*, vol. 114, pp.

16168–16173, 2010.

[12] Y. Yuan, J. Xia, F. Zhang, Z. Wang, and Q. Liu, “Nafion / polyaniline / Zeolitic Imidazolate Framework-8 nanocomposite sensor for the electrochemical determination of dopamine,” *J. Electroanal. Chem.*, vol. 824, pp. 147–152, 2018.

[13] D. Zhang, J. Zhang, H. Bai, R. Zhang, H. Shi, and B. Yuan, “ZIF-9 with Enhanced Surpercapacitor and Electrocatalytic for Oxygen Evolution Reaction Performances in Alkaline Electrolyte,” *Chem*, vol. 11, pp. 7519–7526, 2016.

[14] K. T. Butler, S. D. Worrall, and C. D. Molloy, “Electronic structure design for nanoporous , electrically conductive zeolitic imidazolate frameworks,” *J. Mater. Chem. C*, vol. 5, pp. 7726–7731, 2017.

[15] K. E. Ramohlola, M. Masikini, S. B. Mdluli, G. R. Monama, M. J. Hato, K. M. Molapo, E. I. Iwuoha, K.D. Modibane, "Electrocatalytic hydrogen evolution reaction of metal organic frameworks decorated with poly (3-aminobenzoic acid)". *Electrochimic. Acta*, vol. 246, pp. 1174-1182, 2017.

[16] J. Qian, F. Sun, and L. Qin, “Hydrothermal synthesis of zeolitic imidazolate framework-67 (ZIF-67) nanocrystals,” *Mater. Lett.*, vol. 82, pp. 220–223, 2012.

[17] Y. Huang, D. Liu, Z. Liu, and C. Zhong, “Synthesis of Zeolitic Imidazolate Framework Membrane Using Temperature-Switching Synthesis Strategy for Gas Separation,” *Ind. Eng. Chem. Res.*, vol. 55, pp. 7164–7170, 2016.

[18] V. Sridevi, S. Malathi, and C. S. Devi, “Synthesis and characterization of Polyaniline / Gold Nanocomposites,” *Chem. Sci.*, vol. 2011, pp. 1–6, 2011.

[19] L. Geng, Y. Zhao, X. Huang, S. Wang, S. Zhang, and S. Wu, “Characterization and gas sensitivity study of polyaniline/SnO_2 hybrid material prepared by hydrothermal route,” *Sens. Actuators B. Chem.*, vol. 120, pp. 568–572, 2007.

[20] B. A. Bhanvase, N. S. Darda, N. C. Veerkar, A. S. Shende, S. R. Satpute, and S. H. Sonawane, “Ultrasonics Sonochemistry Ultrasound assisted synthesis of PANI / $ZnMoO_4$ nanocomposite for simultaneous improvement in anticorrosion , physico-chemical properties and its application in gas sensing,” *Ultrason. - Sonochemistry*, vol. 24, pp. 87–97, 2015.

[21] P. Zhao, G. I. Lampronti, G. O. Lloyd, M. T. Wharmby, A. K. Cheetham, and S. *A.* T. Redfern, “Phase transitions in zeolitic imidazolate framework 7: The importance of framework flexibility and guest-induced instability,” *Chem.*

Mater., vol. 26, pp. 1767–1769, 2014.

[22] S. Tanaka, M. Miyamoto, T. Makino, S. Van Der Perre, and V. U. Brussel, “Adsorption and diffusion phenomena in crystal size engineered ZIF-8 MOF,” *J. Phys. Chem. C*, vol. 119, pp. 28430–28439, 2015.

[23] K. E. Ramohlola, G. R. Monama, M. J. Hato, K. D. Modibane, K. M. Molapo, M. Masikini, S. B. Mdluli, and E. I. Iwuoha, “Electrocatalytic hydrogen production properties of polyaniline doped with metal organic frameworks,” Chapter September 2017. In book: Carbon-related Materials in Recognition of Nobel Lectures by Prof. Akira Suzuki in ICCE, p.373, DOI: 10.1007/978-3-319- 61651-3_15

[24] F. Li, Q. Li, X. Bao, J. Gui, and X. Yu, “Preparation and gas permeability of ZIF-7 membranes prepared via two-step crystallization technique,” *Korean J. Chem. Eng.*, vol. 52, pp. 340–346, 2014.

[25] X. Wu, M. Niknam, B. Yuan, and S. Deng, “Synthesis and characterization of zeolitic imidazolate framework ZIF-7 for CO_2 and CH_4 separation,” *Microporous Mesoporous Mater.*, vol. 190, pp. 189–196, 2014.

[26] G. P. Stahly and D. Ph, “*Advantages of a Cu vs . Co X-ray diffraction Source*,” pp. 5629–5630, 2012.

[27] A. Mekki, N. Joshi, A. Singh, and Z. Salmi, “H_2S sensing using in situ photo-polymerized polyaniline–silver nanocomposite films on flexible substrates,” *Org. Electron.*, vol. 15, pp. 71–81, 2014.

[28] G. Singh, R. Thangaraj, and R. C. Singh, “Effect of crystallite size, Raman surface modes and surface basicity on the gas sensing behaviour of terbium doped SnO_2 nanoparticles,” *Ceram. Int.*, vol. 42, pp. 4323–4332, 2016.

[29] L. T. L. Nguyen, K. K. A. Le, H. X. Truong, and N. T. S. Phan, “Metal–organic frameworks for catalysis : the Knoevenagel reaction using zeolite imidazolate framework ZIF-9 as an efficient heterogeneous catalyst,” *Catal. Science & Technol,* vol. 33, pp. 521–528, 2012.

[30] G. Neetika, D. Kumar, and S. K. Tomar, “Thermal behaviour of chemically synthesized polyanilines/polystyrene sulphonic acid composites,” *Int. J. Mater. Chem.*, vol. 2, pp. 79–85, 2012.

[31] C. H. Srinivas, D. Srinivasu, B. Kavitha, N. Narsimlu, and K. S. Kumar, “Synthesis and characterization of nano size conducting polyaniline,” *J. Appl. Phys.*, vol. 1, pp. 12–15, 2012.

[32] D. K. Mahla, S. Bhandari, and M. Rahaman, “Morphology and cyclic voltammetry analysis of in situ polymerized polyaniline/graphene composites,” *Mater. Sci. Eng. C*, vol. 3, pp. 157–166, 2013.

[33] P. Kunzo, Polyaniline/nanoparticle composite for gas sensor*s*, *Sens Actuators*, vol. 43, pp. 2–26, 2015

[34] Z. Du, C. Li, L. Li, M. Zhang, S. Xu, and T. Wang, “Simple fabrication of a sensitive hydrogen peroxide biosensor using enzymes immobilized in processable polyaniline nanofibers/chitosan film,” *Mater. Sci. Eng. C*, vol. 29, pp. 1794–1797, 2009.

[35] B. Y. D. Zhang, J. Zhang, H. Bai, R. Zhang, H. Shi, and A. Yuan, “ZIF-9 with enhanced surpercapacitor and electrocatalytic for oxygen evolution reaction performances in alkaline electrolyte,” *Int. J. Electrochem. Sci*, vol. 11, pp. 7519–7526, 2016.

[36] S. Zhu and J. Gu, “Controlled synthesis of polyaniline inside mesoporous carbon for electroanalytical sensors,” *R. Soc. Chem.*, vol. 20, pp. 5123–5128, 2010.

[37] W. Zhou, J. Jia, and J. Lu, “Recent developments of carbon-based electrocatalysts for hydrogen evolution reaction,” *Appl. Catal. A*, vol. 28, pp. 29–43, 2016.

[38] S. Anantharaj, K. Karthick, and S. Kundu, “Evolution of layered double hydroxides (LDH) as high performance water oxidation electrocatalysts : A review with insights on structure, activity and mechanism,” *Mater. Today Energy*, vol. 6, pp. 1–26, 2017.

[39] A. Mukherjee, S. Chakrabarty, W. N. Su, and S. Basu, “Nanostructured nickel ferrite embedded in reduced graphene oxide for electrocatalytic hydrogen evolution reaction,” *Mater. Today Energy*, vol. 8, pp. 118–124, 2018

[40] K. E. Ramohlola, G. R. Monana, M. J. Hato, K. E. Ramohlola, G. R. Monama, M. J. Hato, K. D. Modibane, M. Masikini, S. B. Mdluli, K. M. Molapo, and E. I. Iwuoha “Polyaniline-metal organic framework nanocomposite as an efficient electrocatalyst for hydrogen evolution reaction,” *Compos. Part B Eng.*, vol. 137, pp. 129–139, 2018.

[41] J. Lim, N. Phiboolsirichit, S. Mubeen, and N. V Myung, “Electrical and gas sensing properties of polyaniline functionalized single-walled carbon nanotubes,” *Nanotechnology*, vol. 21, pp. 406–413, 2010.

[42] G. Korotcenkov, S. Do Han, and J. R. Stetter, “Review of Electrochemical Hydrogen Sensors,” *Chem. Rev.*, vol. 109, pp. 1402–1433, 2009.

[43] D. A. C. Brownson and C. E. Banks, *Interpreting Electrochemistry*. 2014.

[44] L. Nicolae and C. Viespe, “Increased diffusion coefficient of polymetic nanocomposite layer for gas sensing applications,” *Sens. Lett.*, vol. 11, pp. 2327–2332, 2013.

CHAPTER SIX

GENERAL DISCUSSION, CONCLUSIONS AND RECOMMENDATIONS

6.1. GENERAL DISCUSSION AND CONCLUSIONS

This chapter focuses on the general discussion and conclusions of the study and make further recommendations for future electrocatalysts for hydrogen gas sensing application through hydrogen evolution reaction. The overall aim of this work was to fabricate smart sensors with excellent sensitivity, fast response and high accuracy induced by polyaniline (PANI) based zeolitic benzimdazolate framework (ZIF) composite nanofiber for electrochemical detection of hydrogen gas for safety monitoring. The sensing materials studied in this work were selected based on their outstanding properties they offer. PANI particularly half-reduced emeraldine form has been exploited as an excellent tool for hydrogen gas sensing application due to its exceptional electrical conducting, environmental stability and unique acid/base doping process. On the other hand, ZIF was chosen due to its permanent porosity, large surface area and structural diversity, and outstanding chemical and thermal stability, the ZIF crystal structures are based on aluminolilicate zeolitic nets, whereby the tetrahedral Si(AI) sites are replaced by transition metal such as Co and Zn tetrahedrally coordinated by imidazole ligands.

This dissertation was outlined into six chapters. Chapter one (introduction) was on the general background of energy. More focus was on hydrogen technology as an alternative energy carrier to carbon based fuels such as gasoline. However, hydrogen gas feed to the hydrogen fuel cell is highly flammable if its concentration is above 4 wt.% at room temperature. As a result, PANI was chosen as an alternative electrocatalyst to detect hydrogen gas thus ensuring people's safety. This was supported by a well organised aim and objectives of the study. The aim was to fabricate polyaniline decorated with Co-/Zn-zeolitic benzimidazolate framework nanocomposite as effective electrocatalyst for hydrogen gas sensing application through electrochemical HER studies. Chapter two (literature review) was on comprehensive survey of recent developments in polyaniline composites for electrochemical hydrogen gas sensing applications and future prospects. Hydrogen sensing technologies were thoroughly reviewed. Furthermore, the electrochemical

sensing electrodes more especially PANI were reviewed. In addition, the current drawbacks of PANI nanocomposite and future prospect were presented wherein zeolitic benzimidazolade framework was suggested as a possible dopant to enhance the electrochemical sensing performance of PANI nanocomposite. Chapter three (analytical techniques) a short background advantages, disadvantages, previous reports on PANI and ZIF characterisations and their application in this work were reviewed.

The first approach was taken in Chapter four which involves the development of electrochemical gas sensor technology induced by polyaniline doped with cobalt-zeolitic benzimidazolate framework composite for hydrogen safety monitoring. CoZIF was prepared using solvothermal method which allows precise control over the shape, size, crystallinity and controlled morphology, the composite was synthesised through chemical oxidative polymerisation of aniline monomer in the presence of
3.6 wt.% CoZIF. The structural properties of the synthesised materials were studied by employing ultraviolet visible (UV-vis), powder X-ray diffraction (XRD), Fourier transform infrared (FTIR) and Raman spectroscopy, and simultaneous thermal analysis (STA). The scanning electron microscope (SEM/EDS) and transmission electron microscope (TEM/EDX) were used for morphological characterisation and revealed grafting of CoZIF on to the surface of PANI upon composite formation. The XRD diffraction pattern and SAED results showed that PANI and the composite structures are amorphous in nature and the presence of CoZIF did not alter the amorphous nature of PANI. Spectroscopic analyses using FTIR and Raman revealed the coexistence of CoZIF and PANI in the composite displayed by a characteristic peak intensities corresponding to both ZIF and polymer. Furthermore, PANI and the resultant composite possessed the energy band gap of 2.5 and 2.3 eV, distinctively, using Tauc plot which shows that they are both semi-conductors. STA results presented that the resultant composite exhibits an enhancement in thermal stability in comparison to PANI as indicative of improvement of thermal properties. Cyclic voltammetry (CV), Tafel analysis and turn over frequencies (TOFs) were performed to study the electrochemical performance of the synthesised materials through hydrogen evolution reaction (HER) for gas sensing. The PANI-CoZIF composite showed drastic enhancement in the catalytic H_2 evolution and the TOFs as compared to neat PANI. In addition to that the chronoamperometric (CA) results

exhibited the significant improvement in electrochemical hydrogen sensing ability of PANI-CoZIF composite.

The second approach was taken in Chapter five which involves fabrication of polyaniline decorated with zinc based zeolitic benzimidazolate framework nanocomposite as an effective electrocatalyst for hydrogen gas sensing. ZnZIF was prepared using solvothermal method. The composite was synthesised using in-situ chemical polymerisation synthesis of polyaniline in the presence of ZnZIF. (FTIR) spectroscopy and Raman spectroscopy were used to evaluate structure of PANI-ZnZIF composite and the vibrations for functional groups of ZnZIF and PANI in the composite. X-ray diffraction (XRD) and simultaneous thermal analysis (STA) studies showed the co-existence of both PANI and ZnZIF in the composite supported by the decrease in crystallite size and the improvement in the thermal stability, respectively. The Scanning electron microscope (SEM), transmission electron microscope (TEM), energy dispersive X-ray spectroscopy (EDS, EDX), and selected area electron diffraction (HRTEM/SAED) revealed that PANI nanofibers are wrapping the cube nanofiber like structures of ZnZIF. The Square wave voltammetry (SWV), Cyclic voltammetry (CV) and Chronoamperommetry (CA) presented good electrochemical performance indicated by an increase in current response with 3 wt.% loading of ZnZIF. The high electrochemical current response is due to extraordinary specific surface area, more accessible active sites available for the electrolyte provided by ZnZIF and high conductivity supplied by PANI. Moreover, Tafel parameters and Turnover frequency values derived from CV showed an improvement in the catalytic hydrogen evolution of PANI-ZnZIF composite. The resulting PANI-ZnZIF composite was found to be highly responsive to hydrogen gas indicated by higher current response and sensitivity (10.8 $\mu A.mmol.L^{-1}$ H_2), faster steady state response time (4 s) accompanied by lower detection limit (5.27 $\mu mol.L^{-1}$) as compared to pure PANI. These results showed that both PANI-CoZIF and PANI-ZnZIF nanofibers are suitable electrocatalytic for hydrogen gas sensing application through HER in acidic medium. Based on these findings it was observed that PANI-CoZIF have better hydrogen sensing performance indicated by high sensitivity (11.9 $\mu A.mmol.L^{-1}$ H_2) as compared to PANI-ZnZIF (10.8 $\mu A.mmol.L^{-1}$ H_2). This is due to high electron affinity of Co towards hydrogen molecules thus improving the hydrogen gas sensing ability. On the other hand, PANI-ZnZIF showed better electroctrocatalytic performance for HER as compared as PANI-CoZIF. This is due to an increase in electron density

around polymer backbone caused by the excess electrons from the Zn metal centre and the bulkiness of benzimidazole organic linker.

6.2. RECOMMENDATIONS FOR FUTURE WORK

An important innovation in this work was to fabricate an alternative polymer based electrochemical hydrogen gas sensor through HER. In order to improve the electrocatalytic performance of hydrogen gas sensing materials, further improvement of the materials needs to be done. In future characterisation using Brunauer-Emmett-Teller (BET) will be important to know the surface areas of the synthesised PANI, ZIF and PANI-ZIF composite in order to determine the TOF. Furthermore, characterisation using X-ray photon spectroscopy (XPS) will be of great importance to elucidate the interaction mechanism between PANI and ZIF. Furthermore, XPS can reveal the electrochemical hydrogen evolution on the electrocatalyst before and after HER studies. It was observed from this work that PANI-CoZIF and PANI-ZnZIF composites had higher HER responses as compared to neat PANI and ZIF. Moreover, since the PANI-CoZIF and PANI-ZnZIF composites are insoluble and partially soluble, in the conventional solvents such DMSO or DMF and completely decomposed in concentrated acid, it would be useful to consider other solvents that can be used for homogeneous HER applications.

Furthermore, low HER responses of pure PANI and ZIF were due to instability of the radical cations produced during HER experiment in acidic condition. Two alternatives can be utilised in the future to enhance the HER response of the materials. The first approach is to consider alkaline medium as the alternative solvents for HER studies. The second approach is to evaluate the HER of the composites films on interdigitated electrodes in the future through electrochemical polymerisation as heterogeneous HER studies. This is because the results showed that the cross reaction between the PANI-CoZIF and PANI-ZnZIF composites radicals and the electrolytic solution is an important contributing process which influences the HER performance as reflected in the scan rate dependent studies. HER performance of the synthesised materials must be conducted using glassy carbon working electrode which will make it possible to coat. More experimental work needs to be done to optimise the PANI-CoZIF and PANI-ZnZIF composites for electrochemical hydrogen

gas sensing which includes the usage of different ratios of PANI and ZIF as the dopant. HER studies can also be done using different pH's and temperatures to optimise the eletrocatalytic performance of the composites. Even though the materials exhibited good catalytic performance, the stability and durability of the materials during HER studies also needs to be investigated for practical application of these materials. Furthermore, quantification of the amount of hydrogen produced is vital and it can be achieved by coupling CV experiments with gas chromatography or mass spectroscopy to form a hyphened instrument that can reveal the amount of gases in the HER. The substitution of gold electrode with glassic carbon working electrode for hydrogen gas sensing through HER of these materials is a possible alternative route to be employed in future. This will make it possible to coat the synthesised materials on the surface of the electrode instead of preparing them in solutions which can improve electrons movement. The Photo-catalytic hydrogen evolution reaction studies of these materials are also alternative route to be used in future for HER studies. Moreover, it will be important to couple photo-and-electro- catalytic hydrogen evolution studies in future.

The HER mechanism for some of the materials are well known but there are majority of materials whose mechanism are still in their infancy, and it is more than ideal to know the mechanism of all these materials in order to improve their performance. The composites also showed good hydrogen sensing capability deduced by low detection limit, fast response time, greater sensitivity and diffusion coefficient. However sensing parameters such as selectivity, stability and durability are also important. In addition, great progress is being made in the polymer based materials for electrochemical hydrogen gas sensing. Much help has come from the computational tools available today, and we believe that a material which essentially matches metal and metal oxides as an electrocatalyst for hydrogen gas sensing will be found therefore it will be good to implement computational model in hydrogen sensing. In future more work has to be done on achieving selective-long term hydrogen gas sensing electrocatalysts, scalable synthesis techniques, and a real- world electrolyte system.

SUPPORTING INFORMATION

DEVELOPMENT AND STRUCTURAL PROPERTIES OF ELECTROCHEMICAL GAS SENSING TECHNOLOGY INDUCED BY POLYANILINE DOPED WITH COBALT-ZEOLITIC IMIDAZOLATE FRAMEWORK COMPOSITE FOR HYDROGEN SAFETY MONITORING

This chapter was submitted for possible publication in *Electrocatalysis (Revised manuscript is under review with provisional acceptance).*

Gloria Mashao[a], Kwena D. Modibane[a,*], Siyabonga B. Mduli[b], Emmanuel I. Iwuoha[b] , Mpitloane J. Hato[a,d,*], Katlego Makgopa[c],

[a] *Chemistry Department, School of Physical and Mineral Sciences, University of Limpopo (Turfloop), Polokwane, Sovenga 0727, South Africa*

[b] *SensorLab, Chemistry Department, University of the Western Cape, Bellville 7535, Cape Town, South Africa*

[c] *Chemistry Department, Faculty of Science, Tshwane University of Technology (Acardia Campus), Pretoria 0001, South Africa*

[d] *Department of Environmental Sciences, College of Agriculture and Environmental Sciences, University of South Africa, Florida Science Campus, Johannesburg 1710, South Africa*

E-mail address: kwena.modibane@ul.ac.za (K. D. Modibane); mpitloane.hato@ul.ac.za (M. J. Hato).

S1: EXPERIMENTAL SECTION

Polyaniline (PANI) was synthesised according to the route reported previously by Ramohlola *et al*. [1]. The synthesis of polyaniline was achieved by dissolving approximately 1 mL of the distilled aniline monomer in a solution of 10 ml HCl/100 mL distilled water in a 250 mL round-bottom flask. The solution was stirred for 30 minutes at 50 °C whereafter 2.40 g of ammonium persulphate (APS), $(NH_4)_2O_8$ and 1.88 g of $FeCl_3$ were added, respectively, in the solution. The resulted mixture was stirred for another 3 hours at 50 °C, and the content of the reaction was placed in the oven at the same temperature for overnight to evaporate the solvents, and remaining content was washed with ethanol and re-dried. ZnZIF (ZIF-7) was synthesised as described by Quan *et al*. [2] with some modifications wherein methanol, zinc chloride and benzimidazole (BIZ) were used as a solvent, metal center and linker, respectively instead of distilled water cobalt nitrate hexahydrate and 2-methyl imidazole. In a typical synthesis, 0.45 g of zinc chloride was dissolved in 3 mL of deionized (DI) water; then 5.5 g of benzimidazole (BIZ was dissolved in 20 mL of DI water. Those two solutions were mixed and stirred for 6 hours at room temperature, then the resulting precipitates were collected, washed with water and methanol subsequently for 3 times, and finally dried at 80 ^{0}C for 24 hours. PANI-ZnZIF composite was prepared by following a reported procedure of PANI/MOF composite by Ramohlola *et al*. [1] with some modification, ZnZIF was used as a dopant instead of MOF. The synthesis of PANI-ZnZIF composite was achieved by dissolving approximately 1 mL of the distilled aniline monomer and 3.6 wt.% ZnZIF in a solution of 10 ml HCl/100 mL distilled water in a 250 mL round-bottom flask. The solution was stirred for 30 minutes at 50 °C whereafter 2.40 g of ammonium persulphate (APS), $(NH_4)_2O_8$ and 1.88 g of $FeCl_3$ were added, respectively, in the solution. The resulted mixture was stirred for another 3 hours at 50 °C, and the content of the reaction was placed in the oven at the same temperature for overnight to evaporate the solvents, and remaining content was washed with ethanol and re-dried.

S2: REFERENCES

[1] K. E. Ramohlola, M. Masikini, S. B. Mdluli, and G. R. Monama, “Electrocatalytic Hydrogen Production Properties of Polyaniline Doped with Metal-Organic Frameworks,” Springer Int. Publising, pp. 373–389, 2017.

[2] J. Qian, F. Sun, and L. Qin, “Hydrothermal synthesis of zeolitic imidazolate framework-67 (ZIF-67) nanocrystals,” Mater. Lett. vol. 82, pp. 220–223, 2012.

APPENDIX 1

Electrochemical Energy Reviews (ECER) <em@editorialmanager.com>

Tue, Nov 27, 3:03 PM (12 hours ago)
to me

Re: "RECENT DEVELOPMENTS IN POLYANILINE COMPOSITES FOR ELECTROCHEMICAL HYDROGEN GAS SENSING APPLICATIONS"
Full author list: Gloria Mashao; Kabelo E. Ramohlola; Gobeng R. Monama; Mpitloane J. Hato; Katlego Makgopa, PhD; Kwena Desmond Modibane, PhD

Dear Ms Gloria Mashao,

We have just received the submission entitled: "RECENT DEVELOPMENTS IN POLYANILINE COMPOSITES FOR ELECTROCHEMICAL HYDROGEN GAS SENSING APPLICATIONS" for possible publication in Electrochemical Energy Reviews, and you are listed as one of the co-authors.

The manuscript has been submitted to the journal by Dr Kwena Desmond Modibane who will be able to track the status of the paper through his/her login.

If you have any objections, please contact the editorial office as soon as possible. If we do not hear back from you, we will assume you agree with your co-authorship.

Thank you very much.

With kind regards,

Springer Journals Editorial Office
Electrochemical Energy Reviews

APPENDIX 2

Gregory Jerkiewicz <em@editorialmanager.com>

Tue, Feb 5, 5:06 PM

You are being carbon copied ("cc:'d") on an e-mail "To" "Kwena Desmond Modibane" kwena.modibane@ul.ac.za
CC: gregory.jerkiewicz@queensu.ca, "Gloria Mashao" mashaogloria20@gmail.com, "Siyabonga Mdluli" 3680647@myuwc.ac.za, "Emmanuel Iwuoha" eiwuoha@uwc.ac.za, "Mpitloane Hatoa" mpitloane.hato@ul.ac.za, "Katlego Makgopa" makgopak@tut.ac.za, "Kerileng M Molapo" g.molapo947@gmail.com

Dear Dr Modibane,

I have read the revised manuscript and find it ***almost suitable for publication***. However, it still requires the following improvements: (i) the scale bar in the TEM images is hardly visible - correct it; (ii) variables should be in italics (in the text and in the figures); (iii) use the symbol "j" not "i" should be used for current density; (iii) pay attention to how variables are reported; e.g., "Epa" = "E" should be in italics and "pa" in subscript. Overall, I request that you review the format of the manuscript. I encourage you to take into accounts my comments and recommendation when revising the manuscript. Acceptance of your manuscript is contingent on the quality of the revised manuscript. When submitting a revised version, please, explain the extent of your revisions and respond to my comments and criticisms. Please, submit a revised manuscript within 14 days of receiving this notification (Revision Due: 07 Mar 2019).

Yours truly,
Gregory Jerkiewicz, Ph.D., M.Eng.
Editor-in-Chief
Electrocatalysis

APPENDIX 3

--------- Forwarded message ---------
From: **An-Chung SU** <eesserver@eesmail.elsevier.com>
Date: Tue, Mar 5, 2019 at 6:05 PM
Subject: Your Submission
To: <katsmakgopa@gmail.com>

Ms. Ref. No.: MATCHEMPHYS-D-19-00074
Title: Fabrication of polyaniline decorated with zinc based zeolitic benzimidazolate framework nanocomposite as an effective electrocatalyst for hydrogen gas sensing
Materials Chemistry and Physics

Dear Katlego,

Reviewers have now commented on your paper. You will see that they are advising that you revise *your manuscript as it is almost suitable for acceptance in MATER CHEM PHYS*.

For your guidance, reviewers' comments are appended below.

If you decide to revise the work, please submit a list of changes or a rebuttal against each point which is being raised when you submit the revised manuscript. Your revised manuscript should be submitted within 50 days.

Yours sincerely,

An-Chung SU, PhD
Editor
Materials Chemistry and Physics

APPENDIX 4

3rd International Hydrogen Technologies Congress (IHTEC-2018), March 15-18, 2018, Alanya/Antalya, Turkey

Copper(II)phthalocyanine/metal organic frameworks (CuPc/MOF) composite with improved electrocatalytic efficiency for hydrogen production

Emmanuel I. Iwuoha[2], Gobeng Release Monama[1], Kwena Desmond Modibane[1,*], Kabelo Edmond Ramohlola[1], Kerileng Mildred Molapo[2], Mpitloane Joseph Hato[1], Mogwasha Daphney Makhafola[1], Gloria Mashao[1], Siyabonga Beizel Mdluli[2],

[1]University of Limpopo, Private Bag X1106, Sovenga, 0727, South Africa,
[2]University of the Western Cape, Private Bag X17, Bellville, 7535, South Africa

* E-mail: kwena.modibane@ul.ac.za

Abstract

The hydrogen evolution reaction (HER) of CuPc/MOF composite was investigated for hydrogen production. The SEM and EDS analyses showed that CuPc was incorporated into MOF through impregnation method. The electrochemical measurements were studied using cyclic voltammetry (CV) and it was found that CuPc/MOF composite exhibited favourable catalytic activity for HER. The Tafel slope value of the CuPc/MOF composite was found to be 185.3 mV.dec^{-1} and noticeably lower than that of the bare MOF (236.7 mV.dec^{-1}) at 0.30 M of the acid, and the charge transfer coefficients are all close to 0.5, suggesting the Volmer reaction coupled with either Heyrovsky or Tafel reaction for hydrogen production. The exchange current density, (i_0) of all the samples increased with increasing the concentration of the hydrogen source. Nonetheless, the CuPc/MOF composite showed a higher i_0 as compared to bare MOF. These observations provide a platform to synthesize promising low-cost CuPc/MOF electrocatalyst with high efficiency and excellent electrocatalytic performance for HER.

Keywords: Metal organic frameworks; Phthalocyanine; Hydrogen evolution reaction

I. Introduction

In recent years, fossil fuels are considered as the main energy resources. Nonetheless, they possess some disadvantages such as limited resources, global warming and environmental pollution. A numerous efforts have been considered to use alternative energy sources instead of fossil fuels to circumvent these problems. In this context, hydrogen fuel cell technology is one of the promising technology for sustainable energy applications owing to its various advantages such as recyclability, pollution-free and fuel efficiency Ren et al (2013). In addition, H_2 gas yields more energy, which is about 2.75 times greater as compared to traditional gasoline based energy resources. However, the problem for practical usage of H_2 gas as an energy carrier lies in the production and storage technology Ehsan and Wahid (2016). Up to this stage, electrochemical reduction of water is preferred as an effective and alternative route to produce hydrogen with high purity and in large quantity because of its simplicity and economical way Ren et al (2013). A number of porous materials such as carbon nanotubes, metal organic frameworks (MOFs), graphite nanofibers, zeolites and activated carbon were proposed as candidates for HER Ren et al. (2013) and Benck (2014). Among these materials, MOFs hold a greater promise as potential candidates in the design of advanced multifunctional materials due to their unique structures Zheng and Jiao (2017). MOFs are inorganic-organic hybrid compounds built from metal ions or clusters and organic ligands by coordination bonds, providing highly crystalline porous structures with large surface area, high pore volume as well as uniform nanoscale cavities Ramohlola et al. (2017). Thus, MOFs have been used in various applications such as energy storage, CO_2 adsorption, hydrocarbon adsorption/separation, catalysis, advanced sorbents for solids extraction and sensors. However, MOFs possess some drawbacks as HER material because of H_2 embrittlement, moisture instability and poor H_2 adsorption and desorption at ambient conditions Ramohlola et al. (2017). To the best of our knowledge, there are no studies reported on the formation and observation of HER using CuPc incorporated on the MOF surface to prepare an effective electrocatalyst. Therefore, this study reports on the synthesis, characterization and application of the hybrid-hybrid CuPc/MOF composite as a suitable electrocatalyst for HER.

II. Experimental Set-up and Procedure

MOF was synthesized following our recent published work Ramohlola et al (2017). In brief, 4.5 mmol of $Cu(NO_3)_2.3H_2O$ was dissolved in 10 ml of distilled water and then mixed with 0.525 g (2.5 mmol) of H_3BTC dissolved in 10 ml of ethanol. The mixture was stirred for 30 min and then transferred into a 23 ml Teflon stainless-steel autoclave and sealed to react for 36 hours at 120 °C in thermostatic drying oven. Copper phthalocyanine (CuPc) was synthesised from phthalimide according to previous method reported elsewhere Chiang et al. (2012). Typically, a mixture of phthalimide (3.00 g, 0.0200 mol) in the presence of excess urea (3.00 g, 0.0500 mol), ammonium heptamolybdate (0.0800g, 0.0600 mmol) and copper nitrate (1.40 g, 0.0058 mol) in nitrobenzene (15.00 mL) was refluxed for 5 hours at 180 °C to give a target compound. CuPc/MOF composite (Scheme 1) was prepared by

APPENDIX 5

ARTICLE IN PRESS

INTERNATIONAL JOURNAL OF HYDROGEN ENERGY XXX (XXXX) XXX

Available online at www.sciencedirect.com

ScienceDirect

journal homepage: www.elsevier.com/locate/he

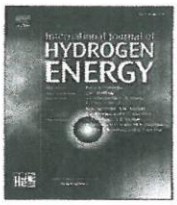

Copper(II) phthalocyanine/metal organic framework electrocatalyst for hydrogen evolution reaction application

Gobeng R. Monama [a], *Kwena D. Modibane* [a,*], *Kabelo E. Ramohlola* [a], *Kerileng M. Molapo* [b], *Mpitloane J. Hato* [a], *Mogwasha D. Makhafola* [a], *Gloria Mashao* [a], *Siyabonga B. Mdluli* [a], *Emmanuel I. Iwuoha* [b,**]

[a] *Department of Chemistry, School of Physical and Mineral Sciences, University of Limpopo (Turfloop), Polokwane, Sovenga 0727, South Africa*

[b] *SensorLab, Chemistry Department, University of the Western Cape, Bellville 7535, Cape Town, South Africa*

ARTICLE INFO

Article history:
Received 5 September 2018
Received in revised form
3 February 2019
Accepted 7 February 2019
Available online xxx

Keywords:
Copper(II)phthalocyanine
Metal organic frameworks
Hydrogen
Electrocatalyst

ABSTRACT

Copper(II)phthalocyanine-incorporated metal organic framework (CuPc/MOF) composite material was synthesized for application as an electrocatalyst for hydrogen evolution reaction (HER). The composite exhibited excellent electroactivity compared to the unmodified MOF, as confirmed by the diffusion coefficients (D) values of 3.89×10^{-7} and 1.57×10^{-6} cm^2 s^{-1} for MOF and CuPc/MOF, respectively. The D values were determined from cyclic voltammetry (CV) experiments performed in 0.1 mol L^{-1} tetrabutylammonium perchlorate/dimethyl sulfoxide (TBAP/DMSO) electrolyte. The Tafel slope determined from the CV data of CuPc/MOF-catalysed HER for 0.450 mol L^{-1} H_2SO_4, was 176.2 mV dec^{-1}, which was higher than that of the unmodified MOF (158.3 mV dec^{-1}). The charge transfer coefficients of MOF and CuPc/MOF were close to 0.5, signifying the occurrence of a Volmer reaction involving either the Heyrovsky or the Tafel mechanism for hydrogen generation. For both MOF and CuPc/MOF, the exchange current density (i_0) improved with increase in the concentration of the hydrogen source (i.e. 0.033–0.45 mol L^{-1} H_2SO_4) Nonetheless, the CuPc/MOF composite had a higher i_0 value compared with the unmodified MOF. Thus CuPc/MOF has promise as an efficient electrocatalyst for HER.

© 2019 Hydrogen Energy Publications LLC. Published by Elsevier Ltd. All rights reserved.

Introduction

Fossil fuels are considered as the primary source of energy; however, they have several drawbacks such as global warming, inadequate resources and environmental pollution. Conversely, other types of fuels have been considered as substitute energy sources to circumvent these problems. In this context, hydrogen gas was identified as one of the favorable fuels for renewable energy applications due to its various advantages such as recyclability, fuel efficiency and pollution-free characteristics [1]. Furthermore, H_2 gas provides energy of approximately 2.75 times with respect to

* *Corresponding author.*
** *Corresponding author.*
E-mail addresses: kwena.modibane@ul.ac.za (K.D. Modibane), eiwuoha@uwc.ac.za (E.I. Iwuoha).
https://doi.org/10.1016/j.ijhydene.2019.02.052
0360-3199/© 2019 Hydrogen Energy Publications LLC. Published by Elsevier Ltd. All rights reserved.

Please cite this article as: Monama GR et al., Copper(II) phthalocyanine/metal organic framework electrocatalyst for hydrogen evolution reaction application, International Journal of Hydrogen Energy, https://doi.org/10.1016/j.ijhydene.2019.02.052

APPENDIX 6

Renewable Energy 119 (2018) 62–72

Contents lists available at ScienceDirect

Renewable Energy

journal homepage: www.elsevier.com/locate/renene

Palladium deposition on copper(II) phthalocyanine/metal organic framework composite and electrocatalytic activity of the modified electrode towards the hydrogen evolution reaction

Gobeng R. Monama [a], Siyabonga B. Mdluli [b], Gloria Mashao [a], Mogwasha D. Makhafola [a], Kabelo E. Ramohlola [a], Kerileng M. Molapo [a], Mpitloane J. Hato [a, *], Katlego Makgopa [c], Emmanuel I. Iwuoha [b], Kwena D. Modibane [a, **]

[a] Department of Chemistry, School of Physical and Mineral Sciences, University of Limpopo (Turfloop), Polokwane, Sovenga 0727, South Africa
[b] SensorLab, Chemistry Department, University of the Western Cape, Bellville 7535, Cape Town, South Africa
[c] Department of Chemistry, Faculty of Science, Tshwane University of Technology (Acardia Campus), Pretoria 0001, South Africa

ARTICLE INFO

Article history:
Received 13 August 2017
Received in revised form
8 November 2017
Accepted 29 November 2017
Available online 30 November 2017

Keywords:
Metal-organic frameworks
Phthalocyanine
Palladium
Hydrogen evolution reaction
Hydrogen spillover

ABSTRACT

Pd-supported copper phthalocyanine/metal organic frameworks (Pd@CuPc/MOF) composite was synthesized by the reaction between CuPc and MOF followed by electroless Pd plating. The structural properties of MOF, Pd@MOF and Pd@CuPc/MOF composite were characterized using X-ray diffraction (XRD), Fourier transform infrared (FTIR), simultaneous thermal analysis (STA), ultraviolet–visible spectroscopy (UV–vis), scanning electron microscopy (SEM/EDS) and Brunauer-Emmett-Teller (BET). The XRD, UV–vis and FTIR analyses showed that Pd was coated on CuPc/MOF composite. SEM and EDS results revealed that Pd nanoparticles were well-dispersed and anchored tightly on the composite. The thermal stability of MOF increased upon addition of Pd and CuPc. The electrochemical hydrogen evolution reaction (HER) performance of the synthesized materials was studied by cyclic voltammetry (CV) and Tafel analysis. The Tafel slope of the composite was 176.9 mV/dec and the transfer coefficient of 0.67 which is close to 0.5. The HER results revealed that the Pd@CuPc/MOF composite has better catalytic characteristic such as high catalytic activity and lowest onset potential compared to MOF. More importantly, the significant enhancement of HER performance at ambient temperature for the composite with Pd content can be ascribed to the hydrogen spillover mechanism in such system.

© 2017 Elsevier Ltd. All rights reserved.

1. Introduction

The growing concern of energy crisis and environmental pollution promotes the development of an effective clean energy technology. Hydrogen gas has a potential to be an alternative energy carrier because it offers clean, efficient and renewable energy characteristics [1]. In addition, H_2 gas yields more energy, which is about 2.75 times greater as compared to traditional gasoline based energy resources [2]. However, the problem for practical usage of H_2 gas as an energy carrier lies in the production and storage technology [2,3]. Electrochemical water splitting ($H_2O \rightarrow H_2 + ½ O_2$) consists of two half reactions known as oxygen reduction reaction (ORR) and hydrogen evolution reaction (HER) [3]. The ORR and HER normally take place on the anode and the cathode, respectively. The reaction mechanism of HER ($2H+ + e- \rightarrow H_2$) in aqueous acid or alkaline solutions proceeds in a series of three elementary reaction steps which comprise of two electrochemical reactions and one chemical reaction [4]. In acidic medium, the HER could proceed via three main steps given in Eqs. (1)–(3) [5]:

$H^+ + e- \rightarrow$ Had Volmer reaction (electrochemical adsorption) (1)

Had $+ H^+ + e- \rightarrow$ H2 Heyrovsky reaction (electrochemical desorption) (2)

Had + Had $\rightarrow H_2$ Tafel reaction (catalytic desorption) (3)

* Corresponding author.
** Corresponding author.
E-mail addresses: mpitloane.hato@ul.ac.za (M.J. Hato), kwena.modibane@ul.ac.za (K.D. Modibane).

https://doi.org/10.1016/j.renene.2017.11.084
0960-1481/© 2017 Elsevier Ltd. All rights reserved.